Summer 2009

Electrohydrodynamic manipulation of multiphase fluids

Sai C. Nudurupati
New Jersey Institute of Technology

Recommended Citation

Nudurupati, Sai C., "Electrohydrodynamic manipulation of multiphase fluids" (2009). *Dissertations*. 921.
https://digitalcommons.njit.edu/dissertations/921

ABSTRACT

ELECTROHYDRODYNAMIC MANIPULATION OF MULTIPHASE FLUIDS

by
Sai Chaitanya Nudurupati

In microfluidic devices, the fluid can be manipulated either as continuous streams or droplets. The latter is particularly attractive as individual droplets can not only move but also split and fuse, thus offer a greater flexibility in applications such as a laboratory-on-a-chip. In this thesis, a technique is developed that uses an externally applied electric field for manipulating and removing particles trapped on the surface of a drop. The drop is assumed to be immersed in another liquid with which it is immiscible, and the electric field is generated by placing electrodes on the sides of the microdevice. Both experiments and direct numerical simulation (DNS) approaches are used to study these problems.

The DNS approach used in this thesis is based on a finite element scheme in which the fundamental equations of motion for the droplets and the surrounding fluid are solved exactly within numerical errors. The interface is tracked by the level set method and the electrostatic forces are computed using the Maxwell stress tensor approach. The distributed Lagrange multiplier method is used for tracking particles.

One of the main results of this work is that the distribution of particles on the surface of a drop can be manipulated by subjecting it to a uniform electric field and these concentrated particles can then be removed by further increasing the electric field intensity. Specifically, it is shown that particles can be concentrated into well-defined regions on the drop surface while leaving the rest of the surface particle free. Experiments show that when the dielectric constant of the drop is greater than that of the ambient liquid, particles for which the Clausius–Mossotti factor is positive move along to

the two poles of the drop. Particles with a negative Clausius–Mossotti factor, on the other hand, form a ring near the drop equator. This motion is due to the dielectrophoretic force that acts upon particles because the electric field on the surface of the drop is nonuniform, despite the fact that the applied electric field away from the drop is uniform. Experiments also show that when small particles collect at the poles of a deformed drop, the electric field needed to break the drop is smaller than it is without the particles. Also, the experimental results for the dependence of the dielectrophoretic force on the parameters of the system such as the particles' and drop's radii and the dielectric properties of the fluids and particles are studied, and a dimensionless parameter regime for which the technique is guaranteed to work is defined. Also it is shown that this technique can be used to separate particles experiencing positive dielectrophoresis on the surface of a drop from those experiencing negative dielectrophoresis, and form a composite (Janus) drop by aggregating particles of one type near the poles and of another near the equator.

The DNS approach is used to study the transport of particles via the traveling wave dielectrophoretic (twDEP) forces. This technique offers a promising method for transporting particles along the length of a channel without having to pump the liquid itself. Since the magnitudes of twDEP forces and torque vary with the frequency of the electric field, a variety of complex dynamical regimes are possible. The DNS approach is used to analyze the various dynamical regimes for yeast cells in terms of the forces that act on the cells, i.e., the conventional dielectrophoretic and traveling wave dielectrophoretic force and torque, the viscous drag exerted by the fluid on the particle, and the electrostatic and hydrodynamic particle-particle interactions.

ELECTROHYDRODYNAMIC MANIPULATION OF MULTIPHASE FLUIDS

by
Sai Chaitanya Nudurupati

A Dissertation
Submitted to the Faculty of
New Jersey Institute of Technology
in Partial Fulfillment of the Requirements for the Degree of
Doctor of Philosophy in Mechanical Engineering

Department of Mechanical Engineering

August 2009

APPROVAL PAGE

ELECTROHYDRODYNAMIC MANIPULATION OF MULTIPHASE FLUIDS

Sai Chaitanya Nudurupati

8/13/09

Dr. Pushpendra Singh, Dissertation Co-Advisor   Date
Professor, Department of Mechanical Engineering, NJIT

8/17/09

Dr. Nadine Aubry, Dissertation Co-Advisor   Date
Professor and Head, Department of Mechanical Engineering, CMU

8/13/09

Dr. Ian S. Fischer, Committee Member   Date
Professor, Department of Mechanical Engineering, NJIT

8/13/09

Dr. Anthony Rosato, Committee Member   Date
Professor, Department of Mechanical Engineering, NJIT

8/13/2009

Dr. Zhiming Ji, Committee Member   Date
Associate Professor, Department of Mechanical Engineering, NJIT

8/13/09

Dr. Denis Blackmore, Committee Member   Date
Associate Professor, Department of Mathematics, NJIT

BIOGRAPHICAL SKETCH

Author: Sai Chaitanya Nudurupati

Degree: Doctor of Philosophy

Date: August 2009

Undergraduate and Graduate Education:

- Doctor of Philosophy in Mechanical Engineering,
  New Jersey Institute of Technology, Newark, NJ, 2009

- Bachelor of Science in Industrial Production Engineering,
  Chaitanya Bharati Institute of Technology, India, 2003

Major: Mechanical Engineering

Journal Publications:

Nudurupati, S., Janjua, M., Aubry, N. and Singh, P. (2009). Electrostatic particle-particle interactions on the surface a drop, (in preparation).

Nudurupati, S., Janjua, M., Aubry, N. and Singh, P. Removal of particle distributed on the surface of a drop, Soft Matter, (Submitted, in review).

Nudurupati, S., Janjua, M., Aubry, N., and Singh, P. (2009). Electrohydrodynamic removal of particles from drop surfaces, Physical Review E, 80, 010402.

Janjua, M., Nudurupati, S., Fischer, I., Singh, P. and Aubry, N. (2009). Electric field induced alignment and self-assembly of rods on fluid-fluid interfaces, Mechanics Research Communications, 36, 55-64.

Nudurupati, S., Janjua, M., Aubry, N. and Singh, P. (2008). Concentrating particles on drop surfaces using external electric fields, Electrophoresis, 29, 1164-1172.

Aubry, N., Singh, P., Janjua, M., and Nudurupati, S. (2007). Micro- and nano-particles self-assembly for virtually defect-free, adjustable monolayers, PNAS, 105, no.10, 3711-3714.

Nudurupati, S., Aubry, N., and Singh, P. (2006). Electrohydrodynamics of yeast cells in microchannels subjected to travelling electric fields, J. Phys. D: Appl. Phys. 39.

Conference Publications:

Nudurupati, S., Janjua, M., Singh, P., and Aubry, N. (2009). Redistribution and removal of particles from drops surfaces, 13th IACIS International Conference on Surface and Colloid Science and 83rd ACS Colloid and Surface Science Symposium

Nudurupati, S., Janjua, M., Singh, P., and Aubry, N. (2008). Motion of particles on the surface of a Droplet Subjected to Electric Fields, ASME Annual Meeting, Boston, Massachusetts.

Nudurupati, S., Janjua, M., Aubry, N. and Singh, P. (2008). Transport and Deformation of Droplets in a Micro-Device using Dielectrophoresis, FACM'08 Conference: Frontiers in Applied and Computational Mathematics, Newark, NJ, May 19-21.

Aubry, N., Singh, P., Janjua, M., and Nudurupati, S. (2008). Self-assembly of Particles into 2D Lattices with Adaptable Spacing, Proceedings of FEDSM2008-55248, ASME Fluids Engineering Division Summer Meeting and Exhibition, August 10-14, 2008, Jacksonville, FL, USA.

Aubry, N., Singh, P., Nudurupati, S., and Janjua, M. (2008) Removal of Particles from the Surface of a Droplet. Proceedings of FEDSM2008-55247, 2008 ASME Fluids Engineering Division Summer Meeting and Exhibition, August 10-14, Jacksonville, FL, USA.

Aubry, N., Singh, P., Janjua, M., and Nudurupati, S. (2008). Self-assembly of particles for 2d lattices with adaptable spacing, XXII ICTAM, 25-29 August 2008, Adelaide, Australia.

Janjua, M., Nudurupati, Singh, P., and Aubry. N. (2007). Direct Numerical Simulation (DNS) of suspensions in spatially varying electric fields, ASME annual meeting, Seattle, Washington.

To

Lord, Sai Baba who is always with me and looked after me

Father, Sai Baba, Mother, Sarada and to my dear wife Jyothi Sri

ACKNOWLEDGMENT

First and foremost, I would first like to thank Lord, Sai Baba who gave me everything in my life. Then I would thank my parents who were very supportive and taught the value and importance of education. They also taught me good morals which I treasure for my entire life. I also thank my wife who is a wonderful person and also who gives me motivation and reminds me of my responsibilities in my day to day activities.

I would now like to thank key people who helped me become a better researcher. First I would like to thank Dr. Singh for his guidance and encouragement. He taught me to be a hard worker and succeed in this competitive world. He is an excellent mentor and a unique guide who takes utmost care of his students both professionally and personally by teaching good work ethics. My work would not go as smoothly if not for the enthusiasm and help from Dr.Aubry. She is also a wonderful person to work with.

I also extend my thanks to Dr. Rosato, Dr. Fischer, Dr. Ji, and Dr. Blackmore for taking interest in my research. I have a learned a lot from these professors over the years.

My friends have supported me immensely during my work. I am thankful to my group members, Dr.Mansoor, Sathish and Bhavin. Dr. Mansoor was a very good friend and a good researcher to work with. My stay in NJIT would not have been the same without his help. Both, Sathish and Bhavin were very compatible and fun to work with and made my stay in NJIT more exciting. I would also like to thank Jaskirat and Mahesh.

TABLE OF CONTENTS

TABLE OF CONTENTS
(Continued)

..

LIST OF FIGURES

Figure   **Page**

Figure   **Page**

CHAPTER 1

INTRODUCTION

In recent years, enormous efforts have been made in the field of electrohydrodynamics to develop miniaturized devices for a wide range of applications. Specifically, there has been an explosion of interest in microsystems for biological, chemical, and bio-chemical applications with a particular emphasis on the development of a "Lab-on-a-chip". This concept of the Lab-on-a-chip integrates several functional units such as identification, separation, concentration, and transportation system all on a single microchip, with potential applications in a wide range of fields, such as diagnosis and cure of complex diseases to screening combinatorial libraries.

The aim of this research was to study the transport, sorting, and separating mechanisms of micron sized particles, droplets, or droplets containing particles using uniform and non-uniform A.C. electric fields. There are additional applications of microfluidics, such as pumping liquids and powders, creating artificial or zero gravity, separating minerals, sorting live from dead cells, removing abnormal from normal particles, and many more scientific applications, where the results of the present study can be employed.

1.1 Literature Review

In the last two decades, dielectrophoresis (DEP) has received a lot of interest from both the research community and industry, especially because of its potential ability to manipulate biological particles. Specifically, several different types of particle have been manipulated using DEP forces, including yeast cells [3, 4], bacteria [5-7], viruses [8-11],

1

DNA [12], mammalian cells [13-15] and also synthetic materials like polymers and polystyrene beads [16, 17]. Pohl [1] (in 1950) was first to note that "Dielectrophoresis does not require ionized particles but rather depends on asymmetrical induction and attraction of displacement charges within the particles". He was able to suspend water droplets in mid-air. Later, he published these experimental results in his classical book [2]. Even before the discovery of dielectrophoresis, Winslow [18] saw that dielectric particles suspended in fluids form chains when subjected to uniform electric fields, which lead to the discovery that the effective viscosity of a fluid can be changed and also can be controlled by varying the electric field strength.

In recent years there has been a push towards smaller systems called Lab-on-a-chip [19-21] where the manipulations of cells can be done faster and with improved efficiency. The goal is to replace the bulky systems, which are used until now, with their scaled-down versions which can be integrated on a single chip of about a few millimeters [22, 23]. This miniaturization allows us to use very small amounts of materials and reagents which make the analysis done using these devices less expensive. Lab-on-a-chip applications reach across various disciplines, such as medical, bioengineering, electronics, mechanical, and chemical engineering. Often the manufacturing techniques have come from microelectronics, and have thus utilized silicon wafers etc, but glass/plastics also have been used by Karniadakis and Beskok (2002). Also, as nano-technology progresses, there is a rapidly growing need to manipulate small objects, such as carbon nano-tubes, nanoparticles, etc., for which these micro devices are clearly better suited.

Another appealing approach for controlling fluids and particles in micro devices is the use of droplets which can transport various types of fluids and particles. This approach has been referred to as "digital microfluidics." One advantage of this technique compared to those using fluid streams is the possibility of using programmable micro-chips in which bio-chemical reactions occur within individual droplets.

Until the late 1980's, the core of the technology was developed based on continuous flow-systems where solutions are pumped, mixed and regulated in micro channels. These tend to require complicated structures to be built which increases the cost and complexity of the system. Also, every new application would require serious remodeling since these systems are application specific. Alternatives to these systems are the open structure systems where independently-controlled droplets are manipulated. By using very small amounts of fluid, the microfluidic functions can be reduced to a set of repeatable operations. This also facilitates the use of a cell-based approach for biochip design which offers a much more flexible system than the one considered until the late 1980's.

Droplets can serve as carriers for various types of reactions [40], the transcription and translation of single genes for the creation of new enzymes [41], therapeutic agents for targeted drug delivery and microfabrication of materials, e.g., the synthesis of supraparticles initially contained within droplets [42]. Current challenges for increasing the efficiency of such biochemical processes include the controlled production, transport, splitting and coalescence of droplets at a certain location and at a given time within the same device [43, 44], mixing, concentrating and separating particles carried by the droplets, and fluid/particles separation.

There are numerous applications in which the presence of small particles on drop surfaces is important. First, it is well known that foams and emulsions can be stabilized by using submicron sized solid particles which become adsorbed at fluid-fluid interfaces [45-48], a technique often used in diverse applications. However, the physics behind the process by which stabilization occurs is not completely understood. Second, in recent years, partly as a result of the attention given to nano particles (and nanotechnology), there has been much interest in the phenomenon of particles assembly at interfaces, including fluid-fluid interfaces, as a means to fabricate novel nano structured materials [45, 46]. Third, the field of digital microfluidics, which, as noted above, generates and uses droplets - rather than fluid streams - to transport, concentrate and mix fluid and particles, offers a clear advantage in its potential for programmable micro-chips with bio-chemical reactions occurring within single droplets [43, 49, 50].

The goal of this work was to study the influence of an externally applied uniform electric field on the distribution of particles on the surface of a drop as a concentration and separation tool for digital microfluidic applications. The drop is immersed in another liquid and the two liquids involved are assumed to be immiscible. In the absence of the electric field, small particles, *i.e.*, submicron sized particles for which the buoyant weight is negligible, distribute randomly on the drop's surface. Such a presence of small particles is known to stabilize emulsions whose constituents separate spontaneously in the absence of particles [51]. Although the role played by small particles is similar to that of surfactant molecules, the mechanism by which emulsions are stabilized is not entirely understood [45-48].

Furthermore, small particles are readily trapped in liquid–gas and liquid–liquid surfaces, even when they are denser than the liquid(s). Such particles are always surface active by virtue of the effects of capillarity and sometimes have activity mimicking the amphillic properties of surfactants. This is known since the pioneering works by Ramsden [52], who observed that emulsions were stabilized by solid matter at the interface between liquids, and of Pickering [53], who noted that colloidal particles which were wetted more by water than by oil could act as an emulsifying agent for oil-in-water emulsions. More recent work in this area is described in Menon and Wasan [54] and Yan and Masliyah [55]. It is generally accepted that hydrophilic solids stabilize oil-in-water emulsions, while hydrophobic solids stabilize water-in-oil emulsions. The most effective stabilization occurs when particles saturate the surface. Effective covering is promoted by self-assembly due to capillarity which cannot occur without the deformation of the interface.

The approach is to make use of externally applied electric fields to manipulate the distribution of particles on the surface of a drop. Electric fields are particularly powerful in small devices due to the fact that small potentials can generate relatively-large field amplitudes that can be used to transport and even breakup droplets. In this regard, O'Konski and Thacker [56] and Garton and Krasnucki [57] noted that a dielectric drop placed in a dielectric liquid and subjected to a uniform electric field will deform. These observations were later confirmed by Taylor [58], who considered the case where the drop or ambient liquid, or both, are conducting, and introduced a leaky dielectric model. The deformation and breakup of a dielectric drop in a dielectric liquid was analyzed analytically in [59, 60]. It was shown in [58, 61] that for the leaky dielectric model, the

shear stress on the surface of the drop is nonzero, and the fluid inside the drop circulates in response to such shear stresses [62–64].

Next, the theory that explains why particles place in a non uniform electric field are subjected dielectrophoresis and traveling wave dielectrophoresis is described. This is followed by a discussion of the dependence of the drop deformation on the dielectric constants of the drop and suspending liquids, and the breakup of the drop when the electric field strength is above a critical value.

1.2 Theory

1.2.1 Dielectrophoresis

Dielectrophoresis is defined as the lateral motion imparted to uncharged particles as a result of polarization induced by non-uniform electric fields. This phenomenon is often misunderstood to be the same as electrophoresis which is the motion of a charged particle in an electric field. That is, a Coulomb force acts on a charged particle which causes it to move in the direction of electric field if the particle's charge is positive and in the opposite direction if the charge is negative. Dielectrophoresis, on the other hand, involves migration of uncharged particles towards a maximal or minimal of the electric field intensity.

The key to understanding dielectrophoresis lies in the appreciation of the charge distribution at the interface between the particle and the fluid which have different conductivity and permittivity. In the presence of an electric field, charges move and pile up on either side of the particle in the direction of electric field as shown in Figure 1.1. The number of charges inside the interface could be more or less than outside depending

on the polarizability of the particle with respect to the medium. This means that there is a charge density which is created on either side of the particle, which gives rise to an induced dipole moment across the particle. A conducting particle in an insulating medium is an example of a particle more polarizable than the surrounding medium.
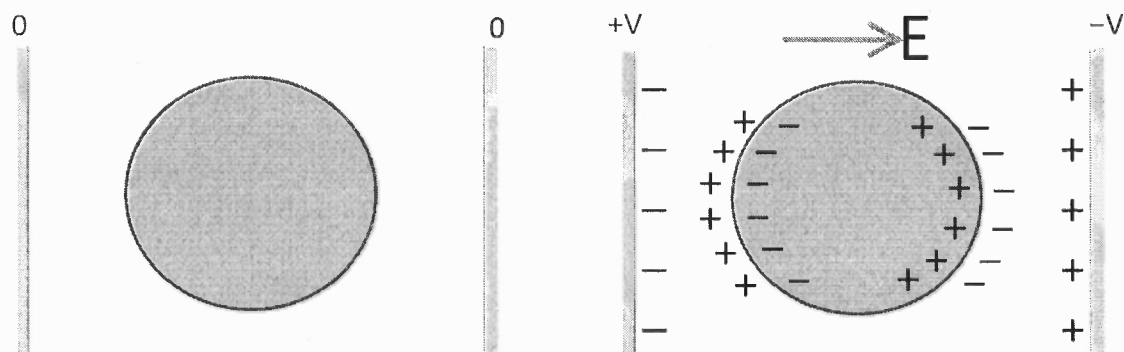
Figure 1.1 The particle on the left is not polarized because no electric filed is applied. The one on the right is subjected to a uniform electric field and is polarized.

More specifically, when an electrically neutral spherical particle is subjected to a uniform electric field, it is polarized, but no net force acts on the particle. However, when the electric field is non uniform, a net electric force acts on the polarized particle. This happens because the field strength on one side of the particle is more than on the other side and so the net electric force acting on the particle is not zero. This force is called the dielectrophoretic force and the technique itself is called dielectrophoresis. If the particle is non spherical, in addition to the above mentioned translatory force, in general, a torque also acts on the particle.

The dielectrophoretic force that acts on a particle causes it to collect either near the local maximums or local minimums of the electric field intensity, depending on the relative polarizability of the particle and the fluid. The magnitude of the net electrostatic force also depends on the gradient of the electric field that acts on the particle. Figure 1.2

shows a particle which is more polarizable than the liquid. The direction of the dipole is aligned with the field, and so that the particle experiences a positive DEP force. The opposite situation arises when the particle is less polarizable than the liquid. The direction of dipole in this case is against the field which gives rise to a negative DEP force.
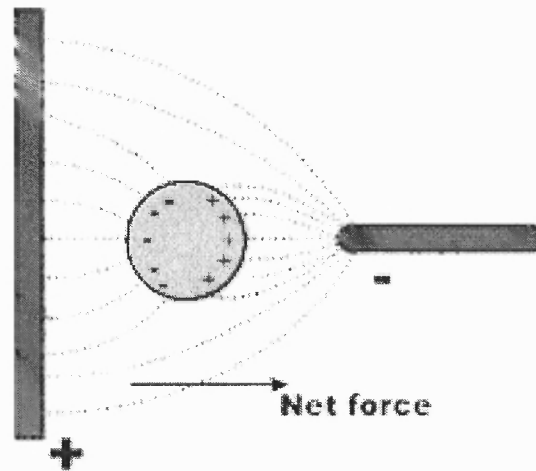
Figure 1.2 A polarized particle in a non uniform electric field. The particle is more polarizable than the surrounding fluid and so is attracted towards the stronger electric field region.
The above picture is taken on August 20, 2009 from "http://www-dsv.cea.fr/en/instituts/institut-de-recherches-en-technologies-et-sciences-pour-le-vivant-irtsv/unites-de-recherche/laboratoire-biopuces-biopuces/projet-medics/dielectrophorese".

For a dielectric spherical particle, the induced dipole moment is given by,

$$p = 4\pi\varepsilon_o\varepsilon_c a^3 \beta(f)$$

where a is the particle radius, ε_c the permittivity of the fluid, $\varepsilon_0 = 8.8542 \times 10^{-12}$ F/m is the permittivity of free space, β is the complex frequency dependent Clausius-Mossotti factor

$\dfrac{\varepsilon_p^* - \varepsilon_c^*}{\varepsilon_p^* + 2\varepsilon_c^*}$, i.e., $\beta(f) = \mathrm{Re}\left(\dfrac{\varepsilon_p^* - \varepsilon_c^*}{\varepsilon_p^* + 2\varepsilon_c^*}\right)$, ε_p^* and ε_c^* being the complex permittivities of the

particles and the fluid, and $\varepsilon^* = \varepsilon - j\dfrac{\sigma}{f}$, where σ is the conductivity, ε is the permittivity

and f is the angular frequency of the applied electric field.

According to the point dipole approximation, the DEP force is given by:

$$\mathbf{F}_{DEP} = \frac{1}{2} p \nabla \mathbf{E}^2$$

where E is the electric field intensity, and p is the dipole moment.

The sign of the Clausius-Mosotti factor (β) determines whether the particle undergoes positive DEP or negative DEP. Specifically, if the sign of β is positive, then particles move to the maximums of the electric field strength and hence undergo positive dielectrophoresis and when β is negative, particles move to a region where the electric field strength is locally minimal. When this value is neither positive nor negative, i.e. it is zero, the DEP force is also zero. Since β varies with the frequency of the electric field, it may be possible to select a frequency for which β is zero. This frequency, when it exists, is called the crossover frequency. This fact can be exploited for separating particles with positive β values from those with negative β values. This is a powerful separation technique which has many practical applications like removal or separation of selected particulate matter from liquid suspensions, classification of micro organisms, separation of minerals, and also, as we show in this work, creation of composite particle structures at fluid-fluid interfaces.

In practice, the separation of particles is often sought in conjunction with their transport. One way to accomplish this is through the field flow fractionation method, which consists of judiciously combining hydrodynamics and dielectrophoresis in a

channel flow [24]. Another technique, referred to as the traveling wave dielectrophoresis (twDEP), is also used to separate particles [25-27].

1.2.2 Traveling Wave Dielectrophoresis

In traveling wave dielectrophoresis, a traveling electric field generated by periodically repeating sets of appropriately phased electrodes is used instead of a field for which the phase of the electric field is constant in space. Thus, as explained below, in addition to a dielectrophoretic force, a particle also experiences a traveling wave dielectrophoretic force and torque. The former can be used to translate particles in the tangential direction to the electrodes and the latter makes particles spin. In conventional dielectrophoresis (cDEP), as explained above, the dielectrophoretic force acting on an isolated, spherical particle is proportional to the in-phase component of the dipole moment induced by the electric field and the field non-uniformity, as given by the gradient of the square of the electric field. In an A.C. electric field, this statement remains valid if the dielectric force considered is the time averaged force and the electric field is replaced by the root mean square (rms) of the electric field. Furthermore, the force is proportional to the real part of the Clausius-Mossoti factor β, which quantifies the mismatch between the dielectric properties of the particle and its suspending medium.

In twDEP, both the real and the imaginary parts of the Clausius-Mossoti factor (β) determine the forces and torques acting on a particle. While the conventional DEP force can be either positive or negative depending on the sign of the real part of the Clausius-Mossoti factor $Re(\beta)$ [28], thus causing particles to move toward the electrodes for $Re(\beta) > 0$, and away from the electrodes for $Re(\beta) < 0$, the traveling wave DEP force is dependent on $Im(\beta)$ and can generate a translatory motion along the electrode array.

However, for such a translation to occur, particles need first to be transported away from the electrodes under the action of negative dielectrophoresis. In other words, the time averaged force acting on an isolated, spherical particle originates from the interactions of the non-uniform electric field with both the in-phase and out-of phase components of the induced dipole moment of the particle. While the first interaction gives rise to a time-averaged force equal to the conventional dielectrophoretic force, which depends on the real part of the Clausius-Mossoti factor and the non-uniformity in the spatial distribution of the square of the electric field magnitude, the second one generates on average a translational force proportional to the imaginary part of the Clausius-Mossoti factor and the square of the electric field magnitude. This translational motion can propel the particles along the channel upstream or downstream (depending on the sign of $\text{Im}(\beta)$), thus avoiding the need to pump the fluid itself. It is thus clear that particle separation can be achieved based on the signs of the real and imaginary parts of β. Further separation capability is due to the fact that the translational particle velocity is a function of the size of the particles and the relative polarizability of the particles versus that of the fluid, and therefore in practical applications the technique has the potential to separate particles according to their size or dielectric properties [29, 30].

Quantitative studies have been performed in the past [31, 32] to compute both conventional DEP and twDEP forces. The actual movement of the particle, however, not only depends on these forces and corresponding torques, but also on the hydrodynamic and electrostatic particle-particle interactions, as well as the viscous drag forces exerted by the liquid. The combined effect of these forces has been analyzed to identify phenomena such as attracting, repelling, and chaining of particles [33]. Computations of

the motion of particles subjected to twDEP in a channel with planar electrodes connecting the two side walls of the channel at its bottom was described in [34], where various regimes were found depending on the real and imaginary parts of β.

1.2.3 Mutual Dielectrophoresis

Particles placed in a spatially non uniform electric field are not only subjected to the DEP force and twDEP forces, but also to the electrostatic particle-particle interaction forces which act even when the electric field is uniform. The electrostatic particle-particle interaction force which is also called the mutual dielectrophoretic force [2], is responsible for the pearl chain formation. These forces arise because when two dipoles are aligned parallel to the line joining their centers they attract. Therefore, since the direction of polarization is parallel to the electric field direction, when the line joining the centers of two particles is parallel to the direction of the electric field, particles attract each other. On the other hand, when the line joining their centers is perpendicular to the direction of electric field, they repel each other.

This is the mechanism by which particles of an electrorheological liquid form chains and columns and align parallel to the electric field direction. It is also imperative that the effective viscosity of the above mentioned ER suspension increases dramatically. As discussed before, Winslow was the first to experimentally study the electrorheological (ER) effects in suspensions of low conductivity subjected to external electric fields. He noted that the viscosity of the suspensions increased due to the formation of particle chains. Since then, many experimental studies of ER fluids have been performed [35-39] to study the dependence of the increase in the viscosity on the parameters such as the shear rate, the electric field strength, the volume fraction of particles, etc.

1.2.4 Electrohydrodynamics of Droplets

When a drop is subjected to a uniform electric field, it becomes polarized like a rigid particle. However, since the distribution of the electric stress on the surface of the drop is non uniform, it elongates in the direction of electric field. The electric field near the drop becomes non uniform because the dielectric constant of the drop and the surrounding fluid are different.

The main objective here is to use this non uniformity of the electric field to concentrate particles distributed on the surface of a drop at its poles or near the equator. This, as noted, requires that the dielectric constant of the drop be different from that of the ambient fluid. The poles are defined as the two points on the drop surface where the applied uniform electric field is normal to the drop surface, while the equator is the curve at equidistance between the two poles and along which the electric field is tangential to the drop surface.

If the drop's dielectric constant is smaller than that of the ambient fluid, the modified electric field distribution is such that the electric field near the equator is smaller and near the poles it is larger, compared to the imposed uniform electric field. If the dielectric constant of the drop is greater than that of the ambient fluid, the electric field is stronger at the poles than it is near the equator. Furthermore, the electric field inside the drop is stronger than the applied field in the former case and weaker in the latter case. An in-detail explanation of this phenomenon is explained in Chapter 2.

Since the electric field strength on the surface of a drop is non-uniform, a particle on the surface is subjected to a dielectrophoretic (DEP) force that causes it to move either to the equator or to one of the poles. The direction of the DEP force that acts on a particle

as discussed before depends on the sign of its Clausius-Mossotti factor which determines the location at which particles eventually aggregate. If the Clausius-Mossotti factor is positive, particles aggregate at the poles if the dielectric constant of the drop is greater than that of the ambient fluid, and at the equator if the dielectric constant of the drop is smaller than that of the ambient fluid. Furthermore, the opposite is true if the Clausius-Mossotti factor is negative. That is, particles aggregate at the equator if the dielectric constant of the drop is greater than that of the ambient fluid, and at the poles if the dielectric constant of the drop is smaller than that of the ambient fluid. For a drop suspended in a fluid and subjected to an AC electric field, the Clausius-Mossotti factor is

$\beta(\omega) = \mathrm{Re}\left(\dfrac{\varepsilon_d^* - \varepsilon_c^*}{\varepsilon_d^* + 2\varepsilon_c^*}\right)$, where ε_d^* and ε_c^* are the frequency dependent complex permittivity of the drop and the ambient fluid, respectively. The complex permittivity is $\varepsilon^* = \varepsilon - j\sigma/\omega$, where ε is the permittivity, σ is the conductivity and $j = \sqrt{-1}$.

Here one can also note that the above expression for the Clausius-Mossotti factor is not directly applicable to a particle at the drop's surface because it is in contact with both fluids. Clearly, in this case the Clausius-Mossotti factor should depend on the dielectric constants of the particle and the two fluids involved, and also on the position of the particle within the interface. The position of a particle within the drop's surface, i.e., the position of the contact line on the particle's surface which determines the fraction of the particle in the two fluids, depends on the contact angle and the buoyant weight of the particle.

The fact that the locations where the particles aggregate depend on the Clausius-Mossotti factor can be used to separate particles for which the sign of the Clausius-

Mossotti factor is different. More specifically, the approach allows us to aggregate one type of particles at the poles and the second type at the equator. Furthermore, since the Clausius-Mossotti factor depends on the frequency, it is possible to separate particles by selecting a suitable frequency.

Once particles concentrate near the poles or the equator, the electric field strength is increased above a critical level at which the drop breaks. The drop deforms because the electric stress distribution on its surface is non-uniform. The deformed shape, assuming that the deformation is small, was determined in [65-74] by the balance of the surface tension force, which tends to make the drop spherical, and the force due to the electric stress, which tends to elongate the drop [68]. The following expression for the drop deformation can be obtained

$$D = \frac{9}{8\pi} We .$$ (1.1)

where $We = \dfrac{a\varepsilon_0 \varepsilon_c E_0^2 \beta^2}{\gamma}$ is the electric Weber number, a is the drop radius, γ is the interfacial tension between the two fluids, ε_c is the dielectric constant of the fluid, $\varepsilon_0 = 8.8542\times10^{-12}$ F/m is the permittivity of free space and E_0 is the RMS value of the electric field. Equation 1.1 is also valid for a DC electric field where E_0 is simply the electric field intensity. This expression implies that the deformation increases as the square of the electric field strength and the square of the Clausius-Mossotti factor. Moreover, it varies inversely with the surface tension coefficient and is proportional to the electric Weber

number. The deformation is defined by the parameter $D = \dfrac{L - B}{L + B}$, where L and B are

respectively the major and minor axes of the drop, assuming that the shape of the drop is

approximately ellipsoidal. The deformation parameter D varies between 0 and 1; for a

spherical drop, D is zero and its value increases with increasing deviation from the

spherical shape.

The rest of the thesis is organized as follows. In the next chapter, the electric field

around a drop in a uniform electric field, and the forces that act on a particle located on

the drop's surface are described. The finite element method used for this study is also

discussed in detail. In the next chapter, experimental results which show that it is possible

to concentrate and remove particles trapped on the surface of a drop by applying an

electric field are described. The particle-particle interactions on the surface of a droplet

are discussed in chapter 4. Finally, the DNS results for the transport of yeast cells by

traveling wave dielectrophoresis in a micro device are discussed, and followed by

conclusions.

CHAPTER 2

REDISTRIBUTION OF PARTICLES ON DROP SURFACE

2.1 Governing Equations

Consider a drop of fluid with viscosity η_d and density ρ_d, placed in an ambient fluid with viscosity η_L and density ρ_L. The drop is assumed to be immiscible with the ambient fluid and its dielectric constant is different from that of the ambient fluid. The system is subjected to a non-uniform electric field which is generated by the electrodes mounted in the bottom surface of the micro device. Since the dielectric constants of the drop and the ambient fluid are different, a spatially varying electric stress acts on the interface which causes the drop to deform and translate.

Denote the domain containing the liquid and the drops by Ω, and the domain boundary by Γ. The governing equations for the two-fluid system are

$$\nabla \cdot \mathbf{u} = 0 \tag{2.1}$$

$$\rho \left[\frac{\partial \mathbf{u}}{\partial t} + \mathbf{u}.\nabla \mathbf{u} \right] = -\nabla p + \nabla.(2\eta \mathbf{D}) + \gamma \kappa \delta(\phi)\mathbf{n} + \nabla.\sigma_M , \tag{2.2}$$

$$\mathbf{u} = \mathbf{u}_L \text{ on } \Gamma \tag{2.3}$$

where $\mathbf{u}$ is the velocity, p is the pressure, η is the viscosity, ρ is the density, $\mathbf{D}$ is the symmetric part of the velocity gradient tensor, $\mathbf{n}$ is the outer normal, γ is the interfacial

17

tension, κ is the surface curvature, ϕ is the level set function defined to be the signed distance from the interface, δ is the delta function and σ_M is the Maxwell stress tensor. Only the case in which the density and viscosity of the drop are the same as those of the ambient liquid are considered, although these assumptions could be easily relaxed. The bulk imposed velocity of the liquid is assumed to be zero and solid walls are placed at the domain boundary. No-slip boundary conditions (i.e. zero liquid velocity) are imposed there.

In order to compute the electric stress acting on the drop surface, first the electric potential V has to be obtained by solving $\nabla \cdot (\varepsilon \nabla V) = 0$ subjected to the voltage boundary conditions [75, 76]. The dielectric constant ε is equal to ε_c for the ambient liquid and ε_d for the drop. The voltage V is prescribed on the electrodes and its normal derivative is taken to be zero on the remaining domain boundary. The electric stress is given by the Maxwell stress tensor

$$\sigma_M = \varepsilon \mathbf{EE} - \varepsilon(\mathbf{E} \bullet \mathbf{E})\mathbf{I}/2 \tag{2.4}$$

where $\mathbf{I}$ is the identity tensor and $\mathbf{E} = -\nabla V$ is the electric field [75, 76]. We will assume that both the liquid and the drop are perfect dielectrics. The results thus obtained, as noted earlier, are also applicable to the case of AC electric fields, provided that the RMS value of the electric field is used, that β is replaced by the real part of the complex frequency dependent Clausius-Mossotti factor and that the force is the time averaged force.

The governing Equations 2.1 - Equation 2.4 can be non-dimensionalized by assuming that the characteristic length, time, velocity, pressure, stress and electric field scales are a, a/U, U, ρU^2, $\eta U/a$, and βE_0 respectively, where U is the characteristic fluid velocity, $E_0 = V_0/L$ is the strength of the electric field, and L is the distance between the electrodes. It is easy to show that the non-dimensional equations after using the same symbols for the dimensionless variables are

$$\nabla \cdot \mathbf{u} = 0$$

$$\left[\frac{\partial \mathbf{u}}{\partial t} + \mathbf{u}.\nabla \mathbf{u}\right] = -\nabla p + \frac{1}{Re}\nabla.\sigma + \frac{1}{Re\ Ca}\ \kappa\ \delta(\phi)\mathbf{n} + \tag{2.5}$$

$$\frac{1}{Re\ Ma}\frac{a}{L}\nabla.\left(\varepsilon\ \mathbf{EE} - \varepsilon\ (\mathbf{E}\bullet\mathbf{E})\mathbf{I}/2\right)$$

Notice that the spatial gradient of the electric field is nondimensionalized using the characteristic length L. The dimensionless dielectric constant ε is obtained by dividing by ε_c, the dielectric constant of the continuous phase. The above equations contain the following dimensionless parameters: the Reynolds number $Re = \rho U a/\eta$, which is the ratio of inertial and viscous forces, the capillary number $Ca = U\eta_0/\gamma$, which is the ratio of viscous and surface tension forces, the Mason number $Ma = \dfrac{\eta U}{\varepsilon_0 \varepsilon_c a \beta^2 E_0^2}$ which is the ratio of the viscous and electric forces, and the length ratio a/L. Another useful parameter which gives the relative importance of the electric and interfacial tension forces is the electrical Weber number $We = \dfrac{\varepsilon_0 \varepsilon_c a \beta^2 E_0^2}{\gamma}$. Notice that We can also be

defined as the ratio of the capillary and Mason numbers. Also another point is that the definition of the Weber number in this work differs from the standard definition, $We = \dfrac{\varepsilon_0 \varepsilon_c a E_0^{\,2}}{\gamma}$, by a factor β^2 (which is dimensionless) and, as discussed below, this allows for a better estimate of the electric force acting on a drop.

It is worth noting that a drop moving in a micro device deforms also because of the velocity field it experiences. However, when the drop stops moving, as is the case after it is captured at an electrode's edge, the shape of the deformed drop is determined by the balance of the electric and surface tension forces.

2.1.1 Dielectrophoretic Force Induced Drop Deformation

When the drop size is sufficiently small compared to the length scale over which the non-uniform electric field varies, the point dipole approach can be used to estimate the dielectrophoretic force. The drop, however, also elongates along the direction of the local electric field. This latter complexity is not present for the case of rigid particles.

Even though the analysis based on the point dipole is not strictly valid in a typical device used for dielectrophoresis for which the drop size is of the same order as the device size [75], it is still useful for estimating the order of magnitudes of the forces. The critical electric field strength below which the drop deformation remains small can be estimated from the result obtained by Allen and Mason [59] for the case of a drop placed in a uniform electric field. The deformed shape in their analysis is determined by the balance of the surface tension force, which tends to make the drop spherical, and the force due to the electric stress, which tends to elongate the drop. The electric stress

distribution on the surface of the drop is deduced by assuming that the drop remains spherical. Allen and Mason obtained the following expression for the drop deformation

$$D = \frac{9 a \varepsilon_0 \varepsilon_c E_0^2 \beta^2}{8 \pi \gamma} = \frac{9}{8 \pi} We \qquad (2.6)$$

This expression implies that the deformation increases as the square of the electric field and the square of the Clausius-Mossotti factor. Moreover, it varies inversely with the surface tension coefficient and is proportional to the electric Weber number We. The deformation is defined as the parameter

$$D = \frac{L - B}{L + B},$$

where L and B are respectively the major and minor axes of the drop, assuming that the shape of the latter is approximately ellipsoidal. The deformation parameter D varies between 0 and 1; for a spherical drop, D is zero and its value increases with increasing deformation from a sphere.

To ensure that the drop deformation is small, one may assume that We is such that D is less than 0.1. From equation 2.6, this implies

$$We \leq \frac{0.8 \pi}{9} \approx 0.28$$

2.1.2 DEP Forces on Particles

Next, the point dipole approach is used to estimate the magnitude of the DEP force acting on a particle that causes it to migrate towards the poles or the equator. The drop is assumed to be spherical. The approach assumes that the electric field is not altered by the

presence of the particle, the particle size is small compared to the length scale over which the electric field varies and the electric field gradient at the center of the particles can be used to estimate the DEP force. The particle's center is assumed to be outside the drop at a small distance from the drop's surface, and thus the non uniform electric field distribution outside the drop is used to estimate the DEP force. Note that the electric field inside the drop is constant, and thus, since its gradient is zero, the DEP force on a particle inside the drop, within the point dipole approximation, is zero.

The r- and θ-components of the rms electric field outside a spherical drop of radius a can be shown to be given by,

$$E_r = E_0 \cos\theta\left(1 + \frac{2\beta a^3}{r^3}\right), \quad E_\theta = -E_0 \sin\theta\left(1 - \frac{\beta a^3}{r^3}\right) \tag{2.7}$$

where E_0 is the rms value of the applied ac electric field which is along the z-direction of the spherical coordinate system, r is the distance of the particle from the center of the drop, $\beta(\omega) = \mathrm{Re}\left(\dfrac{\varepsilon_d^* - \varepsilon_c^*}{\varepsilon_d^* + 2\varepsilon_c^*}\right)$ is the Clausius-Mossotti factor. Here ε_d^* and ε_c^* are the frequency dependent complex permittivity of the drop and the ambient fluid, and ω is the frequency of the ac field. Here the complex permittivity $\varepsilon^* = \varepsilon - j\sigma/\omega$, where ε is the permittivity, σ is the conductivity and $j = \sqrt{-1}$.

The DEP force acting on a particle of radius R outside the surface of the drop is given by $F_{DEP} = 4\pi\beta' R^3 \varepsilon_0 \varepsilon_c \nabla\left(E^2/2\right)$. Here ε_0 is the permittivity of free space,

$$\beta'(\omega) = \text{Re}\left(\frac{\varepsilon_p^* - \varepsilon_c^*}{\varepsilon_p^* + 2\varepsilon_c^*}\right), \quad \varepsilon_p^* \text{ is the frequency dependent complex permittivity of the particle,}$$

and E is the electric field magnitude:

$$E^2 = E_0^2 \left(1 + \cos^2\theta\left(\frac{4\beta a^3}{r^3} + \frac{4\beta^2 a^6}{r^6}\right) + \sin^2\theta\left(-\frac{2\beta a^3}{r^3} + \frac{\beta^2 a^6}{r^6}\right)\right)$$

The θ-component of the DEP force, which for an undeformed drop is in the tangential direction to the drop's surface, is then given by

$$F_{DEP,\theta} = -4\pi\beta' R^3 \varepsilon_0 \varepsilon_c \left(E_0^2 \cos\theta\sin\theta\left(\frac{6\beta a^3}{r^4} + \frac{3\beta^2 a^6}{r^7}\right)\right)$$

The above equation is also valid for a DC electric field in which case E_0 is denotes the electric field intensity. The force on a particle near the drop's surface can be obtained by substituting $r \approx a$, which gives

$$F_{DEP,\theta} = -12\pi R^3 \frac{1}{a}\varepsilon_0\varepsilon_c E_0^2 \, \beta' \beta(2 + \beta)\cos\theta \, \sin\theta \tag{2.8}$$

Equation 2.8 gives the DEP force in the θ-direction on a small particle near, but outside, the drop's surface. The force is zero both at the poles ($\theta = 0, \pi$) and at the equator ($\theta = \pi/2$), and maximum at $\theta = \pi/4$. Also notice that the magnitude of force on a particle of given radius increases with decreasing drop size. This implies that it is easier to concentrate

particles (of a given radius) on a smaller sized drop which is in agreement with our experimental observations.

From Equation 2.8, the sign of the tangential DEP force acting on a particle, depends on the sign of $\beta'\beta(2+\beta)$. Also, since $|\beta| \le 1$, $(2+\beta) > 0$. Thus, the sign of $\beta'\beta(2+\beta)$ is the same as that of $\beta'\beta$. The magnitude of the factor $(2+\beta)$ for $\beta < 0$, however, is smaller than for $\beta > 0$. Thus, the DEP force is smaller for the former case. Furthermore, although the DEP force is zero at both the poles and the equator, it is easy to see that the sign of $\beta'\beta$ determines the location(s) at which particles eventually aggregate. When $\beta'\beta > 0$ particles aggregate at the poles because they are in a state of stable equilibrium at the poles and in a state of unstable equilibrium at the equator. On the other hand, when $\beta'\beta < 0$, they aggregate at the equator where their equilibrium is stable.

From this a conclusion can be drawn that particles with a positive Clausius-Mossotti factor ($\beta' > 0$) aggregate at the poles if the permittivity of the drop is greater than that of the ambient fluid, and at the equator if the permittivity of the drop is smaller than that of the ambient fluid. The opposite statement holds for particles with a negative Clausius-Mossotti factor ($\beta' < 0$). It is important to note that if the fluids and particle conductivities are not negligible, the sign of β' and β, and thus the location where particles collect, may depend on the frequency of the ac field. Furthermore, the electric field induced fluid flow around the drop can also cause the motion of particles trapped on the surface of a drop. This, however, was not the case for the cases investigated in the present study. The use of an ac electric field reduced the role of conductivity.

2.1.3 Finite Element Method

The computational scheme used here is a generalization of the DLM finite-element scheme described in [77, 78]. In this scheme, the fluid flow equations are solved on the combined fluid-solid domain, and the motion inside the particle boundaries is forced to be rigid-body motion using a distributed Lagrange multiplier. The fluid and particle equations of motion are combined into a single combined weak equation of motion, eliminating the hydrodynamic forces and torques, which helps ensure the stability of the time integration. For the sake of simplicity, in this section, it is assumed that there is only one particle. The extension to the multi-particle case is straightforward.

The solution and variation are required to satisfy the strong form of the constraint of rigid body motion throughout $P(t)$. In the distributed Lagrange multiplier method, this constraint is removed from the velocity space and enforced weakly as a side constraint using a distributed Lagrange multiplier term. It was shown in [77, 78] that the following weak formulation of the problem holds in the extended domain:

For a.e. $t > 0$, find $\mathbf{u} \in \overline{W}_{u\Gamma}$, $p \in L_0^2(\Omega)$, $\lambda \in \Lambda(t)$, $\mathbf{U} \in \mathbf{R}^3$ and $\omega \in \mathbf{R}^3$, satisfying

$$\int_\Omega \rho_L \left(\frac{d\mathbf{u}}{dt} - \mathbf{g} \right) \cdot \mathbf{v} d\mathbf{x} - \int_\Omega p \nabla.\mathbf{v} \, d\mathbf{x} + \int_\Omega 2\eta \mathbf{D}[\mathbf{u}] : \mathbf{D}[\mathbf{v}] d\mathbf{x}$$

$$+ \left(1 - \frac{\rho_L}{\rho_d} \right) \left(M \left(\frac{d\mathbf{U}}{dt} - \mathbf{g} \right) \cdot \mathbf{V} + I \frac{d\omega}{dt} \xi \right) - \mathbf{F}'.\mathbf{V} = \left\langle \lambda, \mathbf{v} - (\mathbf{V} + \xi \times \mathbf{r}) \right\rangle_{P(t)}$$

$$\text{for all } \mathbf{v} \in \overline{W}_0, \mathbf{V} \in \mathbf{R}^3, \text{ and } \xi \in \mathbf{R}^3, \qquad (2.9)$$

$$\int_\Omega q \nabla.u \, dx = 0 \qquad \text{for all } q \in L^2(\Omega), \qquad (2.10)$$

$$\langle \mu, \mathbf{u} - (\mathbf{U} + \omega \times \mathbf{r}) \rangle_{P(t)} = 0 \qquad \text{for all } \mu \in \Lambda(t), \tag{2.11}$$

$$\mathbf{u}\,|_{t=0} = \mathbf{u}_0 \qquad\qquad \text{in } \Omega, \tag{2.12}$$

as well as the kinematic equations and the initial conditions for the particle linear and angular velocities. Here $\mathbf{F}'$ is the additional body force applied to the particles to limit the extent of overlap (Glowinski, et al. 1999) and λ is the distributed Lagrange multiplier

$$\overline{W}_{u\Gamma} = \{\mathbf{v} \in H^1(\Omega)^3 \mid \mathbf{v} = \mathbf{u}_\Gamma(t) \quad \text{on} \quad \Gamma\},$$

$$\overline{W}_0 = H_0^1(\Omega)^3,$$

$$L_0^2(\Omega) = \{q \in L^2(\Omega) \mid \int_\Omega q\,d\mathbf{x} = 0\}, \tag{2.13}$$

and $\Lambda(t)$ is $L^2(P(t))^3$, with $\langle .,. \rangle_{P(t)}$ denoting the L^2 inner product over the particle, where Γ^- is the upstream part of Γ. In our simulations, since the velocity and μ are in L^2, we will use the following inner product

$$\langle \mu, \mathbf{v} \rangle_{P(t)} = \int_{P(t)} (\mu.\mathbf{v})\,d\mathbf{x}. \tag{2.14}$$

In order to solve the above problem numerically, we will discretize the domain using a regular tetrahedral mesh T_h for the velocity, where h is the mesh size, and a regular tetrahedral mesh T_{2h} for the pressure. The following finite dimensional spaces are defined for approximating $\overline{W}_{u\Gamma}$, $\overline{W}_0$, $L^2(\Omega)$ and $L_0^2(\Omega)$:

$$W_{u\Gamma,h} = \{v_h \in C^0(\overline{\Omega})^3 \mid v_h \mid_T \in P_1 \times P_1 \times P_1 \text{ for all } T \in T_h, v_h = u_{\Gamma,h} \text{ on } \Gamma\},$$

$$W_{0,h} = \{v_h \in C^0(\overline{\Omega})^3 \mid v_h \mid_T \in P_1 \times P_1 \times P_1 \text{ for all } T \in T_h, v_h = 0 \text{ on } \Gamma\} \quad , \quad (2.15)$$

$$L_h^2 = \{q_h \in C^0(\overline{\Omega}) \mid q_h \mid_T \in P_1 \text{ for all } T \in T_{2h}\},$$

$$L_{0,h}^2 = \{q_h \in L_h^2 \mid \int_\Omega q_h \, dx = 0\}, \quad (2.16)$$

The particle inner product terms in Equation 2.9 and Equation 2.11 are obtained using the discrete L^2 inner product defined in Glowinski, et al. (1999). Specifically, we choose M points, $x_1, \ldots, x_M$ that uniformly cover $\overline{P}(t)$, and define

$$\Lambda_h(t) = \left\{ \mu_h \mid \mu = \sum_{i=1}^M \mu_{h,i} \, \delta(x - x_i), \quad \mu_{h,1}, \ldots, \mu_{h,M} \in R^3 \right\} \quad .$$

Using these finite dimensional spaces, it is straightforward to discretize Equations 2.9 – Equation 2.12.

2.1.4 Time Discretization Using the Marchuk-Yanenko Operator Splitting Scheme

The initial value problem (Equations 2.9 - Equation 2.12) is solved by using the Marchuk-Yanenko operator-splitting scheme, which allows us to decouple its three primary difficulties:

1. The incompressibility condition, and the related unknown pressure p_h,

2. The nonlinear advection term,

3. The constraint of rigid-body motion in $P_h(t)$, and the related distributed Lagrange multiplier λ_h.

The Marchuk-Yanenko operator-splitting scheme can be applied to an initial value problem of the form

$$\frac{d\phi}{dt} + A_1(\phi) + A_2(\phi) + A_3(\phi) = f$$

where the operators A_1, A_2 and A_3 can be multi-valued. Let Δt be the time step. We use the following version of the Marchuk-Yanenko operator splitting scheme to simulate the motion of particles in an ER fluid:

Set $u^0 = u_{0,h}$, $U^0 = U_0$, $X^0 = X_0$ and $\omega^0 = \omega_0$, and calculate E by solving $\nabla^2 \varphi = 0$, subjected to the electric potential boundary conditions, and then calculating $E = \nabla \varphi$.

For n = 0, 1, 2,... assuming u^n, U^n, X^n, and ω^n are known, we find the values for the $(n+1)^{th}$ time step using the following steps:

STEP 1:

Find $u^{n+1/4} \in W^{n+1}_{u\Gamma,h}$ and $p^{n+1/4} \in L^2_{0,h}$ by solving

$$\int_\Omega \rho_L \frac{u^{n+1/4} - u^n}{\Delta t} \cdot v \, dx - \int_\Omega p^{n+1/4} \nabla \cdot v \, dx + \alpha \int_\Omega 2\eta_s D[u^{n+1/4}] : D[v]dx = 0$$

$$\text{for all } \mathbf{v} \in W_{0,h},$$

$$\int_{\Omega} q \nabla.\mathbf{u}^{n+1/4}\, d\mathbf{x} \quad = \quad 0 \qquad\qquad \text{for all } q \in L_h^2, \tag{2.17}$$

STEP 2:

Find $\mathbf{u}^{n+2/4} \in W_{u\Gamma,h}^{n+1}$ by solving

$$\int_{\Omega} \rho_L \frac{\mathbf{u}^{n+2/4} - \mathbf{u}^{n+1/4}}{\Delta t}.\mathbf{v}d\mathbf{x} + \int_{\Omega} \rho_L (\mathbf{u}^{n+2/4}.\nabla \mathbf{u}^{n+2/4}).\mathbf{v}\,d\mathbf{x} + \beta \int_{\Omega} 2\eta_s \mathbf{D}[\mathbf{u}^{n+2/4}] : \mathbf{D}[\mathbf{v}]d\mathbf{x} \;= 0$$

$$\text{for all } \mathbf{v} \in W_{0,h} \tag{2.18}$$

STEP 3:

Compute $\mathbf{U}^{n+2/4}$ and $\mathbf{X}^{n+2/4}$ using the prediction procedure

Set $\mathbf{U}^{n,0} = \mathbf{U}^n$, $\mathbf{X}^{n,0} = \mathbf{X}^n$.

Do k = 1,K

Calculate $\mathbf{F}_E\left(\mathbf{X}^{n,k-1}\right)$

$$\mathbf{U}^{*n,k} = \mathbf{U}^{n,k-1} + \left(\mathbf{g} + \left(1 - \frac{\rho_L}{\rho_d}\right)^{-1} \mathbf{M}^{-1}\left[\mathbf{F}'(\mathbf{X}^{n,k-1}) + \mathbf{F}_E\left(\mathbf{X}^{n,k-1}\right)\right]\right)\frac{\Delta t}{K}$$

$$\mathbf{X}^{*n,k} = \mathbf{X}^{n,k-1} + \left(\frac{\mathbf{U}^{n,k-1} + \mathbf{U}^{*n,k}}{2}\right)\frac{\Delta t}{K}$$

$$\mathbf{U}^{n,k} = \mathbf{U}^{n,k-1} +$$

$$\left(\mathbf{g} + \left(1 - \frac{\rho_L}{\rho_d}\right)^{-1} M^{-1} \frac{\mathbf{F}'(X^{n,k-1}) + \mathbf{F}'(X^{*n,k-1}) + \mathbf{F}_E(X^{n,k-1}) + \mathbf{F}_E(X^{*n,k-1})}{2} \right) \frac{\Delta t}{K}$$

$$\mathbf{X}^{n,k} = \mathbf{X}^{n,k-1} + \left(\frac{\mathbf{U}^{n,k-1} + \mathbf{U}^{n,k}}{2} \right) \frac{\Delta t}{K}$$

end do

Then set $\mathbf{U}^{n+2/4} = \mathbf{U}^{n,K}$, $\mathbf{X}^{n+2/4} = \mathbf{X}^{n,K}$. (2.19)

The next step consists of finding $\mathbf{u}^{n+1} \in W_{u\Gamma,h}^{n+1}$, $\lambda^{n+1} \in \Lambda_h((n+2/4)\Delta t)$, $\mathbf{U}^{n+1} \in \mathbf{R}^3$, and $\omega^{n+1} \in \mathbf{R}^3$, satisfying

$$\int_\Omega \rho_L \frac{\mathbf{u}^{n+1} - \mathbf{u}^{n+2/4}}{\Delta t} \cdot \mathbf{v}\, d\mathbf{x} + \left(1 - \frac{\rho_L}{\rho_d}\right)\left(M \frac{\mathbf{U}^{n+1} - \mathbf{U}^{n+2/4}}{\Delta t} \cdot \mathbf{V} + I \frac{\omega^{n+1} - \omega^{n+2/4}}{\Delta t} \xi \right) +$$

$$= \left\langle \lambda^{n+1}, \mathbf{v} - (\mathbf{V} + \xi \times \mathbf{r}^{n+2/4}) \right\rangle_{P((n+2/4)\Delta t)}$$

for all $\mathbf{v} \in W_{0,h}$, $\mathbf{V} \in \mathbf{R}^2$, and $\xi \in \mathbf{R}$ (2.20)

where the center of the particle $P((n+2/4)\Delta t)$ is at the location $X^{n+2/4}$.

Then set $\mathbf{X}^{n+1,0} = \mathbf{X}^n$.

For k = 1, K, follow the do-loop

$$\mathbf{X}^{*n+1,k} = \mathbf{X}^{n+1,k-1} + \left(\frac{\mathbf{U}^n + \mathbf{U}^{n+1}}{2} \right) \frac{\Delta t}{K}$$

$$X^{n,k} = X^{*n,k-1} + \left(1 - \frac{\rho_L}{\rho_d}\right)^{-1} M^{-1} \left(\frac{F'(X^{n+1,k-1}) + F'(X^{*n+1,k})}{2}\right) \frac{(\Delta t)^2}{2K}$$

end do

Then set $X^{n+1} = X^{n+1,K}$. 　　　　　　　　　　　(2.21)

Then set $p^{n+1} = p^{n+1/4}$, and go back to the first step.

Remarks:

1. The problems arising in the first and second steps are solved using the conjugate gradient algorithm described in [77].

2. α_1 and α_2 are assumed to be the same and its value is 0.5.

3. The third step is used to obtain the distributed Lagrange multiplier that enforces rigid body motion inside the particles. This problem is solved by using the conjugate gradient method described in [77, 78]. In this step, we account for the electrostatic forces that arise due to the dielectrophoretic effect and the particle-particle interactions.

2.2 Electric Field Distribution for a Dielectric Drop Placed in a Dielectric Liquid

Now a drop suspended in a surrounding fluid with small solid particles floating at its surface and subjected to an externally applied uniform electric field is considered. The latter in the numerical simulations is generated by placing the drop and its surrounding fluid in a box with electrodes coinciding with the upper and lower walls. The analysis performed below assumes that: (i) both the drop and the ambient liquids are perfect dielectrics, (ii) the drop and the ambient fluids are immiscible and (iii) the drop's dielectric constant is different from that of the ambient fluid. As discussed below, it is

interesting to note that although the applied electric field away from the drop is uniform, the presence of the drop makes the electric field in the neighborhood of the drop non-uniform and, as a result, the particles on its surface are subjected to a non-uniform electric field and thus to the phenomenon of dielectrophoresis. In this subsection, this non-uniformity, and the resulting dielectrophoretic force which acts on particles located either on its surface or near the drop is characterized.
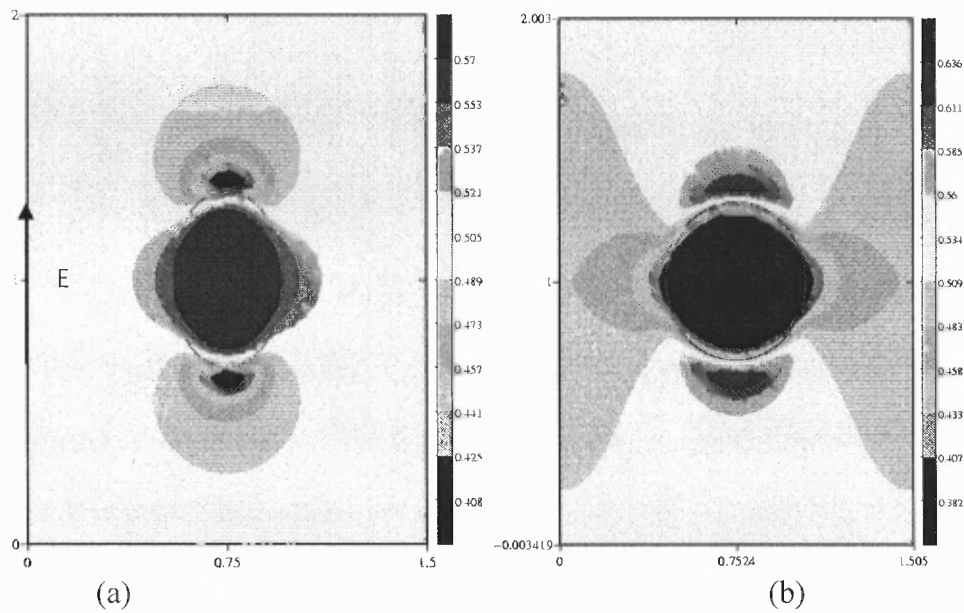
Figure 2.1 The steady deformed shape and the modified electric field around a dielectric drop suspended in a dielectric liquid and subjected to a uniform electric field. (a) The dielectric constant of the drop is 0.5 and of the ambient liquid is one, and We =1.3. Notice that the electric field is no longer uniform, and that it is locally maximum at the equator and locally minimum at the poles. (b) The dielectric constant of the drop is 2.0 and of the ambient liquid is one, and We =1.31. The electric field is locally maximum at the poles and locally minimum at the equator.

For the simulations, the dielectric constant of the ambient fluid is held fixed and assumed to be 1.0. The interfacial tension between the ambient fluid and the drop, and the voltage difference between the electrodes are prescribed. The electric field distribution

and the deformed drop shapes are obtained numerically. The domain dimensions are assumed to be 1.5, 1.5 and 2.0 cm in the x, y and z directions and the undeformed drop radius is assumed to be 0.25 cm. Simulations are started by placing a spherical drop at the center of the domain (see Figure 2.1). The normal derivative of the electric potential is assumed to be zero on the domain side walls, and therefore, since the electrodes completely cover the top and bottom walls, in the absence of a drop, the electric field in the domain is uniform. Furthermore, the drop is assumed to be sufficiently small so that the effect of its presence on the electric field distribution is negligible. The dependence of the dielectrophoretic force, and the resulting drop deformation, are described below for two values of the drop dielectric constant.

Figure 2.1 shows the computed steady state shape of the drop and the electric field distribution around it. The drop considered in Figure 2.1a has a dielectric constant of 0.5 and the dielectric constant of the ambient fluid, as noted above, is one. The modified electric field distribution is such that the magnitude of the electric field near the equator is smaller and near the poles it is larger, compared to the magnitude of the imposed uniform electric field. It is also interesting to notice that the strength of the electric field inside the drop is greater than the applied field strength. This modification makes the electric field strength, and thus also the electric stress distribution, on the drop surface non-uniform.

The modified electric field distribution for the case where the dielectric constant of the drop is greater than that of the ambient fluid is shown in figure 2.1b. Note that the strength of the electric field inside the drop is weaker than that of the applied field, and the electric field strength at the poles is greater than near the equator.

It is worth noting that the electric field strength inside the drop in both cases is constant. This is important because, as discussed below, this implies that a particle placed inside the drop is not expected to experience a dielectrophoretic force, at least within the point-dipole approximation.

(a)   (b)
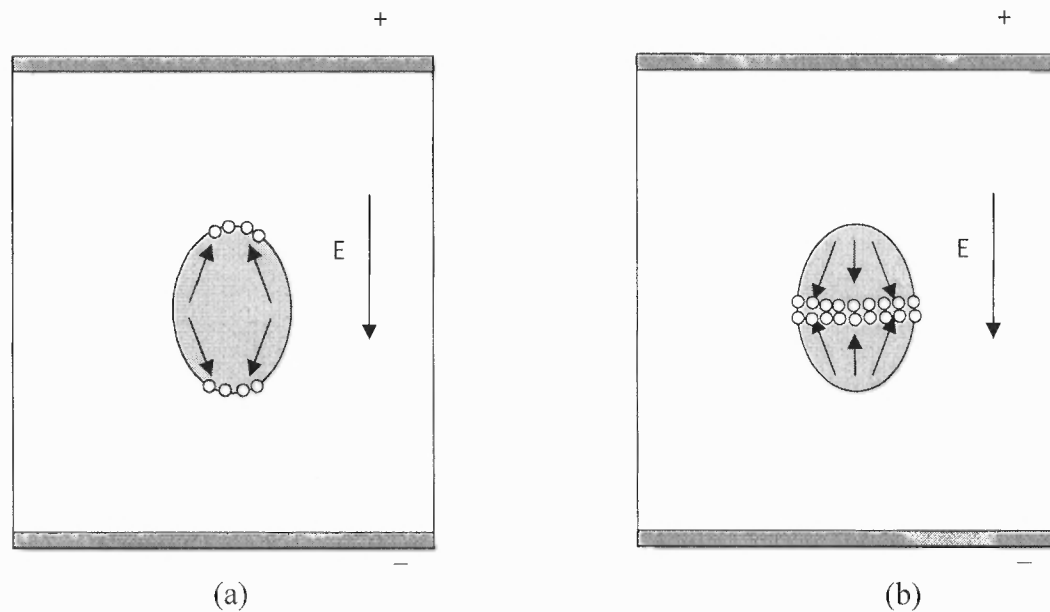
Figure 2.2 The dielectrophoretic force induced motion of small particles on the surface of a drop subjected to a uniform electric field generated by the electrodes placed at the top and bottom of the device. The figure shows the direction of motion for particles for which the effective Clausius-Mossotti factor is positive (The direction is the opposite for particles with a negative effective Clausius-Mossotti factor). The dielectric constant of the ambient fluid is assumed to be one. The dielectric constant of the drop in (a) is greater than one and in (b) it is less than one.

Figure 2.2 shows the direction of the DEP force that acts on a particle for which the effective Clausius-Mossotti factor is positive, and the locations at which the particles are eventually collected. More specifically, if the dielectric constant of the drop is greater than that of the ambient fluid, particles on the drop surface collect at the two poles. On the other hand, if the dielectric constant of the drop is smaller than that of the ambient liquid, particles collect in a ring shaped region near the equator (However, when the

particle's buoyant weight is not negligible and electrodes are mounted on the side walls, they remain near either the top of the drop or sediment to the bottom of the drop while remaining at the equator.) Furthermore, the opposite is true if the effective Clausius-Mossotti factor is negative. That is, particles get collected at the equator if the dielectric constant of the drop is greater than that of the ambient fluid, and at the poles if the dielectric constant of the drop is smaller than that of the ambient fluid. This phenomenon can thus be used to separate two types of particles but where they aggregate (at the poles or at the equator) depends on the dielectric constants of the drop, the ambient fluid and the particles.

2.3 Experiments

2.3.1 Experimental Setup and Materials

This section will begin by describing the experimental procedure employed to investigate the influence of an externally applied electric field on the distribution of particles on the surface of a drop, and the role of various parameters in the process. Experiments were conducted in several devices with rectangular cross-sections in which the electrodes were mounted on the side walls (Figure 2.3). The distance between the electrodes was varied between 2.6 mm and 6.5 mm. The depth of the devices was 6.5 mm and the length 41 mm. The depth of the ambient liquid was approximately 5.5 mm. A variable frequency ac signal generator (BK Precision Model 4010A) was used along with a high voltage amplifier (Trek Model 5/80) to apply voltage to the electrodes. The frequency used in all our experiments was 100 Hz or 1 kHz. The use of an ac field ensured that the role of conductivity and the drop's electric charge, if any, was negligible. The

motion/deformation was recorded using a digital color camera connected to a Nikon Metallurgical MEC600 microscope.

Drops of various sizes were formed at a small distance from the bottom surface by injecting a given amount of liquid into the ambient liquid with a syringe. The density and viscosity of the drops were not equal to the corresponding values for the ambient liquids. In fact, the ambient and drop liquids were selected so that the drop density was slightly larger, which ensured that the drop did not levitate. For all cases reported in this work, drops were allowed to settle to the bottom of the device. The bottom surface was chosen so that its affinity for the ambient fluid was greater than its affinity for the drop.
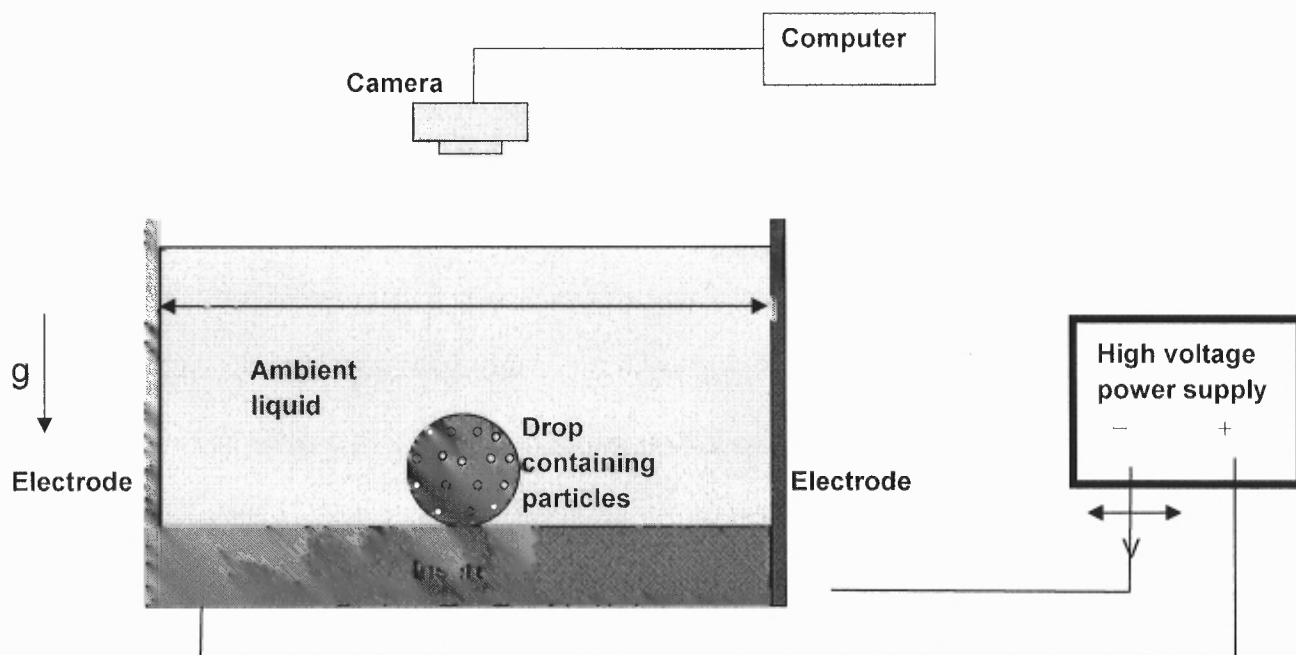
Figure 2.3 Schematic of the setup used in our experiments. The electrodes were mounted on the left and right sidewalls. The electric field was in the horizontal direction, and thus the drops also stretched in that direction. The drop deformation and the motion of particles were recorded using the camera mounted above. An insert was used to ensure that the vertical position of the drop was near the middle of the electrodes. The material used for the insert was such that its dielectric constant was close to that of the ambient liquid.

The liquids used in this study were Millipore water, silicon oil, decane, castor oil, and corn oil with the following properties. The dielectric constant of water is 80.0 and its conductivity is 5.5 x 10^6 pSm^{-1}; the values for silicon oil are 2.68 and 2.67 pSm^{-1}; those for decane are 2.0 and 2.65 x10^4 pSm^{-1}; those for castor oil are 6.0 and 32.0 pSm^{-1} and for corn oil they are 2.87 and 32.0 pSm^{-1}. The densities of water, silicon oil, decane, castor oil and corn oil are 1.00 g/cm^3, 0.963 g/cm^3, 0.730 g/cm^3, 0.96 g/cm^3 and 0.92 g/cm^3, respectively.

In the experiments, a drop with particles distributed on its surface was formed using the following procedure. The first step was to form a dilute suspension by mixing particles in the liquid that was to be used to form the drop. The particle concentration was kept small to ensure that the particle concentration on the surface of the formed drop was small. A fixed volume of this suspension was then injected into the ambient liquid by using a syringe. Since the drop density was slightly larger than that of the ambient liquid, the drop, after being formed, sedimented to the bottom surface of the device. The particles suspended inside the drop sedimented along with the drop. In some experiments, a drop containing two types of particles was formed by merging two or more smaller drops, each containing particles of different types. This ensured that there were enough particles of each type and also ensured that they were not completely mixed. Although the experimental setup did not allow us to photograph the side view of the drops, assumption is made that the drops were deformed from the spherical shape due to their buoyant weights.

Several minutes are then observed until all particles suspended inside the drop reached either the bottom or the top surface of the drop, depending on the density of the

particles compared to that of the drop. Once a particle was trapped at the two-fluid interface, it remained there due to the interfacial tension. The position of a particle within the interface is determined by the three-phase contact angle on its surface and its buoyant weight [79].

(a)   (b)   (c)
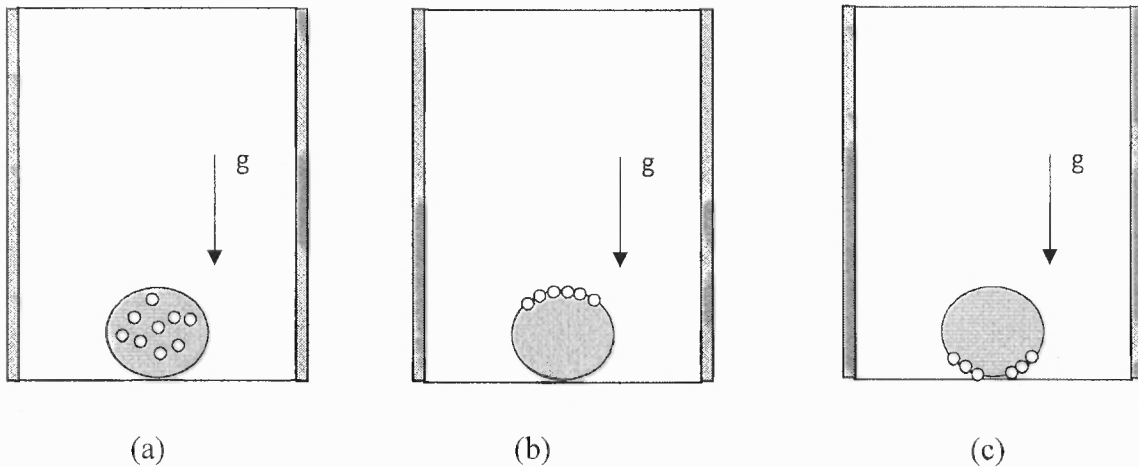
Figure 2.4 Schematic diagram showing the formation of drops containing small particles on their surfaces. (a) The initial state of an injected drop. Particles are present within the drop and not on its surface. (b) The suspended particles are less dense than the drop and so they get accumulated at the top surface of the drop. (c) The suspended particles are denser than the drop and so they get accumulated at the bottom surface of the drop.

Also, relatively large sized particles were used in these experiments to make sure that the motion and the supporting data can be visually monitored after the electric field was applied and thus understand the mechanisms by which particles migrated along the surface of the drop, influenced the drop deformation and were subsequently removed from the drop. However, since the diameter of the particles used was between 4 and 70 microns, their buoyant weight was not negligible and thus, as noted above, particles either settled or rose under the action of gravity as shown in Figure 2.4. Once they were trapped at the interface between the drop and the ambient liquid, they remained trapped

even when the electric field was switched on. When an electric field was applied they moved along the surface of the drop under the action of the dielectrophoretic force which arises because of the non-uniformity of the electric field on the drop's surface. One can also expect smaller, submicron sized particles, for which the buoyant weight is negligible, to behave similarly.

2.3.2 Drop Dielectric Constant Smaller than that of the Ambient Liquid

First the case of particles with a density smaller than that of the ambient liquid is considered, and then the case of particles with a density larger than that of the ambient liquid.

Figure 2.5 shows the top view of the distribution of hollow glass particles, of diameter 18 μm, on the surface of a silicone oil drop suspended in corn oil at four different times after the electric field was switched on. The electrodes are at the top and bottom surfaces of the device. The electric field is perpendicular to the paper, and the voltage applied to the device was 3000 volts, which was held fixed. The drop stretches in the direction of the electric field, but since the viewing direction is parallel to the direction of stretch, this cannot be seen. The density of hollow glass particles being 0.6 g/cm^3, the particles are trapped at the top surface of the drop. In addition, due to the fact that the dielectric constant of the particles is 6.5, which corresponds to a positive Clausius-Mossotti factor, they move to the region where the electric field strength is maximal.
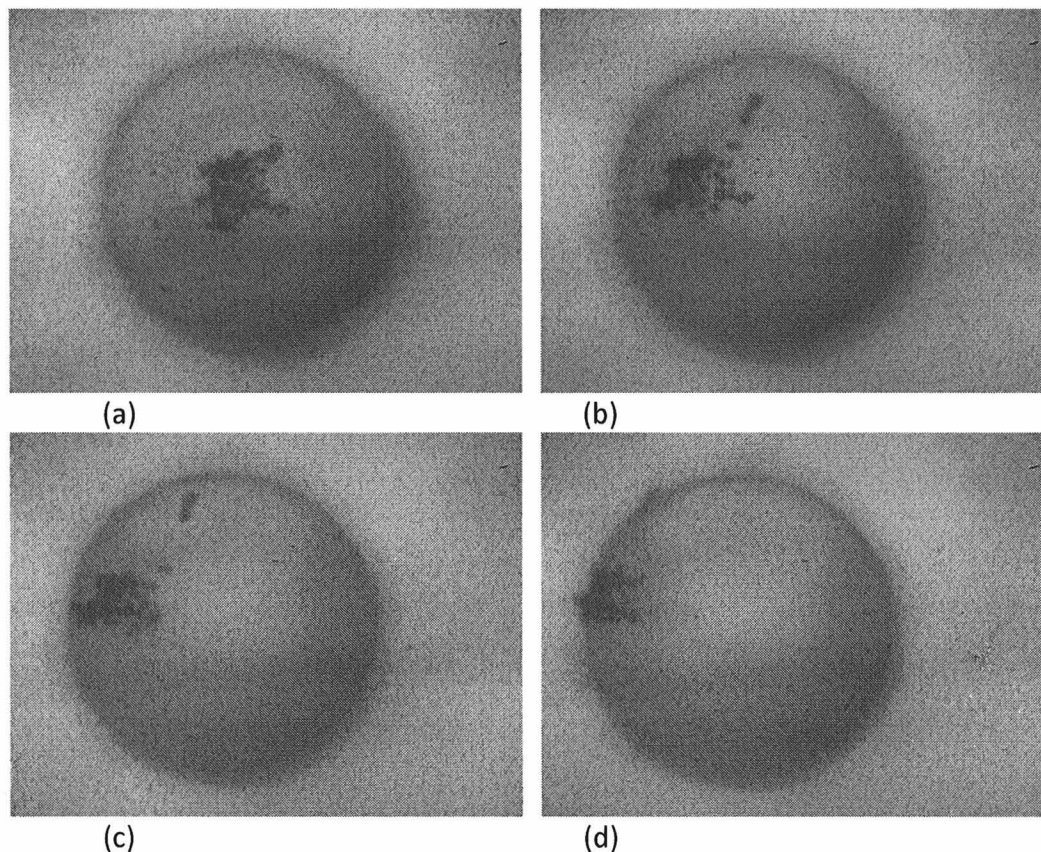
Figure 2.5 Top view of the motion of hollow glass spheres on the surface of a silicone oil drop suspended in corn oil and subjected to a uniform electric field. Electrodes are mounted on the bottom and top surfaces of the device. The electric field is normal to the plane of the paper. The drop diameter is approximately 684 μm. The distance between the electrodes is 6.5 mm and the applied voltage is 3000 volts. The density of hollow glass spheres is 0.6 g/cm^3 and their diameter is approximately 18 μm. The effective Clausius-Mossotti factor is positive and since the electric field is maximal at the equator, after the electric field is switched on, the particles move towards the equator. (a) t=0, (b) t=20 s. (c) t=40 s. (d) t=60 s.

From Figure 2.1 it can be known that when the dielectric constant of the drop is smaller than of the ambient liquid, the electric field is maximal at the equator. In Figure 2.5 the equator is the circular region enclosing the drop. The figure shows that particles move outwards as time increases and eventually most of them get trapped at the equator. Their motion, therefore, is against the buoyancy force which acts in the upward direction as the particles density is smaller than the liquid density. Also notice the presence of

particle chains, which are due to electrostatic particle-particle interactions among particles. Furthermore, most of the particles move together in a cluster which also is a result of the attractive particle-particle interaction force between them.
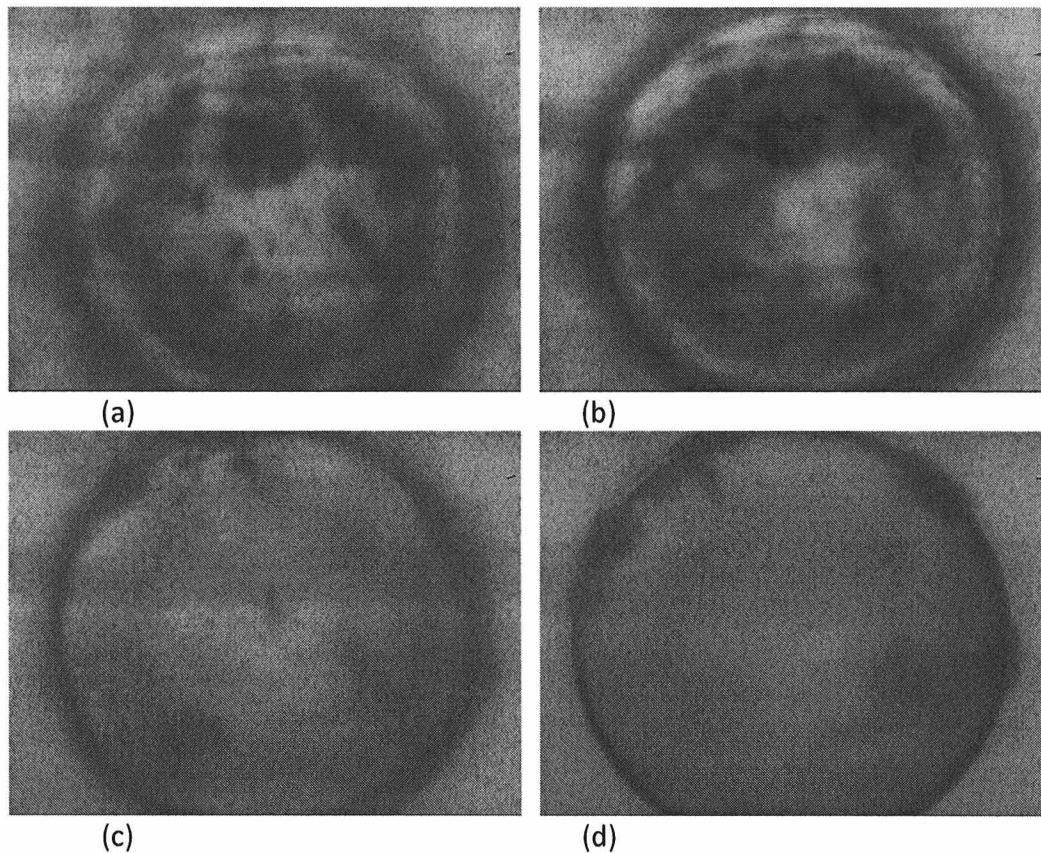
Figure 2.6 Top view of the motion of sodalime glass spheres on the surface of a silicone oil drop suspended in corn oil and subjected to a uniform electric field. Electrodes are mounted on the bottom and top surfaces of the device. The electric field is normal to the plane of the paper. The drop diameter is approximately 940 μm. The distance between the electrodes is 6.5 mm and the applied voltage is 4000 volts. The density of sodalime glass spheres is 2.5 g/cm^3 and their diameter is between 4-10 μm. The effective Clausius-Mossotti factor is positive and since the electric field is maximal at the equator, after the electric field is switched on, the particles move towards the equator. (a) t=0, (b) t=10 s, (c) t=20 s, (d) t=60 s.

Figure 2.6 shows the distribution of sodalime glass particles on the surface of a silicone oil drop suspended in corn oil. The diameter of the particles is between 4-10 μm,

thus smaller than the particles used above, and their density is 2.5 g/cm³, which makes the particles initially migrate toward, and get trapped at, the bottom surface of the drop. The effective Clausius-Mossotti factor is positive since the dielectric constant of particles is 6.5, which is larger than that of the ambient liquid and also of the drop. All particles trapped at the interface move towards the drop's equator where the electric field strength is maximal.

In this case particles move upwards against the bouyant weight which acts downwards as the density of particles is greater than the liquid density. The figure shows that the particles move outwards as time increases and eventually most of them are trapped at the equator. Notice that the middle portion of the drop in Figure 2.6d is virtually free of particles as all have moved to the drop's equator. Again, under the influence of particle-particle interactions, particles are not uniformly distributed along the equator, but rather form particle clusters there.

2.3.3 Drop Dielectric Constant Larger than of the Ambient Liquid

Next the distribution of hollow extendospheres on the surface of a water drop suspended in decane is described. The electrodes in this case were mounted on the left and right side walls of the device. The electric field is horizontal, and the voltage applied to the device was 4000 volts.

The drop stretches in the direction of the applied electric field. The density of hollow extendospheres is 0.75 g/cm³, and thus, as was the case in Figure 2.7, initially the particles are trapped at the top surface of the drop. The dielectric constant of the drop is greater than that of the ambient liquid, and thus the electric field is maximal at the poles. In Figure 2.7 the electric field is horizontal and the poles are the far left and far right most

points on the drop surface. The dielectric constant of particles is 4.5, which is greater than that of decane, but smaller than of the drop.
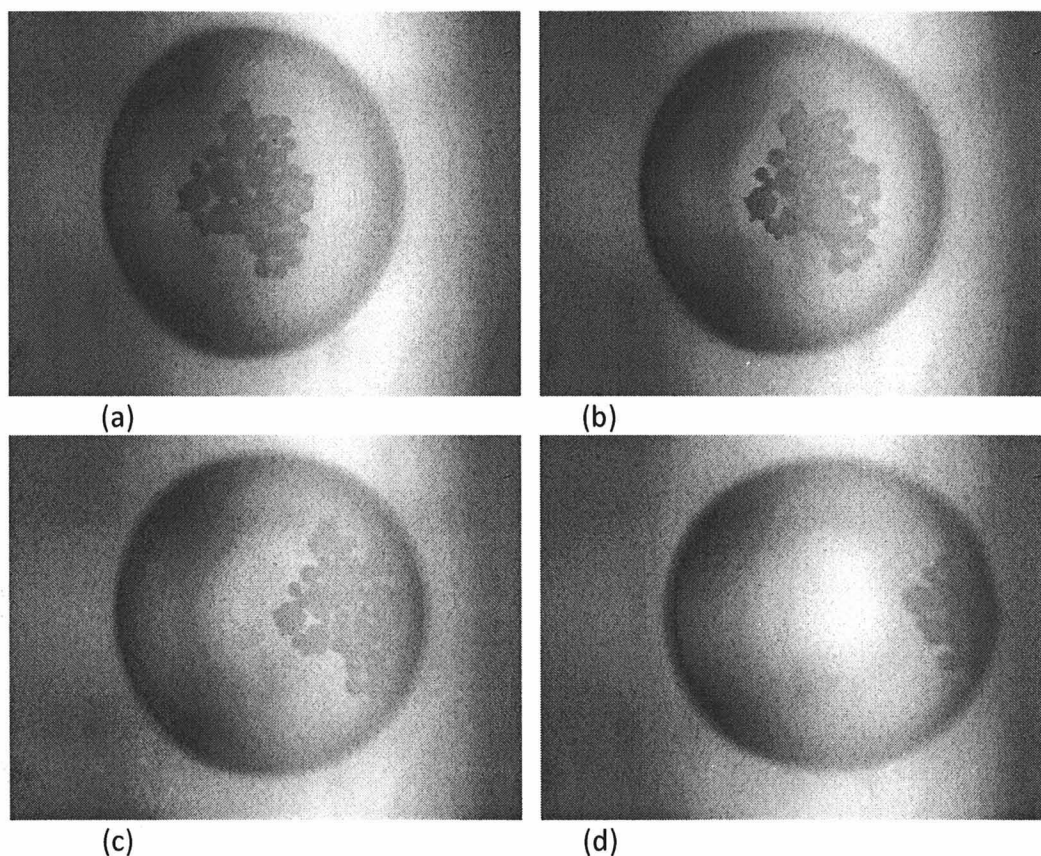
Figure 2.7 Top view of the motion of extendospheres on the surface of a water drop suspended in decane and subjected to a uniform electric field. Electrodes are mounted on the left and right side walls of the device. The electric field is horizontal within the plane of the photographs. The drop diameter is approximately 840 μm. The distance between the electrodes is 6.5 mm. The density of the extendospheres is 0.75 g/cm^3 and their diameter is approximately 55 μm. The effective Clausius-Mossotti factor is positive and since the electric field maximum is located at the poles, after the electric field is switched on, the particles slowly move towards the pole on the right side. Notice that particles move together due to the electrostatic particle-particle interactions. The applied voltage to the electrodes is (a) 0 volts, (b) 1500 volts, (c) 2500 volts, (d) 4000 volts.

The effective Clausius-Mossotti factor of particles in experiments is positive which is indicated by the fact that after the electric field is switched on particles trapped

on the drop surface move to the regions where the electric field strength is maximal. They move closer to the poles with increasing electric field strength. There motion towards the pole is countered by the buoyancy force which tends to bring them to the top surface of the drop.

The figure shows that all the trapped particles move to the right side and are captured near the right pole. Again, particles move together because of the electrostatic particle-particle interactions. It is noteworthy that the effective Clausius-Mossotti factor of particles is positive even though their dielectric constant is much smaller than of the water drop. This indicates that the dielectric constant of the ambient liquid relative to that of the particles is more important in determining the sign of effective Clausius-Mossotti factor.

CHAPTER 3

REMOVAL OF PARTICLES FROM DROP SURFACE

The fact that the location where a particle moves to depends on the particle's Clausius-Mossotti factor (β') can be used, as we discuss earlier in chapter 2, to separate particles trapped on the surface of a drop for which the sign of β' is different, and this, for instance, can be used to form a composite (Janus) drop for which the areas surrounding the poles and the equator are covered by different types of particles. Furthermore, since β' also depends on the frequency of the ac field, this may be achieved by selecting a suitable frequency such that the sign of β' is different for the two types of particles to be separated.

To compare the strength of the DEP force with that of gravity and Brownian forces which act on a particle, the work, W_{DEP}, done on a particle by the DEP force in moving it from one of the poles to the equator of the drop is computed. The work done is given by the integral of the dot product of the DEP force with the displacement along a path on the surface of the drop, from $\theta = 0$ to $\pi/2$:

$$W_{DEP} = \int_0^{\pi/2} F_{DEP} a \, d\theta = -6\pi R^3 \varepsilon_0 \varepsilon_c E_0^2 \, \beta' \, \beta(2 + \beta) \tag{3.1}$$

The work done in moving a particle from the drop's equator to one of the poles is of the same magnitude but has the opposite sign. Also, W_{DEP} is proportional to the square of the electric field intensity and is independent of the drop radius.

45

Obviously, it is possible to manipulate particles trapped on the surface of a drop by applying an electric field only if the DEP force that results is sufficiently large to overcome the particle's buoyant weight. The electric field intensity that is needed to meet this condition can be determined by the requirement that W_{DEP} is greater than the gravitational work done on the particle when it is moved from one of the drop's poles to the equator (or from the equator to one of the poles). The gravitational work done on a particle is given by

$$W_G = \frac{4}{3} \pi R^3 \left(\rho_p - \rho_f \right) g \, a$$

Here g is the acceleration due to gravity, ρ_p is the particle density and ρ_f is the effective fluid density. Using the above expressions, the requirement that the work done by the DEP force must be greater than the gravitational work gives

$$6\pi R^3 \varepsilon_0 \varepsilon_c E_0^2 \, \beta' \, \beta(2 + \beta) > \frac{4}{3} \pi R^3 \left(\rho_p - \rho_f \right) g a$$

The above can be written as

$$G > 1 \qquad\qquad\qquad (3.2)$$

where $G = \dfrac{9\varepsilon_0 \varepsilon_c E_0^2 \, \beta' \, \beta(2+\beta)}{2a(\rho_p - \rho_f)g}$ is an electric gravity dimensionless parameter. Notice that

the above condition is independent of the particle radius R because the buoyant weight and the DEP force are both proportional to the particle's volume. It is noteworthy that the electric field intensity required for manipulating particles increases with increasing particle density. The above condition, in fact, implies that negligibly small electric field is required for manipulating neutrally buoyant particles.

In addition, the above condition implies that the electric field intensity required for concentrating particles decreases with decreasing drop radius. For example, for $\rho_p - \rho_f = 200.0$ kgm^{-3}, g = 9.81 ms^{-2}, $\beta = 0.5$, $\beta' = 0.5, \varepsilon_c = 2.0$, the electric field intensity required for $a = 1.0$ mm is 595.4 kV/m, and for $a = 1.0$ μm is 18.8 kV/m. The electric field strength for the last case is about 32 times weaker than for the first case. This is an important result which states that the electric field intensity required for manipulating micro emulsions is smaller than for emulsions containing larger sized droplets.

Another force, which is especially relevant for small submicron and nano sized particles, is the force that arises due to the Brownian motion of particles. For a given electric field intensity the DEP force decreases with decreasing particle size while the importance of the Brownian forces increases with decreasing particle size, and thus the electric field intensity required for manipulating particles increases with decreasing particle size. The DEP force can be used to concentrate small particles on the surface of a drop only if the work done by the DEP force, W_{DEP}, is greater than kT, where k is the Boltzman constant and T is the temperature. Let us assume that $\beta = 0.5$, $\beta' = 0.5, \varepsilon_c =$

2.0, T = 300 K, kT = 4.28×10^{-21}, and E = 1.0x10^6 V/m. Then, for R = 1 μm, W$_{DEP}$ = 4.9x10^4 kT and for R = 100 nm, W$_{DEP}$ =48.7 kT. This shows that for these parameter values the DEP force is large enough to overcome the random Brownian forces that act on a 1 μm and even 100 nm sized particle trapped on the surface of a drop. The work done by the DEP force is much larger (by 3 orders of magnitude) for a 1μm particle than it is for a 100 nm particle.

Once particles concentrate near the poles or the equator of the drop, the electric field strength is increased further to a level above a critical value at which the drop either breaks near the middle or undergoes tip streaming, thus leading to the removal of particles concentrated near the equator or the poles. A drop placed in a uniform electric field deforms because the electric stress distribution on its surface is non-uniform. The deformed shape, assuming that the deformation is small, was determined in [57-63] by the balance of the surface tension force, which tends to make the drop spherical, and the force due to the electric stress, which tends to elongate the drop.

Furthermore, for certain cases, such as for a water drop immersed in corn oil, there is a critical Weber number at which the drop begins to tip-stream or breaks [80]. Let the critical Weber number at which this happens be We_{crit}, a critical value that we report below. For convenience, a scaled electric Weber number $We' = \dfrac{We}{We_{crit}}$ is defined so that the drop breakup or tip-streaming occurs when $We'=1$.

It is noteworthy that the electric Weber number (We) and the electric gravity parameter (G) both increase as the square of the electric field intensity. The former determines the electric field intensity at which a drop tip-streams or breaks, and the latter

gives the intensity that is needed to manipulate particles. Therefore, depending on the physical properties of the drop and ambient fluids and those of the particles involved, the electric field intensity at which a drop begins to tip-stream can be smaller than the intensity that is needed for manipulating particles. This, in fact, occurred in the experiments for glass particles trapped on the surface of a water drop when the drop diameter was ~ 1 mm or larger. The drop was immersed in corn oil. The drop tip-streamed at an electric field intensity smaller than that needed for manipulating glass particles, and therefore it was not possible to concentrate them. It was only after the drop radius had been reduced, as discussed below, that it was possible to manipulate particles on the surface of the drop.

The ratio of the scaled electric Weber number to the electric gravity parameter can be used to define another dimensionless parameter that quantifies the relative importance of the drop's tendency to tip-stream or break and the tendency of particles to concentrate near the poles or the equator of the drop:

$$\frac{We'}{G} = \frac{4a^2}{9\gamma} \frac{\left(\rho_p - \rho_f\right)g}{\beta'\left(\frac{2}{\beta}+1\right)We_{crit}} \tag{3.3}$$

Notice that the ratio $\dfrac{We'}{G}$ is independent of the electric field intensity and that it only depends on the physical properties of the two fluids and the particles involved. When $\dfrac{We'}{G} < 1$, the drop is not expected to break or tip-stream for the electric field intensity that is needed for concentrating particles on the drop's surface. This is the case

when the interfacial tension γ is sufficiently large, the drop radius is sufficiently small, or the density difference $\rho_p - \rho_f$ is sufficiently small. In fact, neutrally buoyant particles can be manipulated for any value of the drop radius. On the other hand, when $\frac{We'}{G} > 1$, the drop breaks or tip-streams for an electric field intensity that is smaller than that needed for concentrating particles on the surface of the drop.

$$a_{crit} = \frac{3}{2}\left[\frac{\gamma\beta'\left(\frac{2}{\beta}+1\right)We_{crit}}{\left(\rho_p - \rho_f\right)g}\right]^{\frac{1}{2}} \tag{3.4}$$

Furthermore, for a given set of ambient fluid, drop and particles, there is a unique critical drop radius for which $\frac{We'}{G}$ is equal to one (Figure 3.1). From Equation 3.3, the critical radius is given by

If the drop radius is much smaller than a_{crit}, the drop is not significantly deformed for the electric field intensity that is required for concentrating particles. However, if the radius is larger than a_{crit}, the drop tip-streams at an intensity that is smaller than that required for concentrating particles. Clearly, for the latter case, it is not possible to concentrate particles trapped on the surface of a drop. Also notice that for $a = a_{crit}$, the electric field intensity can be adjusted so that both We' and G are equal to one. Furthermore, as discussed below, it is only when the drop radius is smaller than a_{crit} that we can first concentrate and then remove particles from the surface of the drop by further

increasing the electric field intensity, the latter step being possible only if the drop breaks or tip-streams.
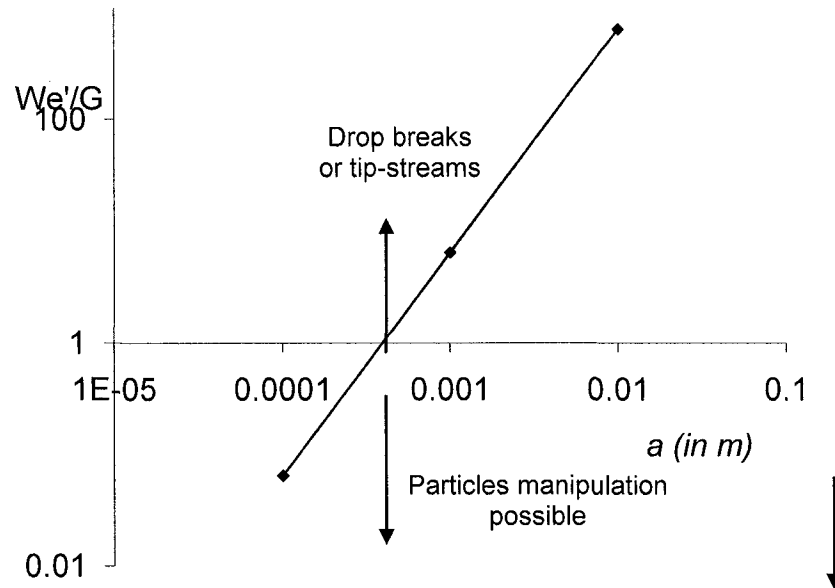
Figure 3.1 The dimensionless parameter $\frac{We'}{G}$ is shown as a function the drop radius on a log-log scale. The parameter values used are: $\rho_p - \rho_f = 1500$ kg/m^3, $\gamma = 0.02$ N/m, $\beta'\left(\frac{2}{\beta}+1\right) = 0.6$ and $We_{crit} = 0.085$. The figure shows that when the drop radius is greater than ~ 0.5 mm, $\frac{We'}{G} > 1$ and so the drop tip-streams for an electric field intensity that is smaller than the intensity required for concentrating particle. On the other hand, for smaller sized drops for which $\frac{We'}{G} < 1$, the electric field intensity needed for concentrating particles is smaller than the intensity at which the drop undergoes tip streaming or breaks up.

3.1 Results

First the results aimed at concentrating particles near the poles or the equator of a drop by applying a uniform electric field is prescribed, and then for separating particles for which the sign of Clausius-Mossotti factor is different, and then removing them from the drop by further increasing the electric field intensity.

3.1.1 Influence of particles on the electric field induced drop deformation

Water drop of diameter 945 μm suspended in corn oil which contained extendospheres on its surface is first considered. The drop sedimented to the bottom of the device as its density was greater than the density of corn oil. Due to their relatively low density (0.91), the extendospheres rose to the top surface of the water drop where they were trapped (see figure 3.2a). Experiments were conducted in a device for which the electrodes were mounted on the left and right sidewalls, thus making the applied uniform electric field horizontal. Hereafter, we define the drop's poles as the left and right most points on its surface. Since the dielectric constant of the drop is greater than that of the ambient liquid, the maximum value of the electric field occurs at the poles of the drop. For extendospheres, the Clausius Mossotti factor is such that $\beta'>0$, and thus the particles were expected to undergo positive dielectrophoresis and collect at the poles. This is indeed what happened in Figure 3.2b which shows that after an A.C. electric field with a frequency of 100 Hz was switched on, the DEP force caused the particles to move towards the poles.

The non uniform electric stress distribution on the surface of the drop caused it to stretch in the direction of the applied electric field. Figure 3.2b, taken at t = 5 s, shows that the drop stretched to an approximately ellipsoidal shape with the deformation

parameter D = 0.179. Notice that in Figure 3.2b particles have started to move towards the poles, while remaining trapped at the drop's surface during this motion. The drop deformation continued to increase as the particles migrated. It took approximately 60 s for all the particles to collect near the poles, and the drop reached a steady shape only after that time. The deformation parameter of the drop for the steady shape (reached at t = 60 s) was 0.207 (see Figure 3.2c).

(a)   (b)   (c)
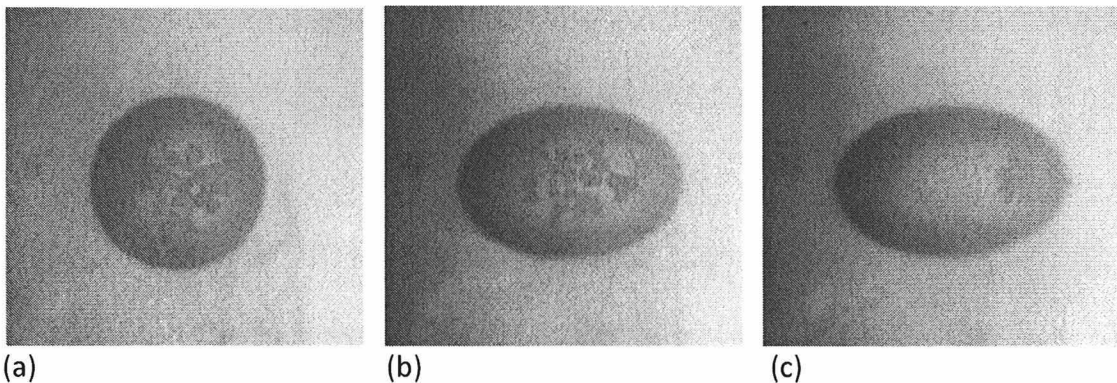
Figure 3.2 Deformation of a water drop immersed in corn oil. The drop carried extendospheres on its surface which rose to its top surface as they were lighter than both liquids. The electrodes were mounted in the left and right side walls of the device, and the distance between them was 6.5 mm. The diameter of extendospheres was ~90 μm.

(a) The applied voltage was zero and the deformation parameter D = 0. The drop diameter was 944.4 μm.

(b) At t = 5 s, shortly after an AC voltage of 3600 volt at 100 Hz was applied, the drop was significantly elongated, but the particles were still located near the center of the drop. The drop deformation parameter was D = 0.179.

(c) t = 60 s. The voltage applied was still 3600 volt. Notice that particles have already reached the poles, although a larger fraction has gone to the right pole. The drop deformation parameter was D = 0.207, which was greater than in (b) as D continued to increase while the particles moved towards the poles. The local radius near the poles was smaller than for the corresponding case without particles shown in Figure 3.3.

To further investigate the influence of particles on the drop deformation, a clean drop (without particles) of the same approximate radius was considered which was subjected to the same electric field intensity (see Figure 3.3a).

(a)   (b)   (c)

(d)
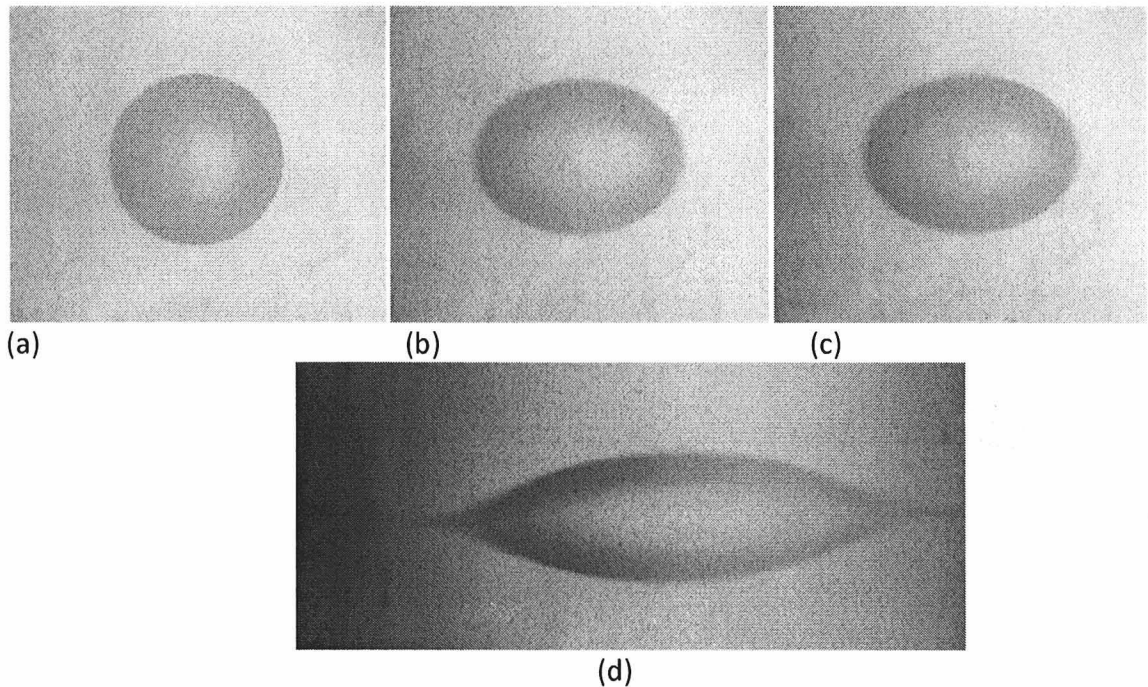
Figure 3.3 Deformation of a water drop immersed in corn oil. The distance between the electrodes was 6.5 mm.

(a) The voltage applied was zero and D = 0. The drop diameter was 954.0 μm.

(b) t = 5 s. Shortly after an AC voltage of 3600 volt at 100 Hz was applied, the drop became elongated with the deformation parameter D = 0.150.

(c) t = 120 s. The voltage applied was 3600 volt at 100 Hz and D = 0.150, which was the same as in (b). This indicates that the drop deformation did not change after 5 seconds.

(d) For another case, when a voltage of 4700 volt at 100 Hz was applied the drop formed pointed ends (Taylor cones) and the fluid was ejected from the tips of the conical ends.

The deformation parameter in Figure 3.3b at t = 5 s was D = 0.150 which did not change afterwards; its value is the same in figure 3.3c at t = 120 s. This, however, was not the case for the drop containing particles described in Figure 3.2 which continued to

deform while the particles migrated to its poles. Also notice that the steady state value of the deformation parameter for the drop containing particles was 0.207 which is larger than the value of D = 0.150 corresponding to a clean drop. Therefore, the presence of particles in this case caused an increase of the drop deformation.

The fact that the drop deformation continued to increase while the particles migrated to the poles suggests that the presence of particles near the poles results in an additional electric force acting on the drop which, for the above case, is in the direction of the outward pointing normal to the drop's surface. This additional force causes an increase in the drop deformation. Moreover, some of the particles protruded out of the drop's surface when the electric field was present (see Figure 3.2c), which we postulate is due to an electric force that acts to pull them out of the drop.

Figure 3.3d shows that when the applied voltage was increased to 4700 V the drop developed conical ends, referred to as Taylor cones, and subsequently a fraction of the fluid inside the drop was ejected out of the conical ends. Notice that after the drop had lost fluid, its final volume was smaller.

In these experiments, the electric field intensity at which tip-streaming occurred increased with decreasing drop size. In addition, as Figure 3.4 shows, the intensity at which tip-streaming occurred varied so that the electric Weber number remained approximately constant. The critical Weber number We_{crit} for these experiments was approximately 0.085. This dependence on the electric field intensity at which a drop tip-streams on the drop radius is in agreement with past experimental and theoretical studies. Also notice that there was a slight decrease in We_{crit} as the drop size increased. This may

be a result of the fact that the larger sized drop deforms more under gravity, and as a result, the electric field necessary to cause tip-streaming is smaller.
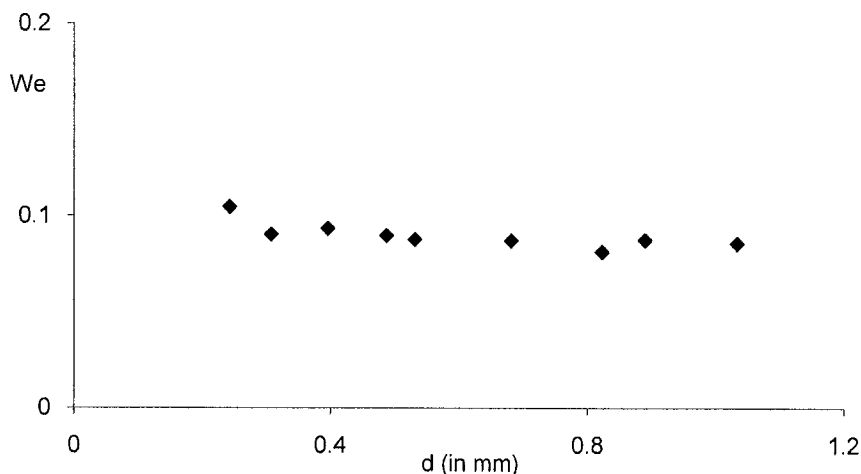
Figure 3.4 The electric Weber number at which tip-streaming occurred for a water drop immersed in corn oil is plotted as a function the drop diameter. The critical Weber number based on this data is approximately 0.085. The frequency was 100 Hz. The distance between the electrodes was 6.05 mm.

For the case described above, the drop was immersed in a liquid whose dielectric constant was smaller than that of the drop itself. Next the case of a silicon drop immersed in castor oil for which the dielectric constant of the liquid is larger than that of the drop is considered. In this case, the maximal and minimal values of the electric field are located at the equator and the poles, respectively. The drop diameter was 944.8 μm and it contained polystyrene particles on its surface (see Figure 3.5a). The drop settled to the bottom of the device as its density was greater than that of castor oil. The density of polystyrene spheres being 1.05, the latter sedimented to the bottom surface of the drop, as shown in Figure 3.5a.

(a)　　　　　　　　　　(b)　　　　　　　　　　(c)
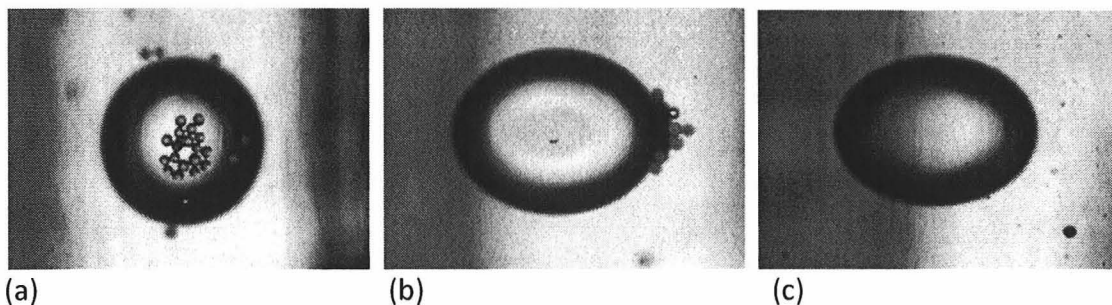
Figure 3.5 Deformation of a silicone oil drop immersed in castor oil. The distance between the electrodes was 6.5 mm.

(a) The voltage applied was zero. The drop contained polystyrene particles and its diameter was 944.8 μm.

(b) After an AC voltage of 5000 volt at 100 Hz was applied, the drop became elongated with the steady state value of the deformation parameter D = 0.106. Notice that particles formed chains and moved together towards the right pole because of particle-particle interactions.

(c) Deformation of a clean drop (without particles) for 5000 volts at 100 Hz. The diameter of the initial (undeformed) drop was 900.8 μm. The steady state value of the deformation was D = 0.128.

After an A.C. electric field with a frequency of 100 Hz was switched on, all particles migrated under the action of the DEP force to the poles where the electric field intensity is minimal (see Figure 3.5b). Polystyrene particles experienced negative dielectrophoresis because their dielectric constant is smaller than that of the ambient liquid. The steady state value of the drop deformation parameter was 0.106 which was attained after all the particles reached the poles. The corresponding deformation for the case without particles was 0.128. Therefore, in this case, the presence of particles caused a decrease in the drop deformation. Recall that for the case in which the drop's dielectric constant is larger than that of the ambient fluid the presence of particles experiencing positive dielectrophoresis near the poles caused an increase in the drop deformation (see Figure 3.2). The drop deformation in Figure 3.5 did not significantly change while particles migrated to the poles. This is different from the case described in Figure 3.2 in

the sense that the drop deformation changed while particles migrated to the poles. Also note that for the experiments the change in the drop deformation due to the presence of particles was insignificant when they concentrated near the equator on the drop's surface.

3.1.2 Dependence of the DEP Force on the Particle Radius

From Equation 3.1, the DEP force that acts on a particle varies as R^3. Therefore, since the only two forces acting on a particle are the DEP force and the buoyant weight which also varies as R^3, the electric field intensity needed to manipulate the particle should be independent of its radius. To validate this result, the electric field intensity needed to move a glass particle from the bottom of a water drop to one of its poles is measured. The drop was immersed in corn oil. Three different glass spheres with the diameters of 45, 64 and 106 μm were considered. The density of glass spheres was 2.6 g/cm^3. The drop diameter was held approximately constant around 500 μm. All other parameters were held fixed in this study.
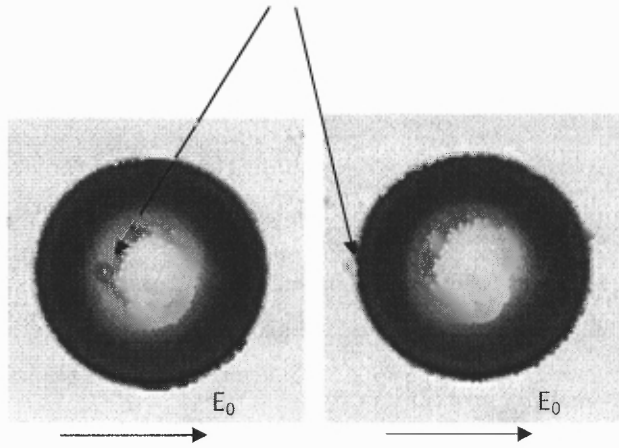
(a)   (b)

Figure 3.6 Manipulation of a glass sphere of diameter 45 μm on the surface of a water drop immersed in corn oil. The distance between the electrodes mounted on the left and right side walls was 6.05 mm. The drop diameter was 496.6 μm.

(a) The glass sphere sedimented to the bottom of the drop as it was heavier than both water and corn oil. The applied voltage was zero.

(b) The glass sphere moved to the left pole when the voltage applied at 100 Hz was slowly increased to 2450 V. For a smaller voltage the particle remained near the bottom surface of the drop.

Figure 3.6 shows the case where a single glass sphere with the diameter of 45 μm was placed in a water drop of diameter 496.6 μm. The drop sedimented to the bottom surface of the device, and the glass sphere sedimented to the bottom of the drop since its density was larger than that of water and corn oil. The voltage applied to the drop was increased slowly to determine the minimal needed to move the glass sphere. Figure 3.6b shows that when the applied voltage reached 2450 V, the glass sphere moved to the drop's left pole. The glass sphere was expected to move to one of the poles since it undergoes positive dielectrophoresis and the drop's dielectric constant was greater than that of the ambient liquid. The above experiment was repeated for two other glass spheres of larger diameters. The voltage required for moving the glass sphere of diameter 64 μm

was 2590 V, and for the sphere of diameter 105 μm was 2530 V. The drop diameter for the former case was 500.0 μm and for the latter was 498.3 μm. These results show that the electric field intensity needed to manipulate a particle is indeed approximately independent of the particle radius. From this one may conclude that the dependence of the DEP force and the buoyant weight on the particle radius is the same. Therefore, since the buoyant weight varies as R^3, the DEP force also varies as R^3. This is an important result because it implies that the same electric field intensity can be used to manipulate both smaller and larger sized particles adsorbed on the surface of a drop. However, as discussed in the beginning of the chapter, submicron and nano sized particles can be manipulated only when the work done by the DEP force on a particle W_{DEP}, which varies as R^3, is greater than kT. For such small particles the DEP force must be large enough to overcome the Brownian motion and the requirement that the DEP force must overcome the buoyant weight is less restrictive.

3.1.3 Dependence of the DEP Force on the Drop Radius

According to Equation 2.8, the DEP force acting on a particle is inversely proportional to the drop radius. To verify the validity of this expression, experiments were conducted in which the electric field intensity needed to move a given extendosphere from the drop's equator to its pole was measured as a function of the drop radius. To ensure that the particle's properties did not change, the same extendosphere was used throughout the experiment while the diameter of the water drop was varied between 390 μm and 700 μm by injecting or removing water from the drop. The drop was immersed in corn oil. For the results presented in Figure 3.7 the radius of the extendosphere was 130 μm. While the

study was repeated for several extendospheres of slightly different diameters, the results obtained are not shown here as they were similar.

Figure 3.7 shows that the electric field intensity (E_0) needed to move an extendosphere from the drop's equator to its pole varied with the drop diameter d so that $\frac{E_0}{d^{0.5}}$ (or equivalently $\frac{E_0^2}{d}$) was approximately constant. Since these results were obtained for a fixed particle and only the drop diameter was varied, all other parameters, including the particle's buoyant weight, remained constant.
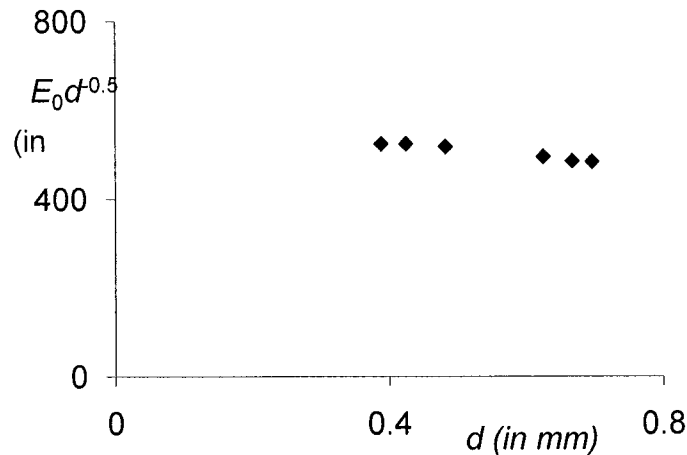
Figure 3.7 The electric field intensity (E_0) needed to move a fixed extendosphere from the drop's equator to a pole divided by the square root of the drop diameter (d) is plotted as a function of the drop diameter. The frequency of the ac field was 100 Hz. The drop diameter of the extendosphere was 130 μm. The drop was immersed in corn oil. The figure shows that when the drop diameter was varied between 0.39 and 0.7 mm, $\frac{E_0}{d^{0.5}}$ remained approximately constant.

As noted earlier, to move a particle from the drop's equator to its pole, the DEP force must overcome the buoyant weight of the particle, which remained constant. Experimental results therefore are in agreement with Equation 2.8 which states that the DEP force acting on a particle behaves as E_0^2 and varies inversely with the drop radius,

and thus the square of the electric field intensity needed to move a particle increases linearly with increasing drop diameter. The inverse dependence of the DEP force on the drop diameter is an important result which essentially shows that the electric field non uniformity on the drop's surface, and thus the DEP force, is greater when the drop size is smaller. Consequently, for example, particles distributed on the surface of micron sized droplets can be manipulated by applying a smaller electric field intensity than that needed for millimeter sized droplets.

3.1.4 Removal of Particles from the Surface of a Drop

Next the removal (from the drop) of particles concentrated either near the poles or the equator of a drop will be discussed. This was achieved by increasing the electric field strength to another critical value so that the electric Weber number was larger than the critical value We_{crit}. The approach, obviously, is likely to work only if the drop tip-streams or breaks when a sufficiently strong electric field is applied. In addition, as discussed in section 3.1.2, the drop radius must be smaller than the critical radius given by Equation 2.8, because otherwise the drop breakup or tip-streaming would occur for smaller electric field intensity than that required for concentrating particles. The latter concentration is an essential first step in the technique without which the removal of all of the particles from the drop's surface would not be possible.

3.1.4.1 Removal of Particles Concentrated at the Poles

Figure 10 describes the case of a water drop suspended in decane which contained extendospheres on its surface. The electrodes were mounted in the left and right side walls. Figure 10a displays the initial distribution of particles at the drop surface. The

dielectric constant of the drop being larger than that of the ambient fluid, which was also the case in Figure 3.2, the electric field was maximal at the poles.

(a)   (b)   (c)

(d)   (e)
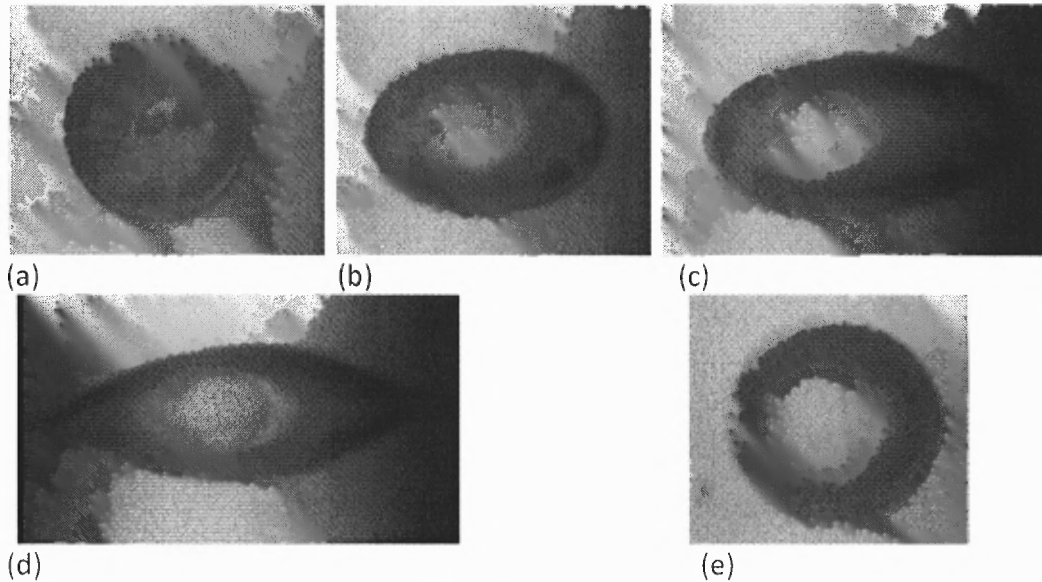
Figure 3.8 Removal of extendospheres from a water drop immersed in decane. The distance between electrodes was 6.5 mm.

(a) The drop diameter was 932.6 μm. The initial distribution of extendospheres on the drop's top surface. The voltage applied was zero.

(b) The voltage applied was 3000 volt at 1 kHz. Particles moved towards the two poles.

(c) The voltage applied was 3500 volt at 1 kHz. All of the particles accumulated at the two poles and formed particle chains. Notice that the radius of curvature near the poles was smaller.

(d) Shortly after the voltage of 3800 volt at 1 kHz was applied, the drop shape near the poles became conical, and all of the particles had already ejected from the drop via tip-streaming.

(e) After the electric field was switched off, the drop assumed a spherical shape. The drop was clean and its diameter was 832.7 μm.

For extendospheres $\beta' > 0$, and so as expected the spheres experienced positive dielectrophoresis. After the electric field was switched on, the drop elongated in the field direction and particles started to move towards the poles (see Figures 3.8b, c). Figure

3.8c, corresponding to the case of a larger voltage, shows that particles had already aggregated near the poles and that the drop was considerably more deformed than in Figure 3.8b.

The radius of curvature at the poles decreased with increasing voltage and ultimately led to the formation of Taylor cones at the two ends of the drop when a voltage of 3800 volts was applied (see Figure 3.8d). The drop's liquid was then ejected out of the conical ends, and along with the liquid all the particles aggregated near the poles were also ejected by means of a tip-streaming mechanism. In this case, since all the particles were already concentrated near the poles before tip-streaming occurred, they were all ejected and the final drop was free of particles. The particles ejected from the drop then rose individually to the top surface of decane as they were lighter than the ambient liquid, thus separating themselves from the liquid. Also it is observed that after the particles were ejected there were small droplets present which were formed because the drop lost not only the particles but also some of the liquid. The final drop size in Figure 3.8e, which was taken after the electric field had been switched off, was therefore smaller than the drop initial size (Figure 3.8a). The above method offers a systematic way for removing particles from the surface of drops in a contactless fashion.

It is noteworthy that the development of conical ends for a clean drop (without particles) occurred at a voltage of 4700 V, which was smaller than the voltage in Figure 3.8a for the case with particles. Therefore, when particles experiencing positive dielectrophoresis accumulated at the poles, not only was the drop deformation enhanced, as described in the previous subsection, but also there was a decrease in the minimal voltage at which the drop tip-streamed.

It was noted in Figure 3.4 that the electric field intensity at which the drops started to tip-stream decreased with increasing drop radius so that the electric Weber number (corresponding to tip-streaming) was approximately constant. Furthermore, it is found that applying a voltage that was sufficiently large to cause tip-streaming right away did not provide an effective method for removing particles from the surface of the drop. This is due to the fact that in this case particles did not have sufficient time to move to the poles and as a result the fluid inside the drop alone was ejected during tip-streaming. For the method to work properly, the voltage needs to be increased in two steps. In the first step, the drop must be subjected to a sufficiently large voltage for a certain period of time during which all the particles accumulate near the poles without causing tip-streaming. Only then a higher voltage, that causes the accumulated particles to tip-stream, should be applied to remove the latter from the drop.

3.1.4.2 Removal of Particles Concentrated near the Equator

In order to address the removal of particles concentrated near the equator, we used a device whose electrodes were separated by a smaller distance. Specifically, experiments showed that when the distance between the electrodes was about three times the drop diameter or smaller the drop bridged the gap between the electrodes when a sufficiently high voltage was applied and subsequently broke-up into two or three major droplets.
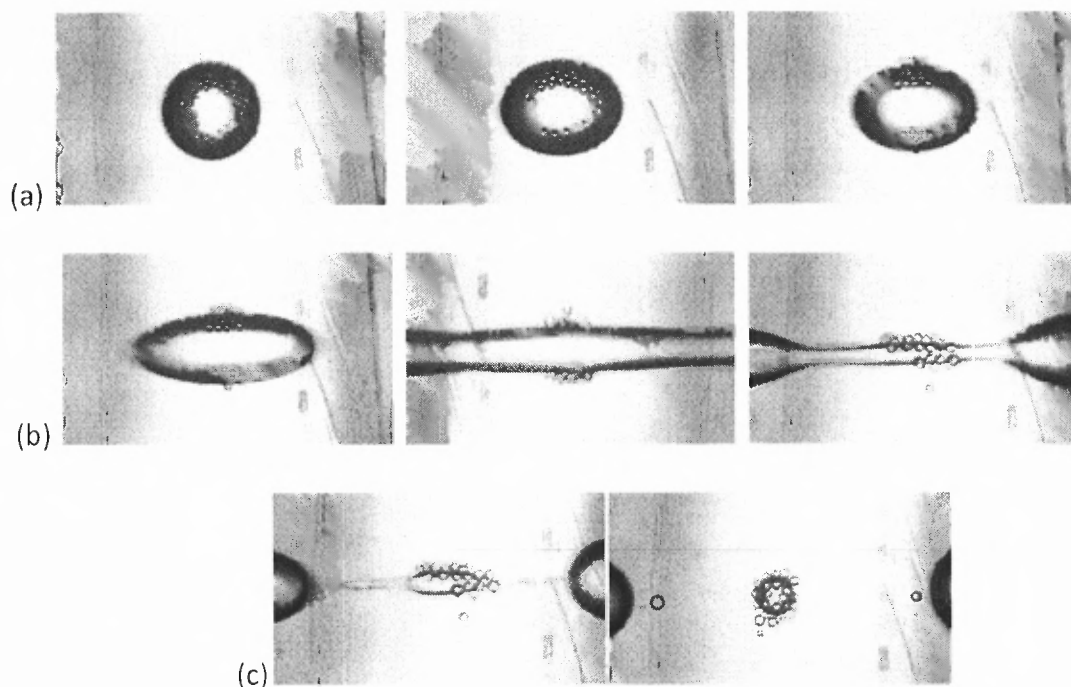
Figure 3.9 Removal of polystyrene spheres from a water drop immersed in corn oil. The distance between the electrodes was 2.65 mm.

(a) The drop diameter was 932.6 μm. Polystyrene spheres sedimented to the bottom of the drop as they were heavier than water. The applied voltage was zero.

(b) The applied voltage was 1400 volts at 1 kHz. Particles moved towards the equator and collected in a ring shaped region around the equator; D = 0.15.

(c) The applied voltage was 1800 volts at 1 kHz. Particles continued to moved towards the equator while the drop quickly stretched with time (the sequence is shown in five photographs), and broke into three main droplets. The droplet in the middle contained all of the particles, and the larger sized droplets on the left and right sides were particle free. Notice that there were some particles outside the drop which remained outside throughout the experiment and that some particles were expunged from the surface of the drop because the number of particle became larger than that could be accommodated on the surface of the middle droplet.

On the other hand, as discussed in the previous subsection, when the distance was about more than five times larger than the drop diameter only tip-streaming occurred when the applied voltage was above a critical value. In a smaller device, there is an increase in the electric field intensity in the gap between the electrodes and the drop's surface, and this increases the stretching electrostatic force experienced by the drop,

causing it to bridge the gap between the electrodes and subsequently break in the middle due to the capillary instability. Experiments described below shows that when particles were located approximately in the middle of the drop, after the drop broke they were contained within a smaller droplet in between the two larger sized droplets. Furthermore, the voltage needed for deforming and breaking the drop was smaller not only because the distance between the electrodes was smaller (and so for the same voltage applied the electric field was stronger), but also because of the enhancement of the electric field intensity in the gap between the drop and the electrodes which in turn enhances the extensional electrostatic force acting on the drop.

First the case of a water drop, carrying polystyrene particles, immersed in corn oil is studied. Since the density of polystyrene particles is 1.05 which is larger than that of the liquids involved, particles settled to the bottom surface of the drop (Figure 3.9a). When a voltage of 1400 volts was applied, the drop elongated and particles began to collect near the equator at the bottom surface of the drop (Figure 3.9b). This shows that particles experienced negative dielectrophoresis as well as a buoyancy force which was non-negligible. For a voltage of 1800 volts, the drop deformation was even larger and particles collected in a ring shaped region near the equator. The drop continued to stretch until it bridged the gap and assumed a dumbbell like shape. The distance between the electrodes was about three times the drop diameter. The filament in between the two ends of the dumbbell continued to thin with time and eventually the capillary instability caused it to break near the middle. The breakup near the middle occurred quickly after the filament diameter became smaller than the thickness of the region occupied by the particles. The size of the middle droplet, as discussed below, was found to increase with

increasing concentration of particles. The middle droplet was formed because not all of the fluid and none of the particles contained in the filament were transferred to the two main droplets. The last photograph in Figure 3.9c shows that the drop has broken into three major droplets and a few additional smaller droplets. All of the particles were contained in the smaller central droplet or were around it, and the two larger droplets on the sides were clean. Notice that the particle concentration in the middle droplet is rather large as most of the liquid was transferred to the two larger drops and this caused some of the particles to be expunged from the drop's surface into the outside ambient fluid.

Figure 3.10 describes a similar process for a water drop suspended in corn oil, with extendospheres on its surface. Extendospheres rose to the top surface of the drop as their density was smaller than that of the drop and ambient liquids. For an A.C. voltage of 2000 volts at 1 kHz particles remained near the top of the drop, implying that either particles experienced negative dielectrophoresis or the DEP force was not large enough to overcome the buoyancy force. Recall that at the frequency of 100 Hz extendospheres undergo positive dielectrophoresis for the same two fluids. The drop deformation then increased quickly which was followed by its breakup into three major droplets. As was the case in Figure 3.9, the droplet in the middle contained all of the particles, leaving the other two droplets particle-free.
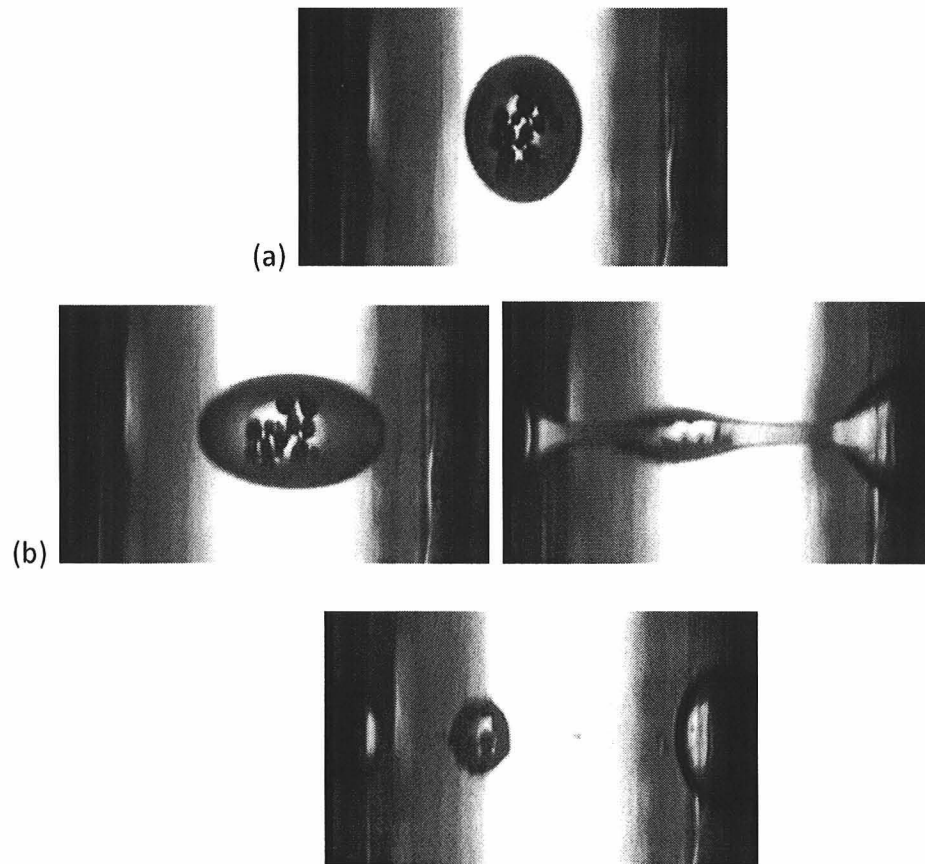
Figure 3.10 Removal of extendospheres from a water drop immersed in corn oil. The distance between the electrodes was 2.65 mm.

(a) The drop diameter was 796.0 μm. Extendospheres were trapped on the drop's top surface. The voltage applied was zero.

(b) The voltage applied was 2000 volt at 1 kHz. Particles remained at the equator while the drop stretched and broke into three main droplets (the sequence is shown in 3 photographs). The droplet in the middle contained all of the particles, and the droplets on the left and right sides were particle free. Notice that at t=0.2s the distribution of particles was slightly to the left and as a result the middle droplet with the particles was also slightly to the left.

For the cases described in this subsection the drops elongated to bridge the gap between the electrodes and eventually broke in the middle due the capillary instability. The drops were able to bridge the gap because the distance between the electrodes was only approximately three times larger than the drop diameter. In fact, experiments showed that for a device with a given distance between the electrodes there was a critical

drop diameter for which the drop bridged the gap between the electrodes. The drops smaller than this size underwent tip streaming, whereas the larger sized drops bridged the gap and broke up in the middle.
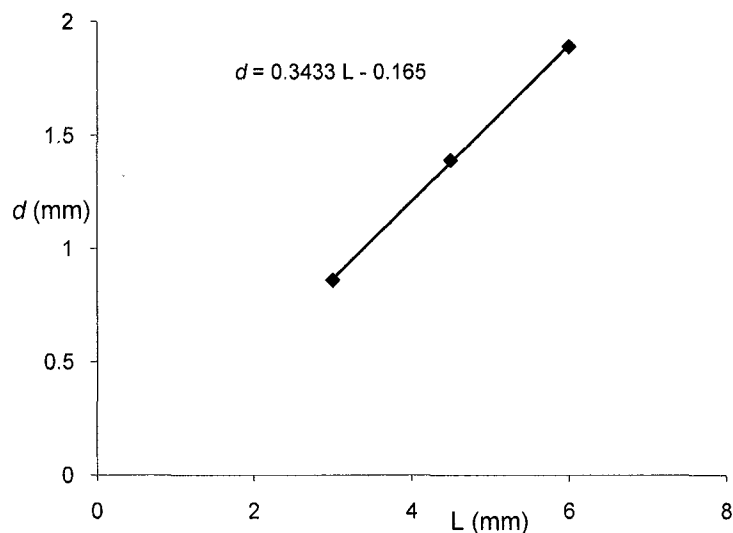
Figure 3.11 The diameter d of the smallest water drop that bridged the gap between the electrodes is plotted as a function of the distance L between the electrodes. Tip-streaming occurred for the drops that were of the smaller diameter. The drops were immersed in corn oil. The frequency was 1 kHz. The best linear fit is also shown.

In Figure 3.11 the diameter of the smallest drop that bridged the gap as a function of the distance L between the electrodes is plotted, i.e., the drops for which the diameter was smaller only tip-streamed. Notice that the drops bridged the gap when their diameter was about one third of the distance between the electrodes. This is an expected result due to the fact that there are two relevant length scales in the problem, the drop diameter and the distance between the electrodes. The actual ratio of the drop diameter and the distance between the electrodes at which the drop bridges the gap, however, depends on the physical properties of the ambient and drop fluids involved.

(a) t=0 s   t=10.5333 s   t=10.6667 s   t=11.5 s

(b) t=0 s   t=16.6 s   t=16.8667 s   t=17.1667 s
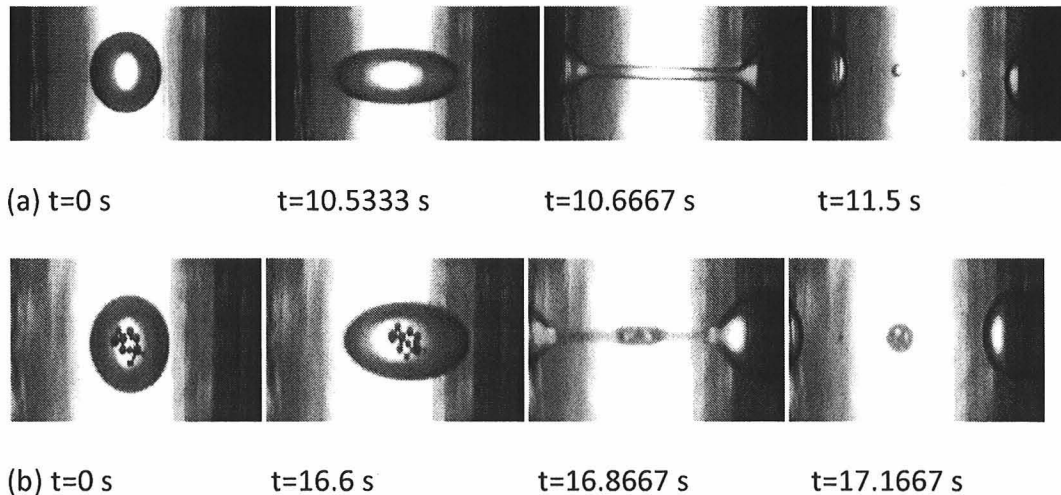
Figure 3.12 Removal of extendospheres from a water drop immersed in corn oil. The distance between electrodes was 2.65 mm. The voltage applied was 2000 volt at 1 kHz.

(a) A clean drop with a diameter of 828.1 μm shown at t = 0, 10.533, 10.6667 and 11.5 s. The drop stretched and broke into two main drops, although three additional small droplets were also generated in the middle.

(b) A drop carrying particles with a diameter of 844.2 μm shown at t = 0, 16.6, 16.8667 and 17.1667s. Particles remained at the equator while the drop stretched and broke, leaving particles in a small droplet in the middle. The particle concentration was smaller than in figure 12, and so was the size of the central drop carrying the particles in the final stage.

To understand the mechanism by which the breakup takes place and why the middle droplets containing particles are formed, similar experiments for the drops that were clean (without particles) was plotted. Figure 3.12a shows the breakup of a clean water drop immersed in corn oil.

The drop stretched in the direction of the electric field and continued to stretch until its ends touched the side walls. Notice that at this point, the drop assumed a dumbbell like shape, with an elongated cylindrical filament in the middle and two spherical ends of larger diameters (see the third photograph of Figure 3.12a). The diameter of the filament continued to decrease with the fluid moving out into the two spherical ends. When most of the fluid was pulled into the two ends and the diameter of

the filament became sufficiently small it broke due to the capillary instability resulting in the formation of a line of small droplets in the middle. The size of the central droplets was smaller than in Figure 3.10 for the case where the drop contained particles.

To further investigate the influence of particles on the formation of the middle droplet, the particle concentration in the drop was reduced, as shown in Figure 3.12b. As in Figure 3.10, particles remained at the equator while the drop stretched. In addition, the filament was similar to that in Figure 3.12a, except that it contained particles. The presence of particles, however, resulted in the formation of a larger sized droplet in the middle which contained all of the particles (see Figures 3.12b). The size of this middle droplet adjusted to the volume of particles in the drop. For example, in Figure 3.12b, the size of the middle droplet was smaller than in Figure 3.10, as the volume of particles in the former case was smaller.

3.1.5 Separation of Two Types of Particles and Formation of Janus Drops

The case in which a water drop contained two types of particles with different dielectric properties is finally considered. The drop immersed in corn oil contained hollow extendospheres and glass particles as seen from Figure 3.13. The goal here was to show that we could separate two different types of particles trapped at the surface of a drop. This was achieved by controlling the electric field intensity and frequency so that extendospheres which undergo positive dielectrophoresis moved to the poles while glass particles which undergo negative dielectrophoresis remained near the equator. Once this arrangement of particles was reached the electric field intensity is further increased and hence were able to remove one type of particles (extendospheres) from the drop, leaving the other type (glass particles) on the drop's surface.
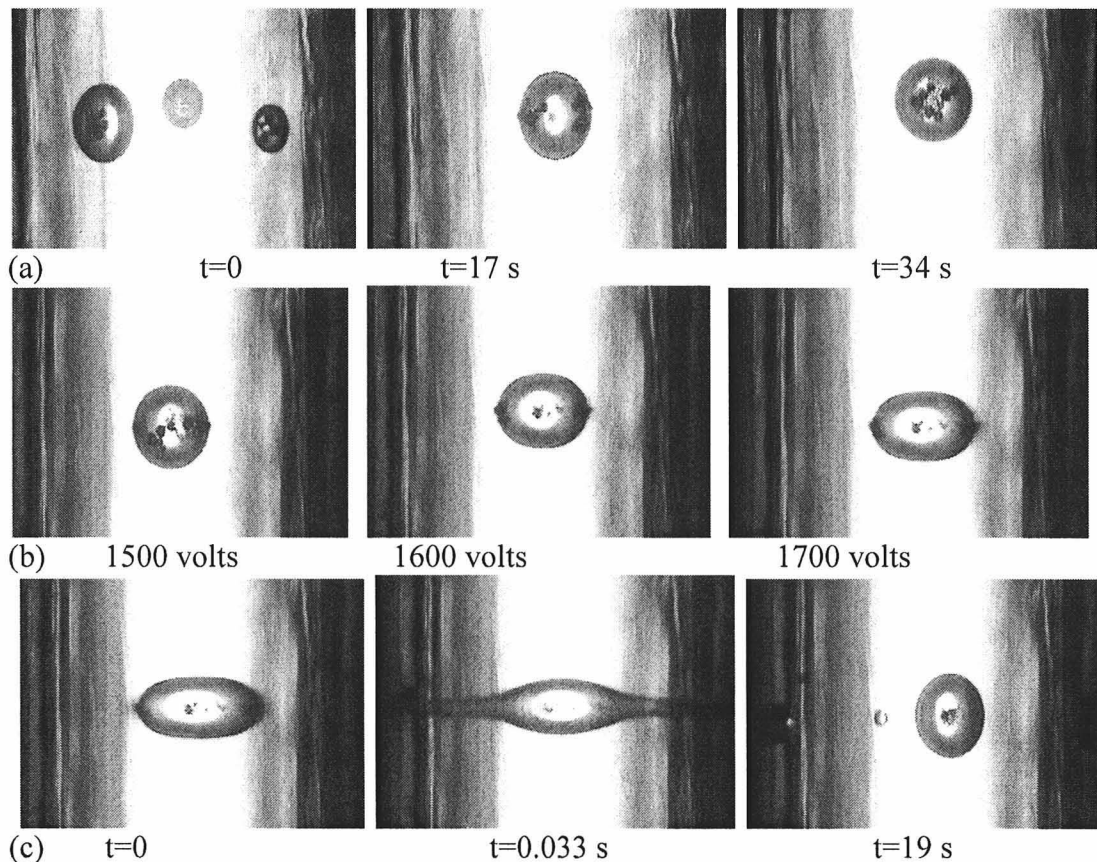
Figure 3.13 Removal and separation of extendospheres and hollow glass spheres from a water drop immersed in corn oil. The distance between electrodes was 2.65 mm.

(a) The electric field induced merging of three drops is shown at t = 0, 17 and 34 s. The middle drop carried glass particles, and the left and right drops carried extendospheres. The drops merged when a voltage of 600 volts at 100 Hz was applied. The electric field was then switched off and at t = 34s particles stopped moving. The diameter of the combined drop was 622.1 μm.

(b) The steady drop shapes are shown for increasing voltages at 100 Hz. The voltage was increased from 1500 to 1700 volts. The extendospheres (larger sized particles) moved to the poles while the glass particles remained at the equator.

(c) The voltage applied was 1825 volts at 100 Hz. The drop is shown at t = 0, 0.033 and 19 s. The extendospheres were ejected out by tip-streaming, and glass particles remained in the drop. The last figure shows small droplets on the left and right sides that carried extendospheres. The main drop carried only glass particles and its diameter was 573.6 μm, which was smaller than in (b). Also notice that the size of the drop was smaller than in figures 12 and 14, and therefore it did not break in the middle as in figures 12 and 14.

In Figure 3.13a, the drop containing glass and extendospheres was formed using three smaller drops as shown. While the middle drop carried glass particles, the two drops on the sides carried extendospheres. The three drops were merged to form a larger drop by applying a voltage of 600 V [74]. After the drops merged, we switched the electric field off and allowed the distribution of particles on the drop surface to reach a steady state. Then a voltage of 1500 V at the frequency of 100 Hz was applied to the device. Figure 15b shows that as the applied voltage was increased to 1600 and then to 1700 V the drop deformation increased. Also, notice that glass particles (which either underwent negative dielectrophoresis or experienced a small DEP force compared to their buoyant weight) remained at the center of the drop whereas extendospheres (which underwent positive dielectrophoresis) began to move towards the poles. After all extendospheres reached the poles, a voltage of 1825 volts was applied. The drop elongated further and the extendospheres accumulated at the poles were ejected from the drop by tip-streaming (see Figure 15c). The electric field was then switched off. The last figure in the sequence shows the drop containing only glass particles while all extendospheres have been removed.

The separation of particles on the surface of a drop, however, requires that the two types of particles do not physically block each other. Figure 3.14 demonstrated that when glass particles and extendospheres were in a mixed state, the former blocked the latter from moving towards the poles. This resulted in the formation of two groups of particles near the top of the drop. The group on the left in Figure 3.14c contained only glass particles while the group on the right contained a mixture of glass particles and extendospheres.

(a) t=0

(b) t=4 s

(c) t=5 s

(d) t=6 s
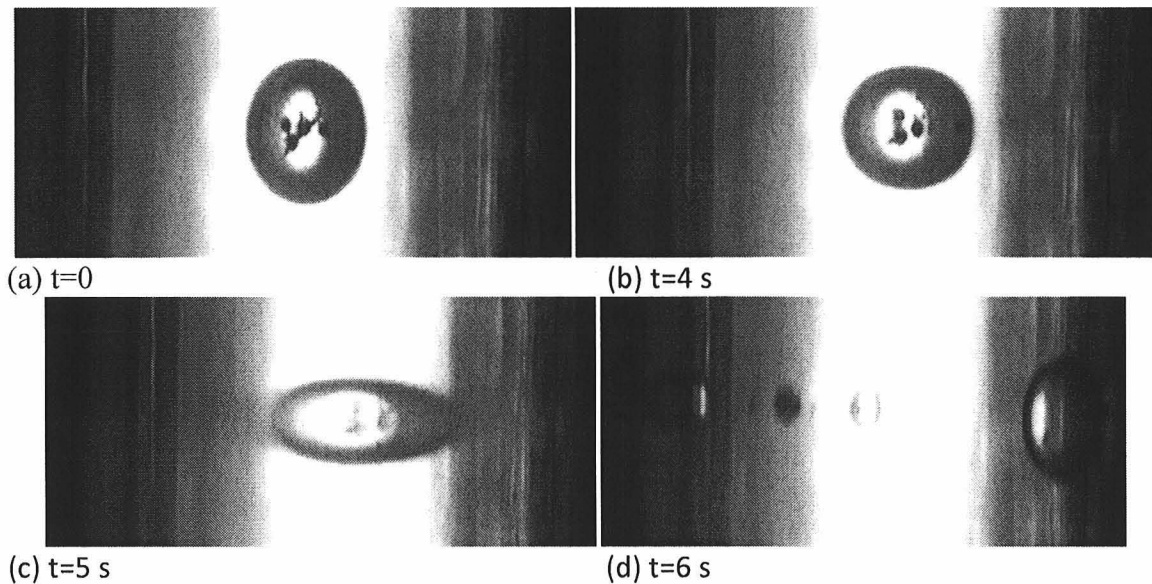
Figure 3.14 Removal and separation of extendospheres and hollow glass spheres from a water drop immersed in corn oil. The distance between the electrodes was 2.65 mm.

(a) At t=0, glass particles and extendospheres were located at the top surface of the drop. The applied voltage was zero.

(b) The applied voltage was 1200 volts at 100 Hz. The drop elongated in the direction of the electric field. Glass particles (which undergo negative dielectrophoresis) stayed near the equator and extendospheres (which undergo positive dielectrophoresis) had a tendency to move towards the poles, but were physically blocked by the glass particles around them.

(c) The applied voltage was 1800 volts at 100 Hz. The drop elongation increased and particles near the top surface separated into two groups, with one group near the equator containing only glass particles and the other one containing a mixture of extendospheres and glass particles and moving slightly towards the right pole.

(d) The drop broke, and particles were contained in the two smaller droplets in the middle, one containing only glass particles and the other one a mixture of glass and extendospheres. The two larger sized droplets were free of particles. The applied voltage was zero.

Under an applied voltage of 1800 volts, the drop broke into four major droplets (Figure 3.14d). One of the two droplets in the middle carried glass particles (left droplet) and the other one a mixture of the two types of particles (right droplet), while the two larger drops on the sides were left free of particles. Notice that before the drop bridged

the gap between the electrodes, glass particles were near the equator, but the cluster containing both extendospheres and glass particles was slightly to the right of the equator. This also shows that if particles are not concentrated within a single cluster near the equator of the drop then after the drop break-up they are not contained in a single droplet. Furthermore, their position away the equator before the drop bridges the gap between the electrodes determines the position of the droplet in which they are captured.
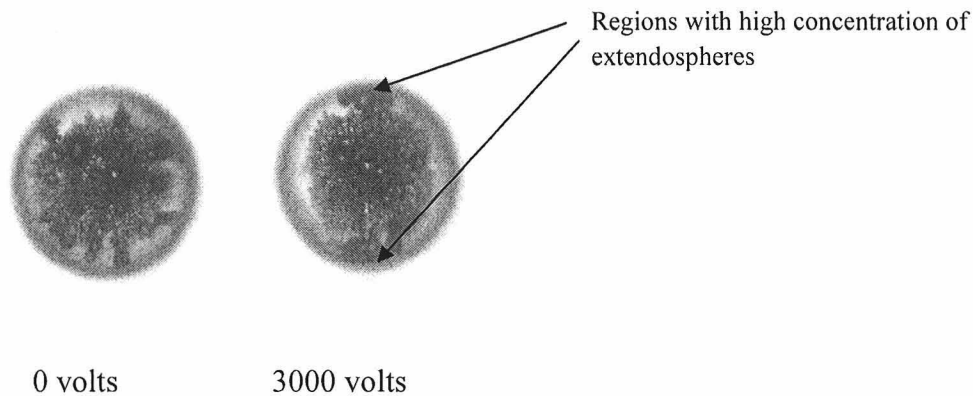
Figure 3.15 Experiments showing that when the electric field was applied glass particles (smaller sized particles, $a \sim 10$ μm) trapped on a water drop moved to the region near the equator and most extendospheres (larger sized particles, $a \sim 55$ μm) migrated to the region near the poles. Some extendospheres remained trapped at the equator because they were physically blocked. The drop diameter was 624 μm and it was immersed in corn oil.

Figure 3.15 shows the case in which glass particles and extendospheres were initially in a mixed state on the surface of a drop, but when the electric field was applied the glass particles remained at the equator while extendospheres moved to the poles. Some extendospheres, however, were physically blocked by the tightly packed glass particles and as a result did not separate. Recall here that both glass and extendospheres remain trapped on the drop's surface, and thus it is rather difficult for a trapped particle to escape since their motion is restricted to the two-dimensional surface of the drop. After

the electric field was removed this distribution remained unchanged resulting in the formation of a drop for which some areas were covered by glass particles alone and some by extendospheres alone, and the remaining surface remained uncovered. This demonstrates that the method can be used to create other distributions of particles on the surface of drops, and the fraction of area covered by a given type of particles can be varied by changing the concentration of those particles. The technique thus offers a way to create composite (Janus) particles with tailored surface structure and composition by freezing these distributions.

CHAPTER 4

PARTICLE-PARTICLE INTERACTIONS ON THE SURFACE OF A DROP

The main objective of this chapter is to use an externally applied uniform electric field to manipulate the distribution of particles on the surface of a drop and to study the dipole-dipole interactions between the particles. Hence a drop that carries particles on its surface and is immersed in another fluid with which it is immiscible is being considered.

4.1 Distribution of particles near the poles

To study the dipole-dipole interactions between particles collected at the poles, first a silicon drop of diameter 1521 μm suspended in corn oil is worked on. Hollow glass spheres with the diameter between 8-16 μm were suspended in the drop. The density of the silicon drop is greater than that of corn oil, and so it sedimented to the bottom of the device along with the suspended particles. However, since the density of hollow glass spheres is ~0.6 g/cm³, they rose to the top surface of the silicon drop where they were trapped (see Figure 4.1a). In addition, since the bottom surface had a greater affinity to corn oil, the silicon drop did not wet the bottom surface.

The experiments were conducted in the device with the electrodes mounted at the top and bottom surfaces as explained in Chapter 2. The dielectric constant of the drop being greater than that of the ambient liquid, the maximum value of the electric field occurs at the poles of the drop, which are located on the top and bottom surfaces of the drop. After an A.C. electric field with a frequency of 1 kHz is switched on, the DEP force causes particles to move towards the poles as shown in Figure 4.1a.

(a) 5000 V

(b) 3000 V

(c) 1000 V

(d) 0 V
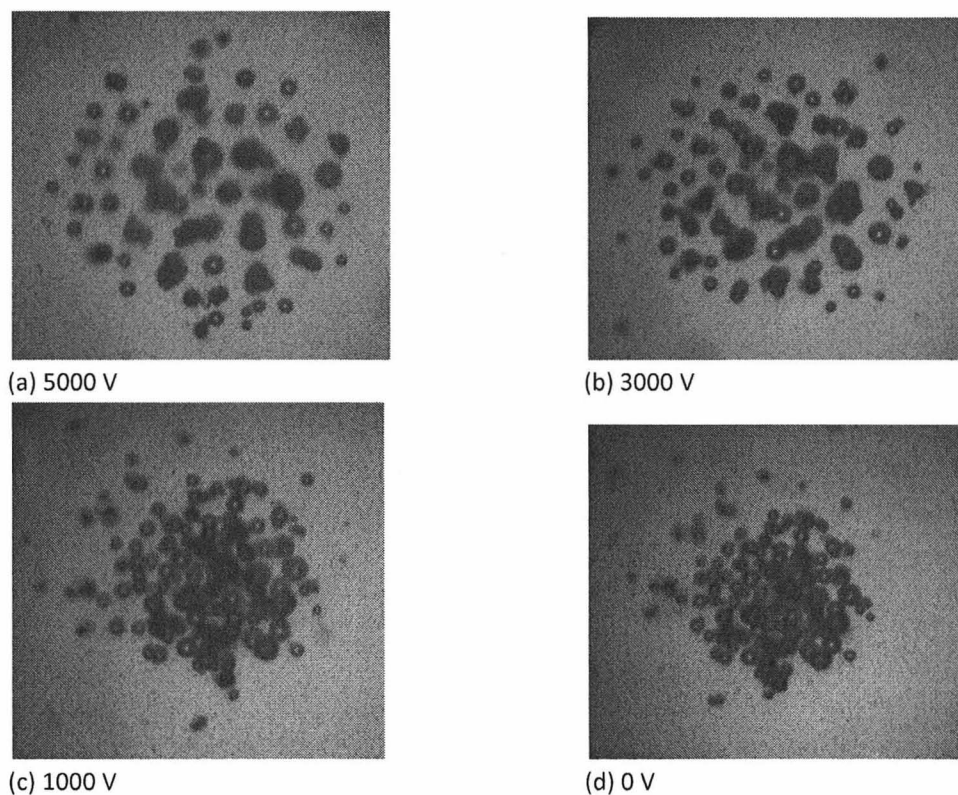
Figure 4.1 A magnified view showing the distribution of hollow glass particles near the pole of a silicon drop immersed in corn oil. The drop carries hollow glass particles which rise to its top surface due to the fact they are lighter than both liquids. The electrodes are in the top and bottom surfaces of the device. The diameter of the undeformed drop was 1521 μm.

(a) The applied voltage is 5000 V. Hollow glass particles rise to the top surface of the drop where they are captured. They remain separated from each other because of the dipole-dipole forces which are repulsive

(b) The applied voltage is 3000 V. The distance between the particles accumulated at the poles is smaller than in (a).

(c) The applied voltage is 1000 V. The distance between the particles is still smaller.

(d) The applied voltage is 0 V. Particles at the poles are in contact with each other since the repulsive dipole-dipole force is not present.

As noted earlier, a particle on the surface of the drop is subjected to a nonuniform electric field and thus to the phenomenon of dielectrophoresis. In this case a voltage of 5000 V was applied before all particles rose to the top surface of the drop. Notice that particles collected close the top pole without touching each other. Also note that in the

present case since particles collect at the poles, and hence can be concluded that particles undergo positive dielectrophoresis.

In Figures 4.1b-d the applied voltage is slowly reduced to 0 V. Notice that the distance between the particles decreases with decreasing voltage. This shows that the dipole-dipole repulsive forces between the particles which keep particles from touching decrease when the applied voltage is decreased. The electric forces between the particles are repulsive because the electric field near the poles is predominantly is in the normal direction to the drop's surface, and therefore the line joining the particles centers is approximately perpendicular to the electric field. For the last figure in the sequence the applied voltage is zero and, as expected, all particles collect at the top surface of the drop.

4.2 Distribution of particles near the equator

Next, consider the case in which particles collect near the equator to study the nature of dipole-dipole interaction between particles in this region. These experiments were conducted in the device with the electrodes mounted at the side walls. A silicon drop of diameter 1624 μm was suspended in castor oil. Polymer spheres of density 1.05 g/cm^3 and the diameter around 70 μm were suspended inside the drop.

The density of the silicon drop is greater than that of castor oil, and so it sedimented to the bottom of the device. The density of polymer spheres, on the other hand, being ~1.05 g/cm^3, they rose to the top surface of the silicon drop where they were trapped (see Figure 4.2a). Also, the bottom surface of the device had a greater affinity to corn oil, and so the silicon drop did not wet the bottom surface.

(a) 0 V   (b) 5000V

(c)   (d)
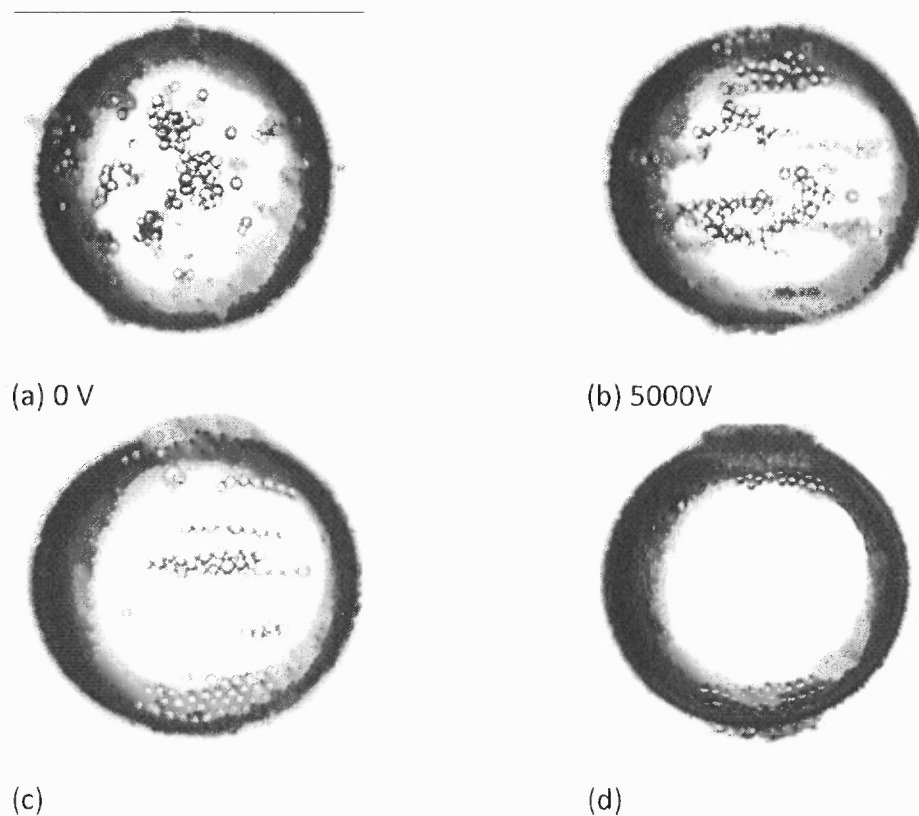
Figure 4.2 The distribution of polymer spheres on the surface of a silicon drop immersed in castor oil is shown. The drop carries polymer spheres which rise to its top surface due to the fact they are lighter than the drop. The electrodes are in the left and right surfaces of the device. The diameter of the undeformed drop is 1624 μm and the applied voltage is 5000 V.

(a) Polymer particles rise inside the drop to its top surface of where they are captured by the interfacial forces.

(b) After the electric field is switched on, particles form chains in the direction parallel to the electric field.

(c) The chains move towards the equator and merge.

(d) Particles and chains remain at the equator, but fall downward along the interface as the density of castor oil is smaller than that of polymer particles.

The dielectric constant of castor oil is smaller than that of the silicon drop, and therefore the electric field is maximal at the poles which are locates at the left and right sides of the drop. The dielectric constant of polymer spheres is smaller than that of castor oil as well as the silicon drop. After an ac electric field with a frequency of 1 kHz is

switched on, the DEP force causes particles to move towards the equator, as shown in Figure 4.2a, indicating that they undergo negative dielectrophoresis. A voltage of 4000 V was applied. Particles collected near the equator and formed horizontal chains. Initially, the chains are at a small distance from each other, but they merge with increasing time to form thicker chains. Also, after reaching the upper surface of the drop they slowly fall downwards as the particle density is smaller than that of the suspending liquid.

The electric field near the equator is predominantly in the tangential direction to the drop surface. Therefore, the fact that the particle chains are horizontal shows that there are dipole-dipole forces between the particles which cause them to align parallel to the local electric field direction.

CHAPTER 5

ELECTROHYDRODYNAMICS OF YEAST CELLS SUBJECTED TO TRAVELING ELECTRIC FIELDS

While traveling wave dielectrophoresis (twDEP) offers a promising method for the control of micro-sized particles suspended in liquids, particularly when the motion of particles along the length of the channel is sought without having to pump the liquid itself, it leads to a variety of complex dynamical regimes which need to be clearly understood for the design of efficient microfluidic devices targeting particular functions. Here, the various dynamical regimes in terms of the forces acting on the particles, are studied i.e., the conventional dielectrophoretic and traveling wave dielectrophoresis force and torque, the viscous drag exerted by the fluid on the particle, and the electrostatic and hydrodynamic particle-particle interactions. Also the variation of the dynamical regimes in three different configurations typical of microfluidic channels whose electrodes are embedded in the bottom wall is considered in this work. The first two configurations have different, i.e. aligned and staggered, electrode geometries, and the third configuration consists of aligned electrodes but energized at different potentials. For these purposes, the direct numerical simulation code based on the distributed Lagrange multiplier method for solving the equations of motion for both the fluid and the individual particles is considered, and the point dipole model to compute the electrostatic forces. The model particles are chosen to have mechanical and electrical properties of yeast cells suspended in an aqueous solution. It is found that the motion of the particles not only depends significantly on the Clausius-Mossotti factor, which is a function of the

electric properties of the fluid and the particles, but also on the specific configuration considered. Particularly, the spinning of particles plays a crucial role on the particle translations and interactions, but the direction of such spinning motion depends on the particular device configuration used.

In this chapter, the motion of particles is investigated for geometries somewhat similar to those described in the experimental work reported by Singh and Aubry in [85]. The electrode geometries studied in this paper are displayed in Figure 5.1. They consist of two arrays of electrodes at the bottom, with each electrode activated at a voltage 90 degrees out of phase with that of the adjacent electrode, thus generating an electric field with a spatially varying phase along the length of the channel (z direction). The voltage phases of the electrodes on both sides of the bottom are indicated in Figure 5.1. Three different configurations are considered, the aligned electrode configurations (i) and (ii) in which the electrodes of the two arrays face each other, and the staggered electrode configuration (iii). In configuration (i), two electrodes facing each other have the same potential, while in configuration (ii) there is a π-shift between the two facing electrodes.
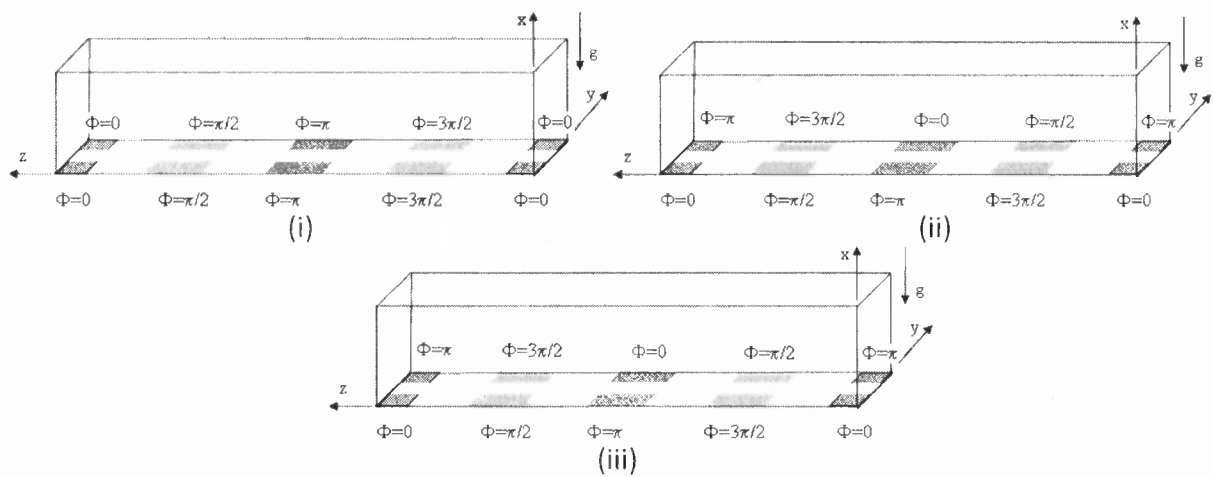
Figure 5.1 Schematic of the three electrode configurations used. (i) Aligned electrode configuration I, (ii) Aligned electrode configurations II, (iii) Staggered electrode configuration.

5.1 Electrostatic Forces

Consider the sinusoidal electric potential oscillating at frequency ω, which, in the phasor

notation, which can be written as $\phi(x,t) = \text{Re}(\tilde{\phi}(x)e^{j\omega t})$, where $j = \sqrt{-1}$, $\tilde{\phi}(x) = \phi_1 + j\phi_2$ and

Re is the real part of a complex variable. The variables ϕ_1 and ϕ_2 are the electric

potentials applied to two different electrodes with a $\pi/2$ phase difference with respect to

each other. The electric field is then deduced from the gradient of the potential as $\mathbf{E}=$

$-\nabla\phi = \text{Re}(\tilde{\mathbf{E}}e^{j\omega t})$, where $\tilde{\mathbf{E}}(x) = -(\nabla\phi_1 + j\nabla\phi_2)$. The potentials are obtained from Laplace's

equation $\nabla^2\phi_i = 0$, $i = 1,2$ subjected to the boundary conditions adapted to the particular

geometry considered (Figure 5.1).

When the electric field is applied, a dielectric spherical particle suspended in a

dielectric liquid becomes polarized. As discussed before in Chapter 2, the polarization is

modeled by the point-dipole (PD) approximation, which was found to lead to results in

good quantitative agreement with computations based on the Maxwell stress tensor,

except if the electric field varied over a length scale comparable with the particle size.

Since this is not the case in the present work, the PD model is adopted and the induced

dipole moment of the particle is $\tilde{\mathbf{p}} = 4\pi\varepsilon_0\varepsilon_c a^3\beta(\omega)\tilde{\mathbf{E}}(x)$, where a is the particle radius, ε_c is

the permittivity of the fluid, $\varepsilon_0 = 8.8542\text{x}10^{-12}$ F/m is the permittivity of free space,

$\beta(\omega) = \dfrac{\varepsilon_p^* - \varepsilon_c^*}{\varepsilon_p^* + 2\varepsilon_c^*}$ is the frequency dependent Clausius-Mossotti factor, and ε_p^* and ε_c^* are the

complex permittivity of the particles and the liquid, with $\varepsilon^* = \varepsilon - j\dfrac{\sigma}{\omega}$, σ being the

conductivity and ε the permittivity. Denoting the complex conjugate by $(.)^*$, the time-

averaged dielectrophoretic force on an isolated particle is expressed as [85]

$$\mathbf{F}_{DEP} = \frac{1}{2}\mathrm{Re}\left((\tilde{\mathbf{p}}.\nabla)\tilde{\mathbf{E}}^*(\mathbf{x})\right) = \pi\varepsilon_o\varepsilon_c a^3 \mathrm{Re}\left(\beta(\omega)\right)\nabla\left(\left|\nabla\varphi_1\right|^2 + \left|\nabla\varphi_2\right|^2\right) -$$

$$2\pi\varepsilon_o\varepsilon_c a^3 \mathrm{Im}\left(\beta(\omega)\right)\nabla\times\left(\nabla\varphi_1 \times \nabla\varphi_2\right) \qquad (5.1)$$

Here, Im(.) denotes the imaginary part. The two terms in Equation 5.1 correspond to the conventional dielectrophoretic force and the *traveling wave dielectrophoretic* (twDEP) force, respectively.

In addition to being exposed to the bulk electric field, two polarized particles i and j close to each other interact electrostatically, with the time-averaged interaction force between them, within the framework of the PD model, being [90]

$$\mathbf{F}_{D,ij} = \frac{3}{8\pi\varepsilon_o\varepsilon_c r^5}\mathrm{Re}\left[\mathbf{r}_{ij}\left(\tilde{\mathbf{p}}_i \cdot \tilde{\mathbf{p}}_j^*\right) + \left(\mathbf{r}_{ij}.\tilde{\mathbf{p}}_i\right)\tilde{\mathbf{p}}_j^* + \left(\mathbf{r}_{ij}.\tilde{\mathbf{p}}_j\right)\tilde{\mathbf{p}}_j^* - \frac{5}{r^2}\mathbf{r}_{ij}\left(\mathbf{r}_{ij}.\tilde{\mathbf{p}}_i\right)\left(\mathbf{r}_{ij}.\tilde{\mathbf{p}}_j^*\right)\right] \qquad (5.2)$$

where $\tilde{\mathbf{p}}_i$ denotes the dipole moment of particle i and $\mathbf{r}_{ij}$ is the unit vector in the direction connecting the center of the ith particle to the center of the jth particle and $r = | \mathbf{r}_{ij}|$. Assuming that $\tilde{\mathbf{E}}_i(\mathbf{x}) = -(\nabla\phi_{1i} + j\nabla\phi_{2i})$ and $\tilde{\mathbf{E}}_j(\mathbf{x}) = -(\nabla\phi_{1j} + j\nabla\phi_{2j})$ are the electric fields at the center of the ith and jth particles, the previous interaction force can be written as

$$\mathbf{F}_{D,ij} = 12\pi\varepsilon_o\varepsilon_c a^6 |\beta|^2 \mathbf{F}'_{D,ij}$$

$$\mathbf{F}'_{D,ij} = \frac{1}{2r^5}[\mathbf{r}_{ij}\left(\nabla\varphi_{1i}.\nabla\varphi_{1j}\right) + \left(\mathbf{r}_{ij}.\nabla\varphi_{1i}\right)\nabla\varphi_{1j} + \left(\mathbf{r}_{ij}.\nabla\varphi_{1i}\right)\nabla\varphi_{1j} - \frac{5}{r^2}\mathbf{r}_{ij}\left(\mathbf{r}_{ij}.\nabla\varphi_{1i}\right)\left(\mathbf{r}_{ij}.\nabla\varphi_{1j}\right) + \mathbf{r}_{ij}\left(\nabla\varphi_{2i}.\nabla\varphi_{2j}\right) +$$

$$\left(\mathbf{r}_{ij}.\nabla\varphi_{2i}\right)\nabla\varphi_{2j} + \left(\mathbf{r}_{ij}.\nabla\varphi_{2i}\right)\nabla\varphi_{2j} - \frac{5}{r^2}\mathbf{r}_{ij}\left(\mathbf{r}_{ij}.\nabla\varphi_{2i}\right)\left(\mathbf{r}_{ij}.\nabla\varphi_{2j}\right)] \qquad (5.3)$$

The net electrostatic interaction force $\mathbf{F}_{D,i}$ acting on the ith particle is the sum of the interaction forces with all other particles, i.e. $\mathbf{F}_{D,i} = \sum\limits_{i=1, i \neq j}^{N} \mathbf{F}_{D,ij}$, which makes the total electrostatic force be $\mathbf{F}_{E,i} = \mathbf{F}_{DEP,i} + \mathbf{F}_{D,i}$. The particle also experiences the following electrostatic torque

$$\mathbf{T}_E = 4\pi\varepsilon_o\varepsilon_c a^3 \, \text{Im}\big(\beta(\omega)\big)\big(\nabla\phi_1 \times \nabla\phi_2\big) \qquad (5.4)$$

Notice that the particle-particle interactions could also have a non-negligible effect on the torque acting on the particles, but this effect is ignored in the present work as it was in previous works.

The previous particle-particle interaction force $\mathbf{F}_{D,i}$ based on the point-dipole approximation, takes into account the modification of the electric field due to the presence of other particles up to the dipole term, but neglects higher order (multipole) terms [86]. The use of this approximation is appropriate when the distance between particles is not much smaller than the particle radius, and not well suited for estimating properties which depend on the behavior of aggregates, such as the viscosity of concentrated suspensions in shear flows. Also ignored is the motion of the suspending liquid due to the presence of the electric field which, under certain conditions, can be quite strong and can drag particles along with it. For example, since most real liquids are at least mildly conducting, the presence of high electric fields can cause significant Joule heating, resulting in electrothermal motion [91].

5.1.1 Governing Equations and Dimensionless Parameters

Consider N solid spherical homogeneous particles, each particle i having an interior denoted by $P_i(t)$, suspended in a Newtonian, incompressible fluid within a domain Ω of boundary Γ. The dimensional governing equations for the fluid and the particles subjected to the appropriate boundary and initial conditions, as well as the equations used for the particle positions. Hereafter, $\mathbf{u}$ is the fluid velocity, p is the pressure, ρ_L is the density of the fluid, η is the dynamic viscosity of the fluid, $\mathbf{U}_i$ and ω_i are the linear and angular velocities of the ith particle, and m_i and I_i are the mass and moment of inertia of the ith particle, and ρ_p, and m the same density and mass of the particles.

The equations governing the fluid and particles motion are nondimensionalized by assuming that the characteristic length, velocity, time, stress, angular velocity and electric field scales are a, U, a/U, $\eta U/a$, U/a and E_0, respectively. The gradient of the electric field is assumed to scale as E_0/L, where L is the distance between the electrodes which is of the same order as the domain width. The nondimensional equations, after using the same symbols for the dimensionless variables, take the expressions:

$$\mathrm{Re}\left(\frac{\partial \mathbf{u}}{\partial t} + \mathbf{u} \cdot \nabla \mathbf{u}\right) = -\nabla p + \nabla \cdot \boldsymbol{\sigma} \qquad \text{in } \Omega \ \overline{P(t)}$$

$$\nabla \cdot \mathbf{u} = 0 \qquad \text{in } \Omega \ \overline{P(t)}$$

$$(5.5)$$

$$\frac{dU_i}{dt} = \frac{6\pi\eta a^2}{mU}\int\left(\frac{-p\mathbf{I}+\boldsymbol{\sigma}}{6\pi}\right)\cdot\mathbf{n}ds + \frac{2\pi a^4\varepsilon_0\varepsilon_c\ \mathrm{Re}(\beta)E_0^2}{mU^2 L}\left((\nabla\phi_1.\nabla)\nabla\phi_1 + (\nabla\phi_2.\nabla)\nabla\phi_2\right) - $$
$$\frac{4\pi a^4\varepsilon_0\varepsilon_c\ \mathrm{Im}(\beta)E_0^2}{mU^2 L}\frac{1}{2}\nabla\times(\nabla\phi_1\times\nabla\phi_2) + \frac{3\pi\varepsilon_0\varepsilon_c a^3|\beta|^2 E_0^2}{4mU^2}\left(\mathbf{F}_{D,i}'\right) \tag{5.6}$$

$$\frac{d\omega_i}{dt} = \frac{5\eta a^2}{2mU}\int(x-X)[(-p\mathbf{I}+\boldsymbol{\sigma})\cdot\mathbf{n}]ds + \frac{8\pi a^3\varepsilon_0\varepsilon_c\ \mathrm{Im}(\beta)E_0^2}{mU^2}\frac{1}{2}(\nabla\phi_1\times\nabla\phi_2) \tag{5.7}$$

which contain the following dimensionless parameters:

$$\mathrm{Re} = \frac{\rho_L Ua}{\eta}, \qquad P_1 = \frac{6\pi\eta a^2}{mU}, \qquad P_2 = \frac{3\pi\varepsilon_0\varepsilon_c|\beta|^2 a^3\ |E_0|^2}{4mU^2}, \qquad P_3 = \frac{2\pi a^4\varepsilon_0\varepsilon_c\ \mathrm{Re}(\beta)|E_0|^2}{mU^2 L},$$

$$P_5 = \frac{4\pi a^4\varepsilon_0\varepsilon_c\ |E_0|^2\ \mathrm{Im}(\beta(\omega))}{mU^2 L}, \qquad P_6 = \frac{8\pi a^3\varepsilon_0\varepsilon_c\ \mathrm{Im}(\beta(\omega))|E_0|^2}{mU^2} \quad \text{and}\quad h' = \frac{L}{a}.\ \text{Each parameter}$$

has a well-defined physical meaning; specifically Re, the Reynolds number, gives the relative importance of the fluid inertia and viscous forces, P_1 is the ratio of the viscous and inertia forces, P_2 is the ratio of the electrostatic particle-particle interaction and inertia forces, P_3 is the ratio of the dielectrophoretic and inertia forces, P_5 is the ratio of the traveling wave dielectrophoretic and inertia forces, and P_6 is the ratio of the traveling wave torque and rotational inertia. In addition, the solids fraction plays an important role.

In previous work done by Singh and Aubry, they have used the ratio $P_4 = \frac{P_2}{P_3} = \frac{3L|\beta|^2}{8a\,\mathrm{Re}(\beta)}$ for comparing the electrostatic particle-particle interaction with the dielectrophoretic force, and have shown the crucial role played by this parameter in the phenomenon of particle chaining both numerically [87] and experimentally [88]. In the case of nano-particles,

the additional Brownian force needs to be not only added to the dynamics but also compared with the other forces as in [89]. In this present work, this additional force will be neglected as the particles considered are of larger size (about 6 μm).

5.1.2 Finite Element Method

Numerical method consists of a finite-element scheme which solves the fluid flow equations in the fictitious domain including both the fluid and the solid particles, and imposes rigid-body motion within the particle boundaries through a Distributed Lagrange Multiplier (DLM) method. Details about the finite element model can be referred from Chapter 2.

5.2 Electric Field

In this study, rigid particles that have the properties of viable yeast cells [33] are considered, including a diameter and a density of 6.0 μm and 1.01 g/cm^3. Regarding the electric properties of the cells, a two-shell model [4] was used, assuming that the dielectric constants of the cell wall, membrane, cytoplasm and medium (aqueous solution) are 10, 6, 50 and 78, the conductivities of the cell wall, membrane, cytoplasm and medium are 50 mS/m, 0.25 μS/m, 0.5 S/m and 40 mS/m and the cell wall thickness is 0.22 μm [33]. The electrohydrodynamics of the system for the following frequencies is considered (i) f = 3000 Hz, (ii) f = 1 MHz, (iii) f = 3 MHz and (iv) f = 5 MHz, corresponding to effective Clausius-Mossotti factors equal to -0.473+0.00092 j, -0.3687+0.264 j, -0.02+0.31 j and 0.1233+0.3357 j, respectively. Notice that since the point dipole model is used to solve the electrical problem, only the effective Clausius-Mossotti factor of the yeast particles is needed.

For the first three frequencies, the real part of β is negative which implies that particles will be repelled away from the electrodes (negative dielectrophoresis) and for the last frequency the real part of β is positive, which means that particles will be attracted to the electrodes (positive dielectrophoresis). In the case of the second frequency, the real part of β, however, is small and therefore the conventional dielectrophoresis force will be small as well. In addition, for the last three frequencies the imaginary part of β is non-negligible, indicating that the effects due to the traveling wave dielectrophoretic force and torque will play a role in the dynamics.

Figure 5.1 shows the channel with the coordinate system used in the simulations. The dimensions of the channel are 32 μm x 48 μm x 128 μm in the x, y, and z directions and all lengths are nondimensionalized with respect to the average cross-sectional length of 40 μm. The periodic boundary condition is imposed in the z-direction for the fluid velocity, pressure, and electric field and the no-slip velocity boundary condition is applied on all walls. Throughout this chapter, the dynamic fluid viscosity is $\eta = 0.01$ poise and the fluid density $\rho_L = 1.0$ g/cm^3. The gravity is taken along the negative x-direction. The domain is discretized by means of a regular pseudo P2-P1 tetrahedral mesh and the number of nodes used is 208,065.

In this study two different electrode geometries are used, which are sketched in figure 5.1, to generate electric fields with spatially varying phases. For the aligned electrode configuration, two electric potential boundary conditions are used to create slightly different electric fields. The electric potential is considered to be periodic in the z-direction, and the normal derivative of the electric potential is taken to be zero on the boundary surfaces not covered by the electrodes. Features of the dimensionless electric

field distributions for the three configurations of Figure 5.1 are depicted in Figures 5.2-5.4. The distributions are qualitatively similar, but there are some important differences, which, as we will discuss later, can result in quite different particle trajectories. The magnitude $|\mathbf{E}|^2$ of the electric field in the x = 0.05 plane (near the bottom of the device) is displayed in Figures 5.2a and 5.3a for the two electrode geometries (Figures 5.1 (i) and (iii)). The electric field magnitudes, as expected, are maximal near the electrodes edges. In the case of the staggered geometry, like the geometry itself, the electric field distribution, as displayed in Figure 5.3a, is not symmetric about the domain mid plane.

(2a)　　　　　　(2b)
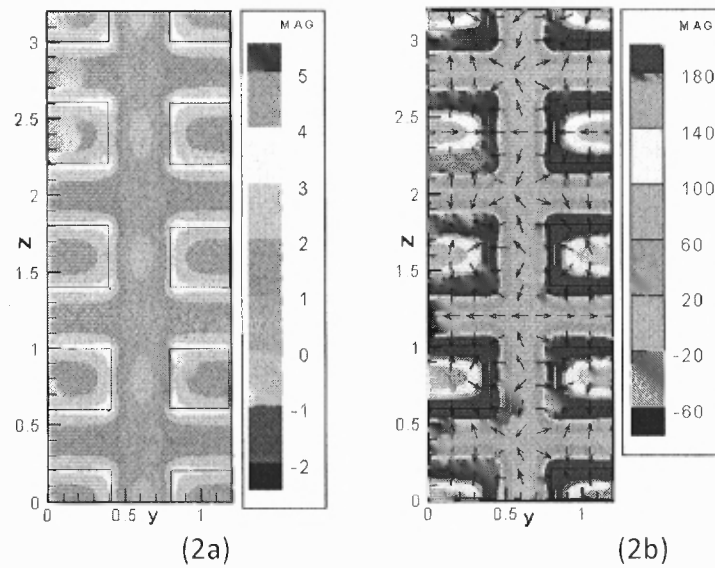
Figure 5.2 Electric field distributions for the aligned configuration I. The electrodes are shown as boxes. (a) Logarithm of $|\mathbf{E}|^2$ in the x = 0.05 plane. The magnitude is maximal near the electrodes edges and decays with increasing distance from these edges. (b) Magnitude and direction of $\nabla(\mathbf{E}^2)$, to which the dielectrophoretic force component is proportional, shown in the x = 0.05 plane. The magnitude is maximal near the electrodes edges and decays with increasing distance from the edges. It also decreases with height. Arrows indicate the direction of the force for positive dielectrophoresis.

In addition, there are four electric field minima in the gap between the two rows

of electrodes in all cases. The particles with negative Re(β) are expected to move to these

regions of electric field minima, and those with positive Re(β) to the electrodes edges

(where the electric field maxima are located). The above minima and maxima become

less pronounced with increasing distance from the bottom plane containing the

electrodes. The direction of the conventional DEP force shown in Figures 5.2b and 5.3b

points away from the minima of $|\mathbf{E}|^2$ and towards the electrodes edges for positive

dielectrophoresis. These figures also show that the domain contains four saddle-node

points.

The magnitude and direction of the term $\nabla \times (\nabla \phi_1 \times \nabla \phi_2)$ in the x = 0.05 and x =

0.25 planes for the two electrode geometries are shown in Figures 5.2c and 5.3c. The

twDEP force is proportional to this term, but points in the opposite direction due to the

negative sign in Equation 5.6. The magnitude of this term is maximal near the electrodes

edges and decreases with increasing distance from the electrodes. It is interesting to note

that for the aligned geometry, the force is in the z-direction in the x = 0.25 plane, but it

varies in direction in the x = 0.05 plane (close to the bottom surface). In the latter plane,

directly above the electrodes, it is in the negative z-direction, but in the central region of

the channel it points mostly in the positive direction. In the staggered geometry case,

directly above the electrodes (in the x = 0.05 plane), the force is in the negative z-

direction, and in the central region the direction is less well defined. Another significant

difference is that in the staggered case the direction of the twDEP force in the x = 0.25

plane directly above the gap between the rows of electrodes is not along the z-direction,

but at an angle. Therefore, the particles that levitate to this height are expected to move

towards the right row of electrodes. The direction of the projection of the force onto the y = 0.5 and y = 0.7 planes varies close to the electrodes, but away from the electrodes the projection points approximately in the z-direction.
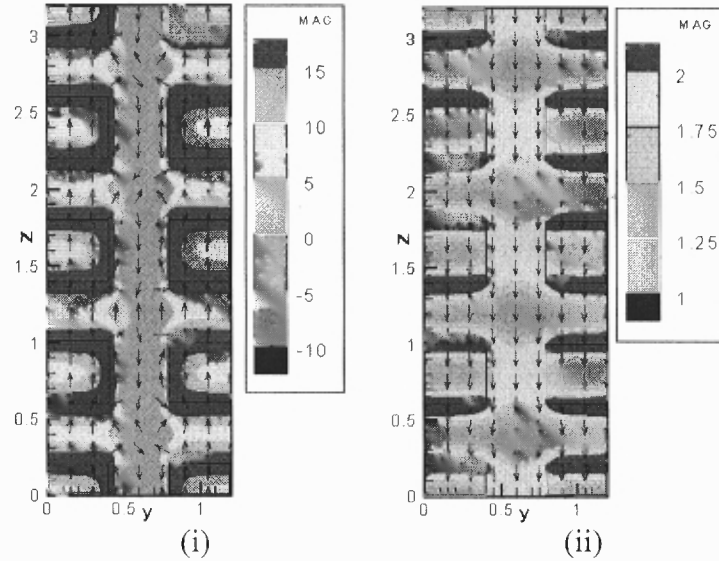
Figure 5.2 (c) Logarithm of the magnitude and direction of $\nabla \times (\nabla \phi_1 \times \nabla \phi_2)$, to which the traveling wave (twDEP) force is proportional, shown in the (i) x = 0.05 and (ii) x = 0.25 planes. The twDEP acts in the opposite direction of the arrows. Its magnitude is maximal at the electrodes. The twDEP force directly above the electrode surface points in the negative z-direction and in between the gap between the electrodes its direction varies. Away from the bottom surface, the force points in the z-direction.

The magnitude and direction of the term $\nabla \phi_1 \times \nabla \phi_2$, to which the traveling wave torque is proportional, are displayed in Figures 5.2d and 5.3d. In the aligned electrode geometry case shown in Figure 2d, the projection of $\nabla \phi_1 \times \nabla \phi_2$ onto the yz-planes is approximately along the y-direction, both near and away from the bottom plane.

(i)   (ii)
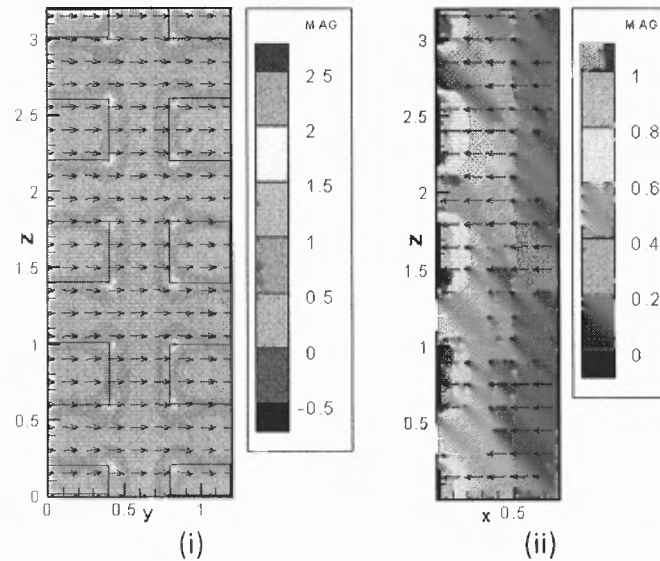
Figure 5.2 (d) Magnitude and direction of the term $\nabla\phi_1 \times \nabla\phi_2$, to which the traveling wave torque is proportional, in the (i) x = 0.05, (ii) y = 0.7 planes. The magnitude is maximal near the electrodes edges and decays with increasing distance from the electrodes. The projection onto the x = 0.05 plane is approximately along the y-direction. The projection onto the y = 0.5 plane is approximately along the negative x-direction. Due to the antisymmetry, the projection onto a plane on the other side of the xz- mid plane is along the positive x-direction.

(3a)   (3b)
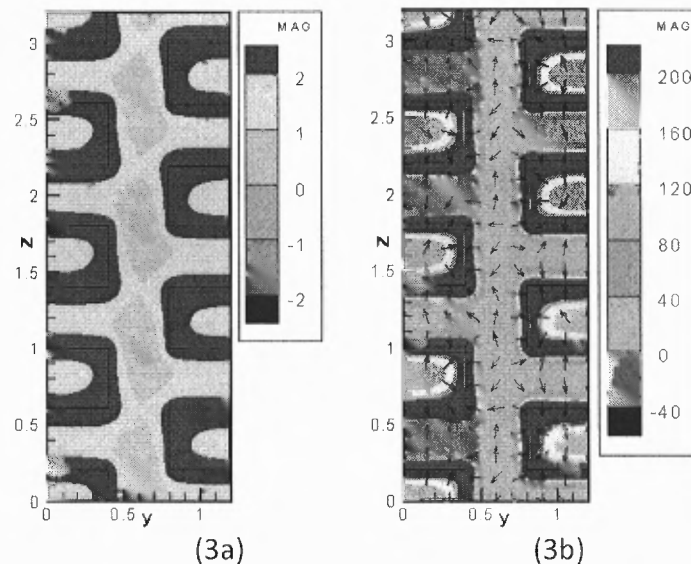
Figure 5.3 The electric field distributions for the staggered configuration. The electrodes are shown as boxes. (a) Logarithm of $|E|^2$ in the x = 0.05 plane. The magnitude is maximal near the electrodes edges and decays with increasing distance from these edges close to the bottom plane. It also decreases with height. (b) Magnitude and direction of the term $\nabla(E^2)$ in the x = 0.05 plane. The magnitude is maximal near the electrodes edges. Arrows indicate the direction of the force for positive dielectrophoresis.

This is, however, not the case in Figure 5.3d which shows that in the central region of the channel between staggered electrodes, the projection of $\nabla\phi_1 \times \nabla\phi_2$ onto the yz-plane makes an angle of approximately 45^0 with respect to the y-axis. This implies that the spin resulting from this torque will be around a line also inclined at an angle of 45^0 with respect to the y-axis, and not along the y-direction, as is the case for the aligned geometry. This change in the direction of spin, as we will discuss later, causes particles to move away from the left row of electrodes and migrate toward the right row.
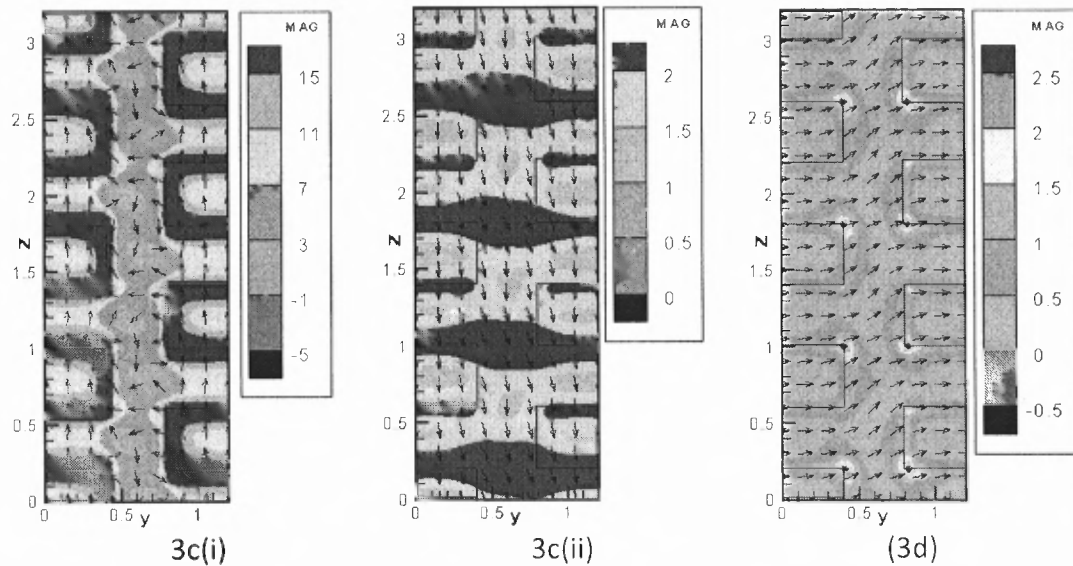
Figure 5.3 (c) Logarithm of the magnitude of $\nabla\times(\nabla\phi_1 \times \nabla\phi_2)$ is shown in the (i) x = 0.05 and (ii) x = 0.25 planes. The twDEP force acts in the opposite direction of the arrows. The twDEP force directly above the electrode surfaces points approximately in the negative z-direction and in between the gap between the electrodes varies in direction. Away from the bottom surface, the force points mostly in the z-direction, but in the gap between the two rows of electrodes the force has a component along the y-direction as well. (d) $\nabla\phi_1 \times \nabla\phi_2$ in the x = 0.05 plane. The projection onto the x = 0.05 is approximately along the x-direction except in the central gap where it contains a component in the z-direction.

The projection of $\nabla\phi_1 \times \nabla\phi_2$ onto the xz-plane is directed approximately along the x-axis, and its magnitude over the electrodes is relatively smaller than that in the gap between the two rows of electrodes. On the left side of the domain mid-plane it is negative (as the arrows point in the negative x-direction) and on the right side it is positive. This implies that when observed from the top, the particles on the left side of the mid plane will rotate in the clockwise direction and those on the right side will rotate in the counterclockwise direction.

4a   4b   4c
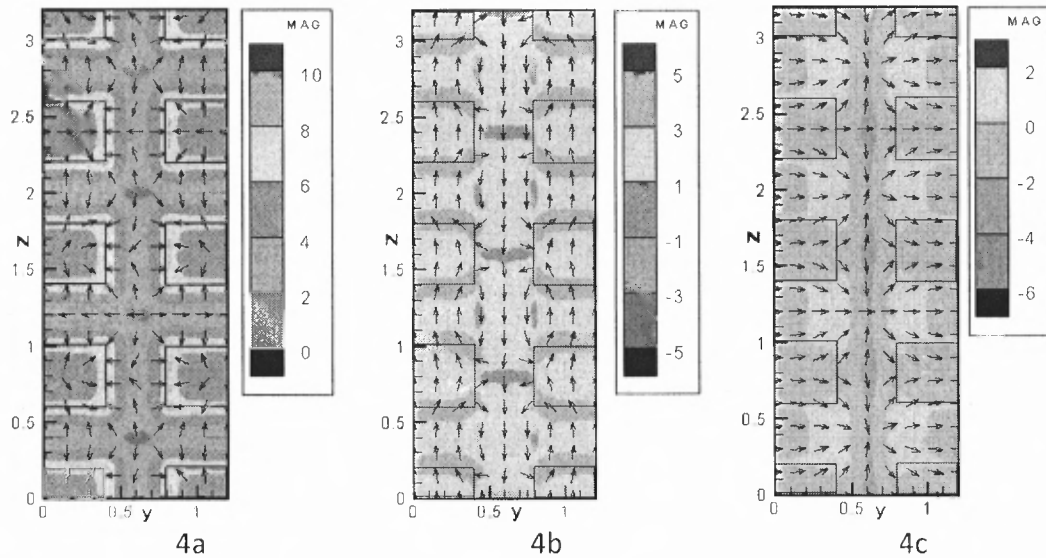
Figure 5.4 Electric field for the aligned configuration II. The electrodes are shown as boxes. (a) Magnitude and direction of $\nabla(\mathbf{E}^2)$ in the x = 0.05 plane. Arrows indicate the direction of the force for positive dielectrophoresis. (b) Logarithm of the magnitude of the term $\nabla\times(\nabla\phi_1 \times \nabla\phi_2)$ is shown in the x = 0.05 plane. The twDEP force acts in the opposite direction of the arrows. The twDEP force directly above the electrode surfaces points approximately in the negative z-direction and in the gap between the electrodes varies in direction. Away from the bottom surface, the force points in the z-direction, as in figure 5.3c(ii) (not shown). (c) Magnitude and direction of the term $\nabla\phi_1 \times \nabla\phi_2$ is shown in the x = 0.05 plane.

In Figure 5.4a-c the electric field distributions are shown for the aligned geometry and the electric potential boundary conditions of Figure 5.1b. A comparison of Figure 5.4a with Figure 5.2b indicates that the fixed points of the cDEP force distribution for the two boundary conditions are at different locations. The cDEP force (for positive dielectrophoresis), however, is still directed towards the electrodes and its magnitude decreases with increasing distance from the electrodes. The qualitative nature of the twDEP force at x = 0.25 shown in Figures 5.2c and 5.4b is similar, i.e., the force in both cases is directed in the negative z-direction. This is also the case at the lower height x = 0.05 just above the electrodes, but in the gap between the electrodes the twDEP force, including its direction, differs in the two cases. The projections of $\nabla\phi_1 \times \nabla\phi_2$ onto the yz-plane shown in Figures 5.2d and 5.4c are similar. In the gap between the electrodes the magnitude of $\nabla\phi_1 \times \nabla\phi_2$ in Figure 5.4c is smaller and on the mid plane it is zero. Thus, for the electric field of Figure 5.4, the spin in the y-direction near the mid plane is expected to be weaker. The projections of $\nabla\phi_1 \times \nabla\phi_2$ onto the xz-planes are primarily along the x-direction.

5.3 Results

First, consider the cases with either two or six particles that were selected to understand the importance of the electrostatic forces and torques, as well as the electrostatic and hydrodynamic particle-particle interactions, on the motion of particles. Since for these cases the solids fraction is relatively small, the motion of particles does not induce bulk motion in the fluid and in this sense the fluid mediated interactions among the particles are rather limited. The initial positions of the particles are selected to be close to the

bottom channel wall either just above the electrodes or in the channel between the electrodes. For the two particle cases the initial positions of the particles are (0.1, 0.4, 1.8) and (0.1, 0.4, 1.96), and for the six particle cases they are (0.1,0.44+0.16*j,1.5+0.16*k), with j=1,2 and k=1,2,3. The real and imaginary parts of β are selected to simulate the particle dynamics at the four frequencies listed earlier in this section.

5.3.1 Aligned Electrode Configuration I

In this subsection, particle motion for the aligned electrode configuration is considered with the voltage boundary condition of Figure 5.1a and first consider the case where $\beta =$ -0.473 + 0.00092j, corresponding to a frequency of 3000 Hz. The dimensionless parameter values are: Re=7.3E-3, P_1= 611.3, P_2= 40491.4, P_3= 11414.0, P_4= 3.5, P_5= 44.4 and P_6= 1776.0.

Top View   Side view
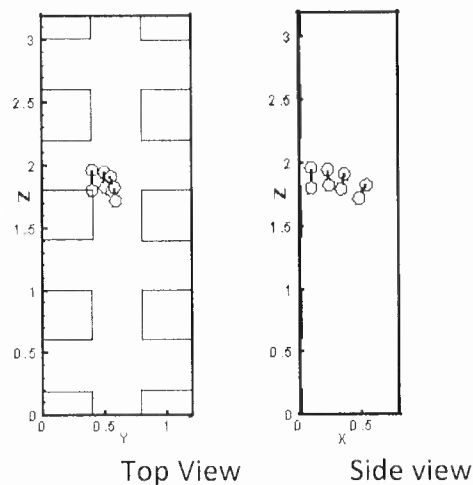
Figure 5.5a Top and side views showing the positions of the two particles at times t = 0, 0.075, 0.243, and 0.618 in the aligned electrode configuration I, for a frequency of 3KHz. The two particles are identified by a line joining the center of one particle to the surface of the other, so that particles can be followed in time.

Since the imaginary part of β is small compared to the real part, the conventional DEP force dominates and the electrostatic torque and twDEP forces are negligible. Simulations show that the particles are pushed away from the electrodes in both the x and y-directions, as is evident from Figure 5.5a. Initially, the conventional DEP force experienced by the lower particle (with a smaller z-value) is larger than that experienced by the upper particle and thus it rises faster. However, as the particles move away from the electrodes in the y-direction, the force on the lower particle decreases and it levitates to a slightly smaller height. The equilibrium height to which a particle rises is determined by the balance of the conventional DEP force and its buoyant weight. Another noticeable aspect is that the particles slowly come close to one another due to the electrostatic particle-particle interaction force.

Next, the case where the frequency is 1 MHz is considered, corresponding to β= -0.3687+0.264 j. The dimensionless parameter values for this case are: Re=6.55E-2, P_1= 68.0, P_2= 460.8, P_3= 110.2, P_4= 4.2, P_5= 157.7, P_6= 6310.4. In this case the electrostatic torque and twDEP force are no longer negligible as the magnitude of the imaginary part of β is not small. As in the previous case, initially the two particles released above the left electrodes rise against gravity, as well as move away from the electrodes in the y-direction. In addition, they spin about the y-axis, rotate together like a dumbbell, and after reaching a certain height, slowly move along the channel length (in the z-direction) (see Figure 5.5b(i)). The nearby spinning particles also come close to each other due to the electrostatic particle-particle interaction force, although relatively slowly due to the fact that the spinning causes lubrication forces on the particles which oppose the motion of the latter towards each other. The spinning is roughly about the y-axis because just above

the electrodes the torque is itself approximately along that direction, as shown by the velocity field distribution (Figure 5.5b(ii)).

Top view   Side view
(i)   (ii)

Top view   Side view
(iii)   (iv)

Figure 5.5b Particle positions and velocity distributions for the aligned electrode configuration I. Results are for the two and six particles cases at a frequency of 1MHz. (i) Top and side views showing positions for the two particle case of Figure 5a at times t = 0.075, 0.9855, 1.293, and 1.65; (ii) Velocity profile in the y = 0.477 plane for the two particle at t = 0.06. Notice that the y-component of the angular velocity of the particles is positive; (iii) Top and side views showing the particle positions for the six particle case at time t = 1.35; notice that four particles levitate and two do not, the latter staying close to the bottom; (iv) Velocity distribution of the particles in the y = 0.6 plane for the six particle case. The figure shows that the y-component of the angular velocity of the particles is positive.

Another run considered six particles released in the gap between the electrodes (Figure 5.5b(iii)). While four of these particles levitate, two are trapped at the local minima of the electric field. The levitated particles form a quadruplet which rotates about the y-axis; the electrostatic torque causes the particles to spin about the y-axis and since in this case the spinning particles are close to each other, they begin to rotate in a global quadruplet spinning motion illustrated in Figure 5.5b(iv). After reaching a certain height above the electrodes, these levitated particles begin to translate along the z-axis, as was the case with two particles. Recall here that due to periodic boundary conditions particles leaving the end of the channel reappear at the entrance. Particles released in the gap between the electrodes also spin about the x-axis, but the x-component of the angular velocity is much smaller than the y-component.

Next, when $\beta = -0.02+0.31$ j, corresponding to a frequency of 3 MHz which lies in the transition range from negative to positive dielectrophoresis. The dimensionless parameter are: Re=0.105, P_1= 42.5, P_2= 84.2, P_4= 2.3, P_4= 36.2 P_5= 72.2, P_6= 2886.6. It has been observed experimentally that in this range cells exhibit an amusing electrokinetic behavior and the corresponding regime was then referred to as the FUN regime [33]. Here, the conventional DEP force is nearly 20 times smaller than in the previous case and therefore it can be considered negligible, except near the electrodes edges. This implies that the particles, instead of being levitated, fall towards the bottom under gravity and that their motion is driven mostly by the combined action of the electrostatic torque and the twDEP force.

The primary direction of the particles spin is along the y-axis right above the electrodes. The particles at higher elevations, on the other hand, in addition to spinning

about the y-axis, also spin about the x-axis. Simulations show that two particles released just above the electrodes spin and rotate about each other and that after several rotations, one particle gets trapped at an electrode tip. Meanwhile, the second particle rises above the electrode edge, falls under the action of the twDEP force and finally stops. Before the particles get captured, their motion is rather erratic, consisting of both rotation about each other and translation, the former being mainly due to the spin arising from the traveling wave torque. These results are qualitatively similar to those reported in [33] for the FUN regime. Six particles released in the middle of the channel are also either eventually captured by the electrodes or in regions where the twDEP force changes sign (see Figure 5.5c).

For all cases investigated the particles did not get transported along the channel in the positive z-direction. In contrast, as particles spin primarily about the y-axis, particles close to the bottom of the channel move along the negative z-direction. Particles in the channel also spin about the negative x-axis, but with a much smaller angular velocity component than about the y-axis. The x-component of the angular velocity for the particles on the left side of the mid plane is negative and for those on the right side of the mid plane it is positive.
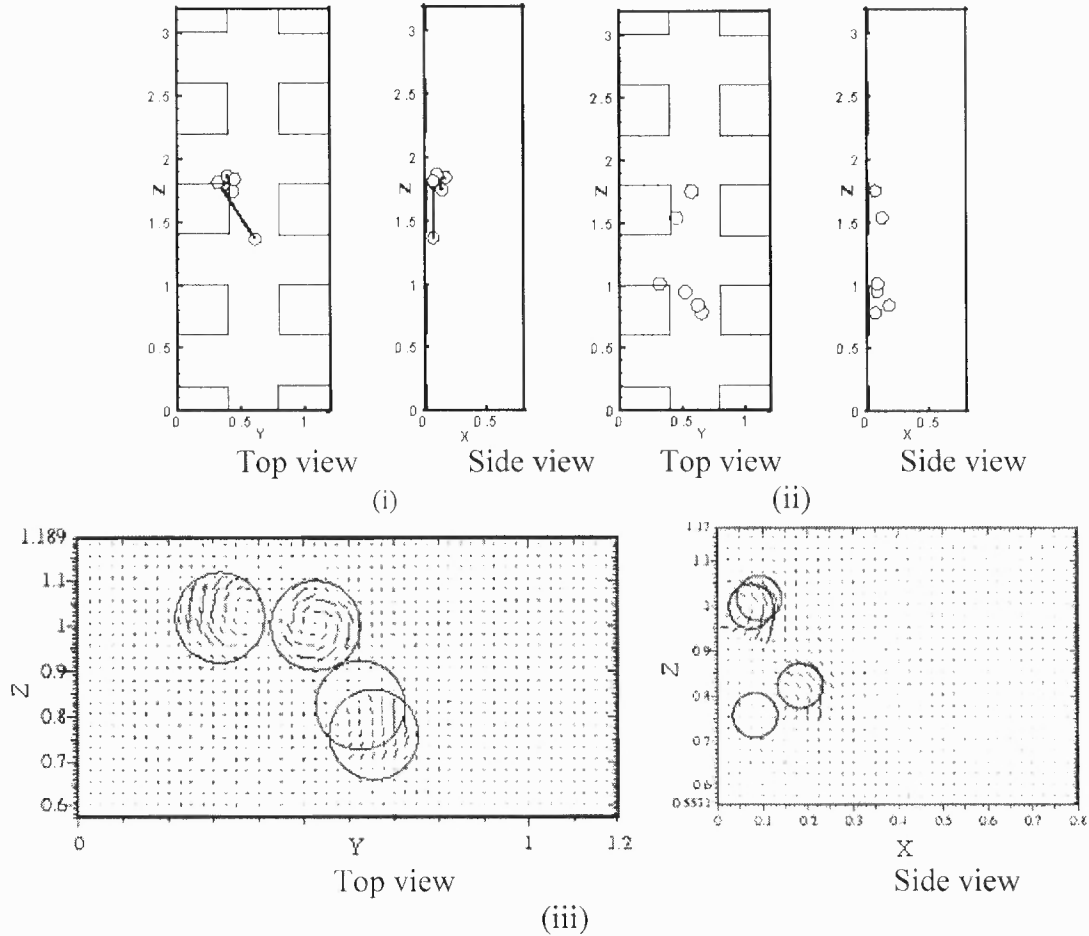
Figure 5.5c Particle positions and velocity distributions for the aligned electrode configuration I. Results are for the two and six particles cases at a frequency of 3 MHz: (i) Top and front views showing positions for the two particle case at times t = 0.0255, 0.039, and 1.923; (ii) Top and side views showing the positions for the six particle case at time t = 1.0395; (iii) Velocity distribution shown in the y = 0.5 and x=0.1 planes for the six particle case at t = 1.0395, showing that the particles spin about both the y- and x-axes. The x-component of the angular velocity is negative for the particles on the left of the mid plane and positive for those on the right.

The last situation a study is done which corresponds to the case where the frequency is increased to the value of 5MHz, for which the Clausius-Mossotti factor becomes β = 0.1233+0.3357 j, and the dimensionless parameters are Re= 5.06E-2, P_1= 87.9, P_2= 478.9, P_3= 61.6, P_4= 7.8, P_5= 335.2, P_6= 13409.7. Since in this case the real part of the Clausius-Mossotti factor is positive, particles move towards the electrodes, even

when they are released in the gap between the electrodes. In the case of two particles, the upper particle attaches to the nearby electrode and the second particle moves in the negative z-direction while maintaining a very close distance to the electrode. This movement is due to the spinning of the particle. The particle is captured near the other end of the electrode, but continues to spin. It is held there by the conventional DEP force which overcomes the hydrodynamic force that arises because of the spinning due to the electrostatic torque.

5.3.2 Aligned Electrode Configuration II

Next, the particle motion for the aligned electrode configuration is considered with the voltage boundary condition of Figure 5.1 (ii). As discussed before, the qualitative distribution of the electric field in the aligned geometry for the two boundary conditions differs near the electrodes and is similar away from the electrodes. For $\beta = -0.473 + 0.00092j$ the real part of β is relatively large, and thus particles move away from the electrodes. Also, since the imaginary part of β is relatively small, the force and torque are small and thus the motion is qualitatively similar to that reported in the previous subsection for the same value of β and is therefore not described here.
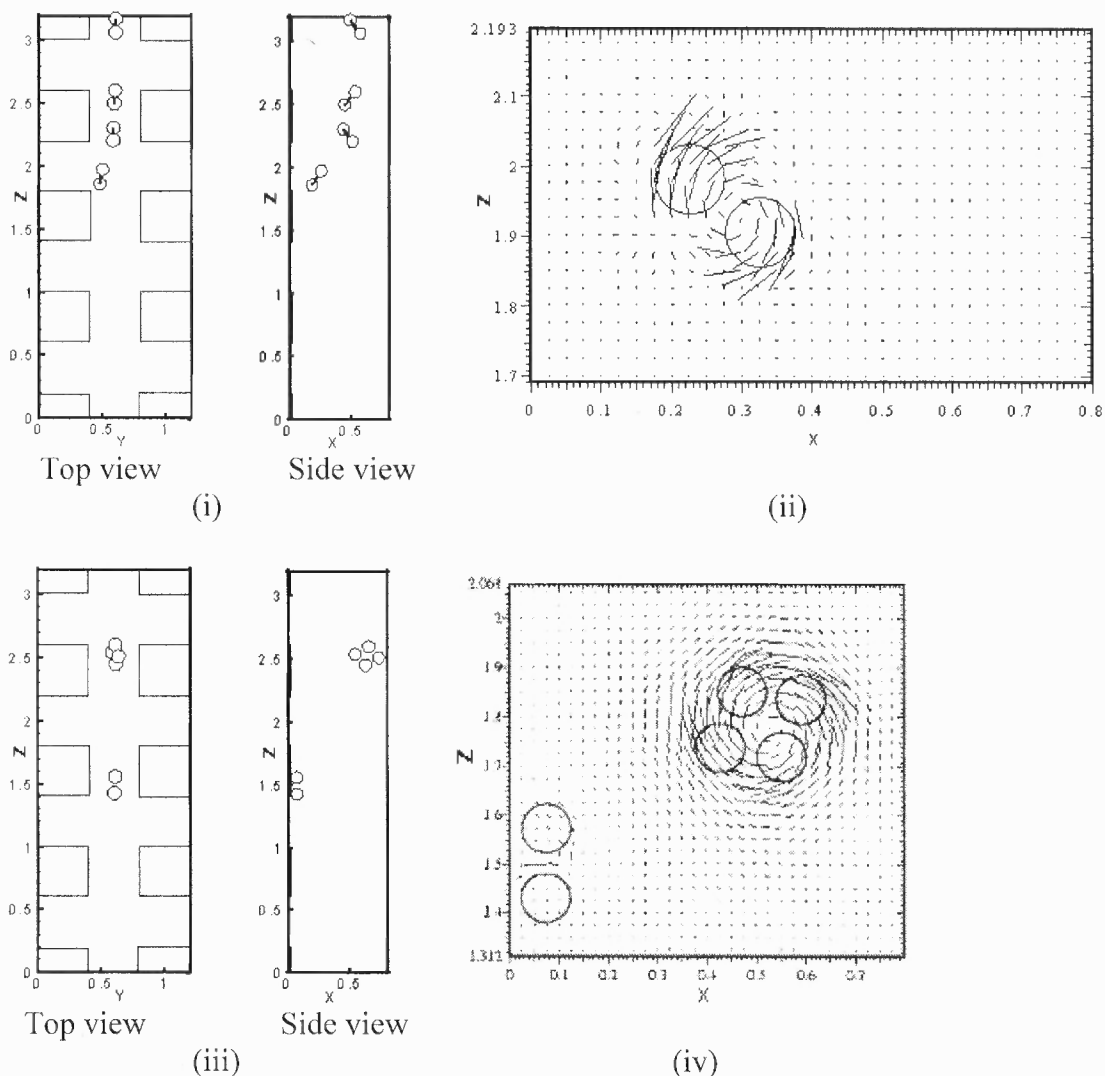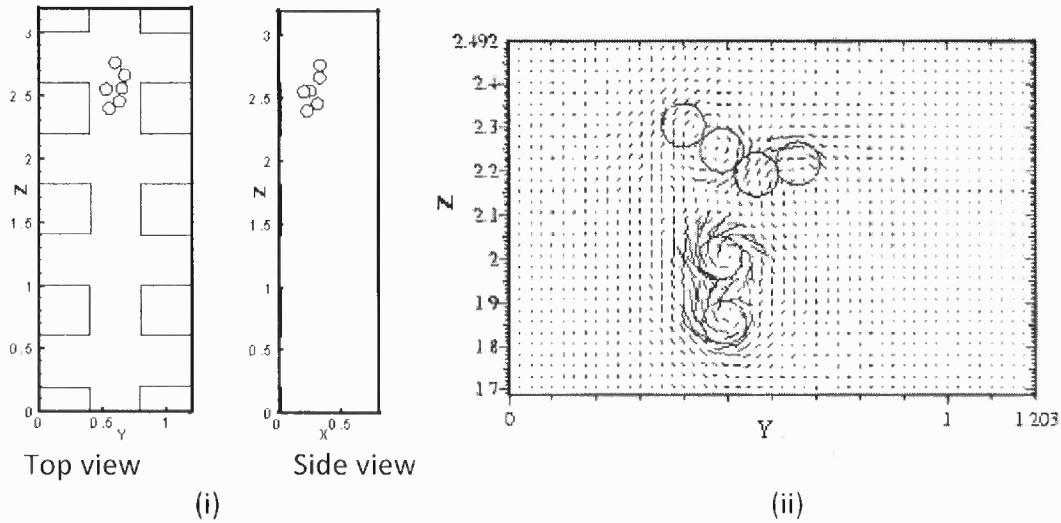
Figure 5.6 Particle positions and velocity distributions for the aligned electrode configuration II. (a) Results are for the six particles case at a frequency of 1 MHz. (i) Position at time t = 0.495. (ii) Velocity distribution shown in the x = 0.2 plane at t = 0.31. The figure shows that the particles spin about the x-axis, the x-component of the angular velocity being negative for those on the left of the mid plane and positive for those on the right.

The same remark is valid for β = -0.3687+0.264 j after particles levitate, reach a certain height and begin to slowly move in the z-direction under traveling wave dielectrophoresis (see Figure 5.6a). However, before they move away from the electrodes, the traveling wave torque causes the particles in the gap to spin. In this case, the torque component in the x-direction is the largest, and thus particles spin primarily about the x-axis. The dimensionless parameter values are: Re=2.9E-2, P_1= 148.5, P_2=2354.9, P_3=646.7, P_4= 3.6, P_5= 340.7 and P_6= 13629.9. Notice that these parameter values differ from the corresponding value for the case described in figure 5.5b, as the velocity of the particles is different.
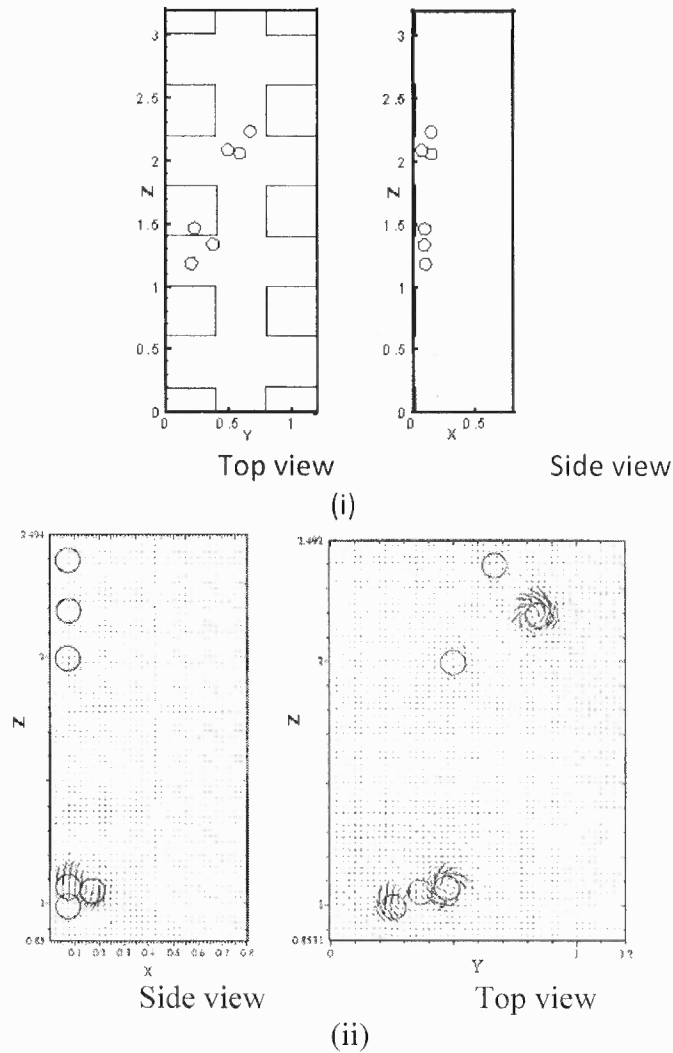
Figure 5.6 (b) Results at a frequency of 3 MHz: (i) Positions at time t = 1.20; (ii) Velocity distribution in the y = 0.6 and x = 0.1 planes at t =0.93. The two views show that the particles are spinning about both the x- and y-axes.

This is a result of the fact that the electric field distributions for the two configurations are different. In addition, since all components of the torque near the domain mid plane are small, the angular velocities of the particles near this plane are small too. This is in contrast to the primary direction of the spin for the aligned electrode configuration I, as described in the previous subsection, which was along the y-direction. The sense of rotation in the x-direction, however, is similar. Specifically, the particles on

the left side of the mid plane have a negative x-component of angular velocity and those on the right side of the mid-plane have a positive x-component.

For β= -0.02+0.31 j, as for the corresponding case discussed in the previous subsection, particles do not levitate and thus move under the actions of the electrostatic torque and the twDEP force. The dimensionless parameter values are: Re=0.31, P_1= 14.4, P_2=9.7, P_3=0.27, P_4= 36.2, P_5= 8.3, P_6= 330.9.

Near the bottom plane, both change periodically in magnitude and direction, and consequently the trajectories of the particles appear erratic [33].The electrostatic torque causes particles to spin about both x- and y-axes, with the former component being the largest. The rotation about the y-axis causes the particles to move along the negative z-axis and that along the x-axis causes the nearby particles to hydrodynamically interact with each other. As was the case above, particles on the left side of the mid plane have a negative x-component of angular velocity and on the right side of the mid plane it is positive (see Figure 5.6b). In the case of six particles released in the middle of the channel, four are captured by the electrodes or in regions where the twDEP force changes sign and the remaining two continue to move. For all cases investigated the particles do not get transported along the channel.

The particle motion for β = 0.1233+0.3357 j was qualitatively similar to that reported in the previous subsection for the same parameter values and is therefore not discussed further.

5.3.3 Staggered Electrode Configuration

Next, the motion of the two particles in the staggered electrode geometry case for the same parameters as above is considered. In the first case, corresponding to a frequency of

3 KHz, the conventional DEP force causes the particles to move away from the electrodes. The dimensionless parameter values are: Re=1.7E-2, P_1= 262.7, P_2= 7479.0, P_3= -2108.2, P_4= -3.5, P_5= 8.2, P_6= 328.0. Particles move in the y- and negative z-directions, towards the region of the electric field minimum. As for the corresponding case shown in Figure 5.5a, particles rise against gravity to a height where the buoyant weight balances the conventional DEP force. As they drift towards the channel center in the inter-electrode gap, they fall because the conventional DEP force becomes weaker with increasing distance from the electrodes.

For the second case corresponding to a frequency of 1 MHz, the particles rise against gravity while simultaneously moving in the y-direction (see Figure 5.7a), as was the case in the aligned configuration reported in Figure 5.6b. The dimensionless parameter values are: Re=3.9E-2, P_1= 113.9, P_2= 1291.5, P_3= -308.7, P_4= -4.2, P_5= 442.1, P_6= 17685. Both particles also spin due to the electrostatic torque which, we recall, makes an angle of approximately 45 degrees with the y-axis (see Figure 5.4d). In addition, the particles in the channel on the left side of the mid plane experience a torque along the negative x-axis, and the particles on the right side of the mid plane experience a torque about the x-axis. Eventually, particles reach the center of the channel where the conventional DEP force, twDEP force and torque are all small. One of the particles falls to the bottom and, because of its spin, drifts away from the second particle. The second particle remains levitated and moves in the positive z-direction under the action of the twDEP force. In general, if a particle rises to a certain height above the electrodes, it moves in the z-direction under the action of the twDEP force. However, if it does not, it gets captured either by the electrodes or at one of the zeroes of the twDEP force. Notice

that the levitated particle slowly drifts to the left as it moves along the z-direction because the average y-component twDEP force in the gap is negative (see figure 5.3c).

Top view   Side view   Top view   Side view

7a   7b(i)   7b (ii)
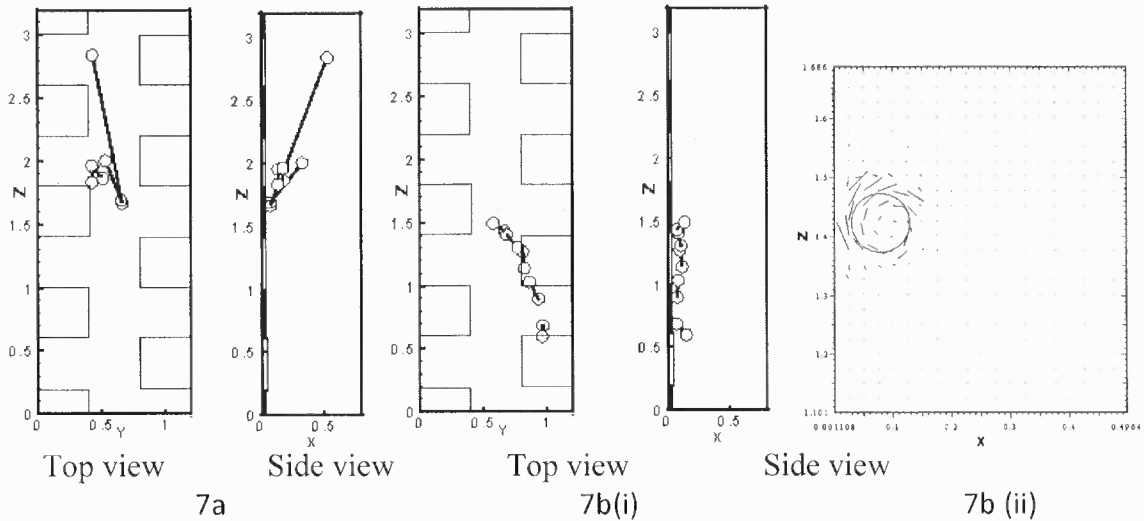
Figure 5.7 (a) Results are for the two particle case at a frequency of 1 MHz. The positions of the two particles are at times t = 0.0135, 0.0465, 0.6015, and 2.2425. (b) Results are for the two particle case at a frequency of 5 MHz. (i) Positions of the two particles are at times t = 0.1125, 0.189, 0.228, 0.3, 0.705, showing the motion of the particles at an angle rather than along the channel length; (ii) Velocity distribution at t = 0.048 (magnified view around particle).

When the frequency takes the value of 3MHz, the motion of particles is similar to that observed for the case of the aligned electrodes I. They first fall towards the electrodes, spin, and get captured near the bottom plane. They continue to spin even after they are captured. The dimensionless parameter values are: Re=0.107, P_1= 41.6, P_2= 81.0, P_3= -2.2, P_4= -36.2, P_5= 69.4, P_6= 2777.2.

For the last case where the frequency is further raised to 5 MHz, particles experience a positive conventional DEP force, a twDEP force and a torque. The dimensionless parameter values are: Re=4.6E-2, P_1= 96.2, P_2= 573.4, P_3= 73.7, P_4= 7.8,

P_5= 401.3, P_6= 16053.5. Figure 5.7b shows that in this case both particles fall downward under gravity and spin. The motion of the particles is generated by both the torque and the proximity of the bottom of the channel. Since the torque, in this case, is at an angle of 45 degrees to the y-axis, the particles move away from the electrode on a trajectory which also makes an angle of approximately 45 degrees with the ý-axis, thus moving downward to the right row of electrodes. Particles continue to spin even after being captured at electrodes edges there.

5.3.4 Motion of 50 or 112 Particles

Now the transient motion of 50 and 112 particles initially arranged on a simple cubic lattice and released at the channel entrance near the bottom wall is described. Since the particles are released close to each other, they influence each others' motion. The parameters and the set of frequencies selected for this investigation are the same as above. Consequently, the dimensionless parameters are approximately the same as for the corresponding case containing two or six particles.

5.3.4.1 Aligned electrode configurations

For β = -0.473 + 0.00092j, particles move primarily under the action of the conventional DEP force, undergoing negative dielectrophoresis. They rise to a height at which the buoyant force is equal to the conventional DEP force (see Figure 5.8a). Figure 5.8a shows that particles also migrate toward the center of the channel, where the magnitude of the electric field is smaller. Also notice that particles come close to each other under the action of the particle-particle electrostatic interaction force and become tightly packed. The results for the two aligned electrode configurations are qualitatively similar.

Next consider the case where $\beta = -0.3687+0.264\,j$, for which both the twDEP and conventional DEP forces are significant. The latter causes particles to levitate, but before they move away from the channel bottom, the spin in the y-direction due to the traveling wave torque causes the particles near the channel bottom to move in the negative z-direction (see Figure 5.8b). The results for the two aligned electrode configurations are qualitatively similar, and therefore only those for the aligned electrode configuration II are presented here. Simulations show that although all particles rotate, the rate of rotation is higher for those near the electrodes than for those near the center of the channel, where the torque is weaker. The conventional DEP force causes particles to move away from the electrodes and levitate. After reaching a certain height above the electrodes, the twDEP force causes particles to move in the z-direction.

Top view   Side view
t = 0.12   t = 0.6015   t = 0.12   t = 0.6015
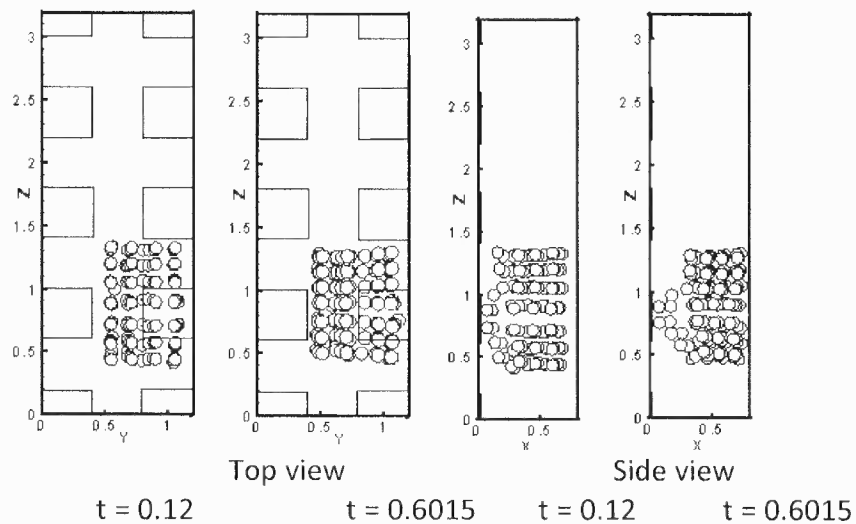
Figure 5.8a Positions of the 112 particles in the aligned electrode configuration I at times t = 0.12, t = 0.6015, for a frequency of 3000 Hz, showing that the particles levitate but do not undergo any traveling wave motion along the length of the channel.

At the frequency of 3MHz, the particles do not levitate and thus their motion is determined by the twDEP force near the bottom plane and the traveling wave torque which causes them to spin (see Figure 5.8c). They first fall and begin to spin about the y-axis. The results are shown only for the aligned electrode configuration II since for the aligned electrode configuration I they are similar. The rotating particles near the channel bottom experience a downward hydrodynamic force that propels them in the -z-direction.
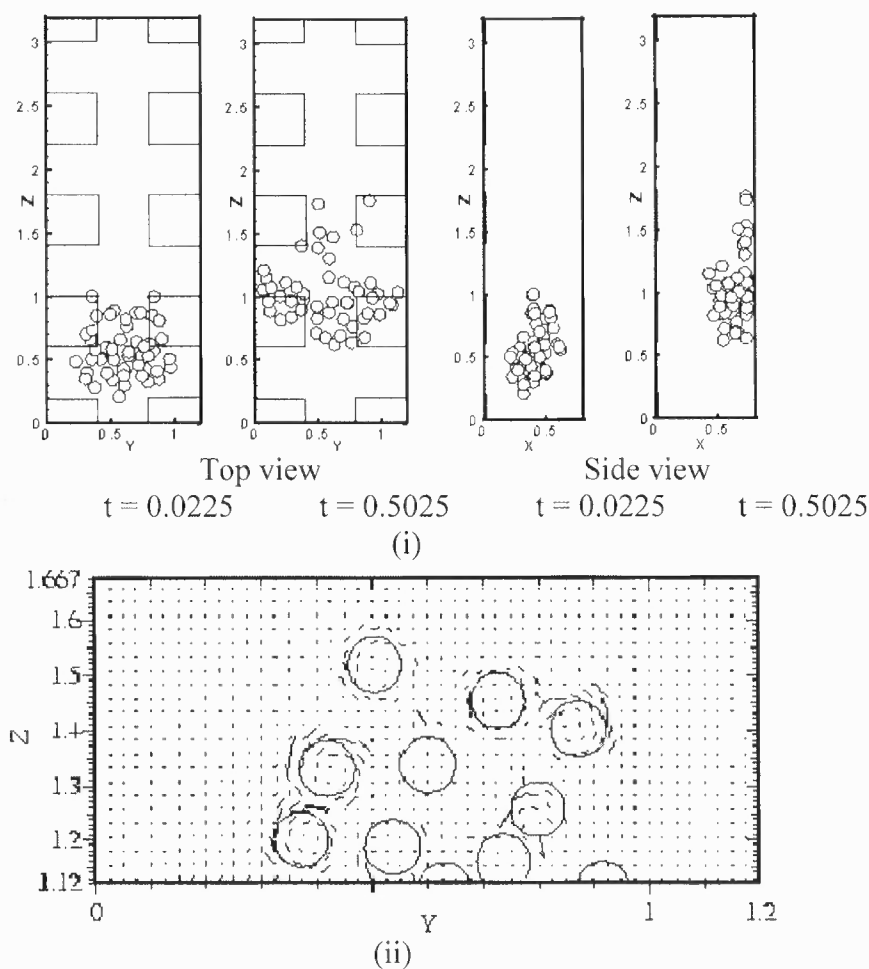
Figure 5.8b Positions and velocity distribution for the case of 50 particles in the aligned electrode configuration II for a frequency of 1 MHz: (i) Positions of the particles showing both levitation and traveling wave motion; (ii) Velocity distribution in the x = 0.1 plane at t = 0.215 (magnified view around some particles), showing that the x-component of angular velocity of the particles is negative for those on the left of the mid-plane and positive for those on the right. The velocity vectors are magnified 100 times and the particles are shown even when they are not in x=0.1 plane.
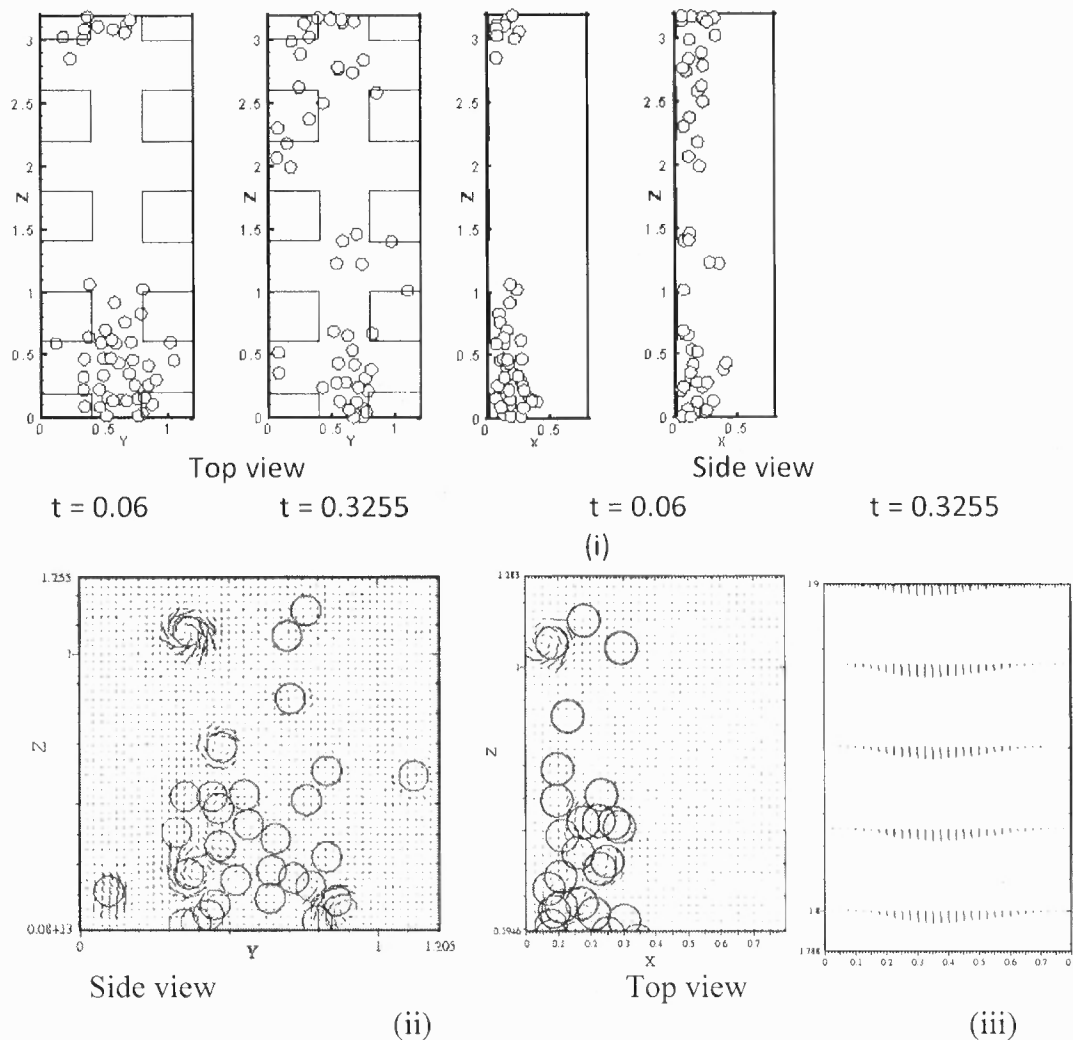
Figure 5.8c Positions and velocity distribution in the aligned electrode configuration II for a frequency of 3 MHz: (i) Positions of the particles traveling motion in the opposite direction of the traveling wave dielectrophoresis; (ii) Velocity distribution in the x = 0.1 plane at time t = 0.235 (magnified view around some particles), showing the spinning of the particles about the y- and x-axes; (iii) Velocity profile in the channel showing a profile in the negative z-direction induced by the bulk motion of the particles. The velocity vectors are magnified 100 times.

The downward motion of these propelled particles drags along other particles in close proximity creating a downward bulk motion of particles. This bulk motion of particles creates a bulk downward motion of the liquid, as can be seen in Figure 5.8c,

which, in turn, creates a downward drag force on all particles. As noted in the previous subsection, for these parameter values isolated particles are not transported along the channel, but instead get trapped at the electrode edges or at the zeroes of the twDEP force.

Therefore one can conclude that the motion of a group of particle in a device is fundamentally different than that of an isolated particle. It is noteworthy that the direction of motion of a group of particles that fall to the channel bottom is the opposite of that remain levitated above the bottom plane. This difference, in principle, could be used to separate particles of the same densities for which the real parts of β differ, i.e., particles with a smaller Re(β) would settle and then move downward, and those with a larger Re(β) would levitate and then move in the upward direction.

For $\beta = 0.1233+0.3357$ j, the conventional DEP force is positive, which implies that particles fall to the channel bottom under the action of positive dielectrophoresis. The traveling wave torque causes them to spin along the y-direction. The spinning particles near the channel bottom are propelled in the negative z-direction, as for the case discussed above and therefore not shown here.

5.3.4.2 Staggered Electrode Configuration

For $\beta = -0.473 + 0.00092$j, as in the previous subsection, particles rise to a height at which the buoyant force is equal to the conventional DEP force. The particles also migrate toward the center of the channel, where the magnitude of the electric field is smaller and come close to each other under the action of the particle-particle electrostatic interaction force and become tightly packed.

Next, consider the case with $\beta = -0.3687+0.264$ j for which particles levitate, but before moving away from the bottom of the channel they spin at 45 degrees to the y-direction due to the traveling wave torque and thus the particles near the channel bottom move in the -z-direction and towards the right electrodes. After particles levitate, they move in the z-direction while drifting to the left under the action of the twDEP force (see Figure 5.9).

Top View
t=0.1875   t=0.9015

Side View
t=0.1875   t=0.9015
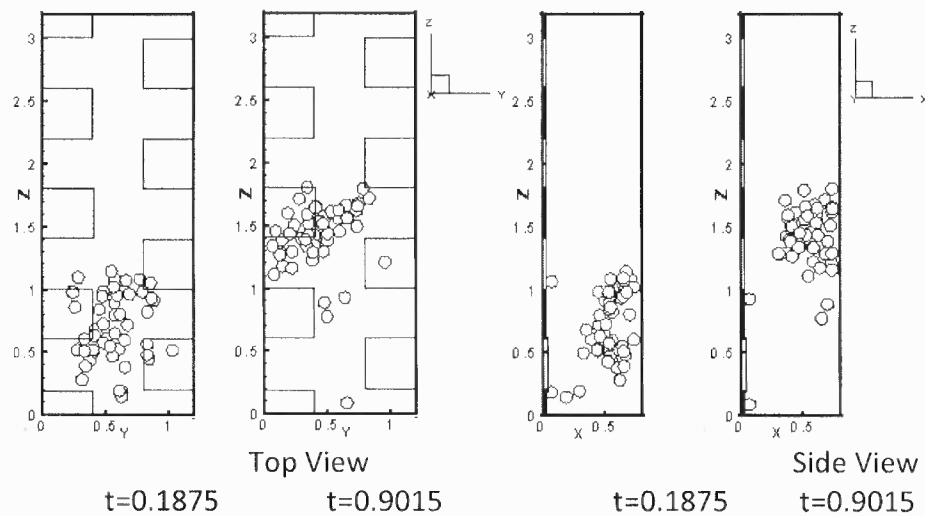
Figure 5.9 Positions and velocity distribution for the case of 50 particles in the staggered electrode configuration for a frequency of 1 MHz. Notice that after levitating particles move to the left side under the action of twDEP force.

For $\beta= -0.02+0.31$ j, particles first fall and begin to spin about the y-axis. Their motion is governed by the twDEP force and the traveling wave torque. The latter is directed at 45 degrees to the y-axis. The rotating particles move in the negative z-direction and towards the right, and drags nearby particles in the same general direction. As noted in the previous subsection, such motion of a group of particles in a device is fundamentally different from that of an isolated particle.

Finally, when β = 0.1233+0.3357 j particles fall to the channel bottom under the action of both positive dielectrophoresis and gravity. The traveling wave torque causes them to spin at 45 degrees to the y-direction. The spinning particles near the channel bottom are propelled downward toward the right.

CHAPTER 6

CONCLUSIONS

This work deals with study of various parameters that influence the process of concentrating, separating and removing particles distributed on the surface of a drop when it is subjected to a uniform electric field and study the influence of traveling electric fields on yeast cells. It is possible to manipulate particles trapped on the surface of a drop because they experience DEP forces due to the non-uniformity of the electric field intensity on the drop's surface (even though the applied electric field away from the drop is uniform). The DEP forces cause particles to aggregate either near the poles or the equator of the drop, depending on the dielectric constants of the fluids and particles involved.

The experimental results, in agreement with the analytical results, show that the DEP force on a particle is inversely proportional to the drop radius. This was shown by measuring the electric field intensity needed for moving a fixed particle trapped on the surface of a drop from the drop's equator to one of its poles for different values of the drop radius, the latter being varied by injecting or removing liquid from the drop. The result that the electric field intensity required to move particles trapped on the surface of a drop decreases with decreasing drop radius is significant because it implies that the electric field intensity required for manipulating particles of micro emulsions is smaller than that needed for emulsions containing millimeter sized droplets.

Experiments also show that the presence of particles on the drop's surface can influence its electric field induced deformation. For the case in which particles aggregate

118

at the poles and the drop's dielectric constant is greater than that of the ambient liquid, it is found that the drop's deformation was larger and that the drop tip-streamed at a smaller electric field intensity than for a clean drop. On the other hand, when particles aggregated near the poles and the drop's dielectric constant was smaller than that of the ambient liquid, the drop deformation was smaller than for a clean drop. Recall that particles undergo positive dielectrophoresis in the former case and negative dielectrophoresis in the latter. This change in the drop deformation is due to the modification in the net electrostatic force that acts on the drop. For cases in which particles aggregated near the equator, the drop deformation was not significantly altered by the presence of particles.

It is possible to concentrate particles only if the electric field intensity is large enough so that the DEP force overcomes the particles' buoyant weight as well as the Brownian motion. The work done on a particle by the DEP force in moving it from one of the drop's poles to the equator was computed for a typical range of parameter values and found to be at least an order of magnitude larger than kT for 100 nm sized particles, thus showing that the DEP force is large enough to overcome the Brownian force. Furthermore, it is shown that the concentration of particles is possible only when the electric gravity parameter G, defined as the ratio of the DEP force and the buoyant weight, is O(1) or larger. Since the DEP force acting on a particle and its buoyant weight both vary as the particle's volume, the electric gravity parameter is independent of the particle radius. The electric gravity parameter G increases with decreasing buoyant weight and also with decreasing drop size. The former implies that negligible electric field intensity is required for concentrating neutrally buoyant particles.

Once particles were aggregated near the poles or the equator, electric field intensity is increased to remove them from the drop. Experiments also show that the electric field intensity at which tip-streaming occurred increased with decreasing drop diameter so that the electric Weber number was approximately constant, which is in agreement with past experimental studies. To remove particles concentrated near the poles, the intensity was increased to a critical value at which particles aggregated at the poles were ejected by means of a tip-streaming mechanism. During this process, the drop also lost some of its liquid. The method was effective in removing all of the particles aggregated near the poles. This required the use of a device for which the distance between the electrodes was larger than approximately five times the drop diameter.

To remove particles aggregated near the equator of the drop, a device for which the gap between the electrodes was approximately three times larger than the drop diameter is used. In this case, after all the particles aggregated near the equator, the applied voltage was increased to a value so that the drop elongated, bridged the gap between the electrodes, and then broke into three major droplets. Experiments show that the drop breakup near the middle occurred due to the capillary instability once the diameter of the filament became smaller than the size of the particle cluster. All of the particles were contained in and around the droplet in the middle, while the two larger sized droplets on the sides were particle free. The middle droplet containing particles was formed due to the fact that the filament diameter decreased due to the transport of the fluid into the two major droplets on the sides while none of the particles was transported. In fact, the size of the middle droplet adjusted to the volume of particles trapped on the

drop's surface, i.e. it increased (decreased) when the volume of particles was increased (decreased).

The drop bridged the gap between the electrodes due to the enhancement of the electric field intensity in the gap between the electrodes and the device walls. Experiments show that the diameter of the smallest drop that bridged the gap between the electrodes varied linearly with the distance between the electrodes. For a water drop suspended in corn oil, the drop bridged the gap when the distance between the electrodes was about three times the drop diameter. The electric Weber number at which the drop bridged the gap between the electrodes was found to be approximately constant and its value was smaller than the critical Weber number at which the drop underwent tip-streaming (which happened when the distance between the electrodes was larger).

The technique described in this thesis for removing particles from drops can work only if the drops break or tip-stream for a larger electric field intensity than that required for concentrating particles. It is shown that for a given drop, ambient liquid and particles combination, there is a critical drop radius below which the electric field intensity needed for concentrating particles is smaller than the intensity at which the drop tip-streams or breaks. Only in the case where the drop radius is smaller than this critical value, it is possible to concentrate particles on the surface of the drop. More specifically, only if the dimensionless parameter is such that $\dfrac{We'}{G}$ <1, it is possible to concentrate particles. On the other hand, if the drop radius is larger than the critical radius, it is not possible to concentrate particles because the drop breakup or tip-streaming occurs at a smaller electric field intensity than that needed for concentrating particles. This suggests that the technique is more effective for the emulsions for which the drop size is smaller. Ideally,

if the goal is also to clean the drop of particles then $\frac{We'}{G}$ should not be much smaller than one because otherwise the electric field intensity required for breaking the drop will be much larger than that required for concentrating particles.

It is also shown that the method can be used to separate particles which undergo positive dielectrophoresis form those experiencing negative dielectrophoresis on the surface of a drop. This is done by aggregating particles of one type at the poles and of another type at the equator. The redistribution of particles remained unchanged after the electric field was switched off because they did not mix. This approach therefore can be used to form composite or "Janus" drops for which surface properties vary because their surface is covered by one type of particles near the equator and by another type of particles near the poles. Once particles were separated on the surface of a drop, the particles aggregated at the poles can be removed from the drop via tip-streaming, thus leaving the drop with only one type of particles. This was demonstrated in a device for which the gap between the electrodes was sufficiently large so that it did not bridge the gap between the electrodes.

In addition to collecting at the poles or the equator, particles interact with each other via dipole-dipole interactions. For the case in which particles aggregate at the poles, we find that particles do not touch each other because there are dipole-dipole repulsive forces between them. The repulsive forces arise because the local electric field is approximately normal to the drops surface and thus perpendicular to the line joining the particles centers.

On the other hand, when particles aggregate near the equator there is a tendency to form particle chains. These chains initially repel each other but later they merge. The

chains are aligned parallel to the local electric field direction which near the poles is approximately tangential to the drop's surface.

The direct numerical simulation approach was used to investigate the dynamical motion of particles in a channel driven by traveling wave dielectrophoretic forces and torques. The traveling wave electric field was generated by a periodic array of electrodes placed in the bottom wall of the channel, typical of Micro-Electro-Mechanical System (MEMS) devices. The problem was studied for two aligned electrode configurations (with the same electrode geometry but different phases between the voltages applied to the electrodes) and a staggered electrode geometry. Our simulations have led to the following conclusions.

Even though the three electrode configurations studied in this paper are rather similar, the generated electric fields differ and so do the forces and torques acting on the particles. This results in different dynamical motions of particles for the three configurations, although in all cases one can clearly distinguish four regimes, depending on the real and imaginary parts of the Clausius-Mossotti factor, $\text{Re}(\beta)$ and $\text{Im}(\beta)$. Although the particles' dynamics were found quite complex in many of the cases studied, they were explained in terms of the forces and torques acting on the particles, consisting of the conventional dielectrophoretic and traveling wave dielectrophoresis force and torque, the viscous drag exerted by the fluid on the particle, and the electrostatic and hydrodynamic particle-particle interactions. We now summarize our findings.

If $\text{Re}(\beta)$ is negative, of sufficiently large amplitude, and $\text{Im}(\beta)$ sufficiently small, particles undergo negative dielectrophoresis and therefore levitate. There is, however, no translation of the particles along the channel, as the traveling wave

dielectrophoresis is not sufficiently large. This behavior is observed for two particles as well as for a group of particles.

If Re(β) is negative and small so that particles do not levitate and Im(β) is large, the particles fall to the bottom of the chamber and spin. The direction of spin is different for the three electrode configurations investigated, which along with the twDEP force, determines the direction in which the particles move. In the staggered configuration they move at a 45 degrees angle to the y-axis. Isolated particles are captured in all cases. A group of particles move downward in all cases.

If Re(β) is positive the particles do not levitate and if Im(β) is large, the particles fall to the bottom of the device and the behavior is similar to that observed in the previous situation.

Perhaps, the most interesting phenomenon highlighted in Chapter 5 which, has not been reported in the literature before, is the phenomenon of particle spinning about various directions. This could be explored in applications where particles are used as stirrers for local mixing at specific sites where chemical or biological reactions are required, or as miniature rotors whose directions of rotation can be varied by simply changing the voltages applied to the electrodes. In addition, although the computations have been carried out with the Clausisus-Mossotti factor values relevant to yeast cells suspended in an aqueous solution, the results remain valid for other types of particles including glass and polymer beads and other biological particles, as well as carbonaceous particles suspended in in-service oils and heavy metals absorbing particles which could be used to filter contaminated water.

REFERENCES

1. Pohl, H. A. (1951). The motion and precipitation of suspensoids in divergent electric fields. Journal of Applied Physics, 22, (7), 869-871.

2. Pohl, H. A. (1978). Dielectrophoresis, Cambridge University press, Cambridge.

3. Holzel, R. (1997). Electrorotation of single yeast cells at frequencies between 100 Hz and 1.6 GHz. Biophysical Journal, 73(2), 1103-1109.

4. Huang, Y., Holzel, R., Pethig, R., & Wang, Y. (1992). Differences in the AC electrodynamics of viable and non-viable yeast cells determined through combined dielectrophoresis and electrorotation studies. Physics in Medicine and Biology, 37(7), 1499-1517.

5. Zhou, R., Wang, P., and Chang, H.C. (2006). Bacteria capture, concentration and detection based on ac dielectrophoresis, electro-osmotic transport and self-assembly of single-wall carbon nanotubes. Electrophoresis, 27, 1376-1385.

6. Lapizco-Encinas, B.H., Simmons, B.A., Cummings, E.B., and Fintschenko, Y. (2004). Insulator-based dielectrophoresis for the selective concentration and separation of live bacteria in water. Electrophoresis, 25, 1695-1704.

7. Huang, Y., Yang, J.M., Hopkins, P.J., Kassegne, S., Tirado, M. (2003). Separation of simulants of biological warfare agents from blood by a miniaturized dielectrophoresis device. Biomedical Microdevices, 5, 217-225.

8. Docoslis, A., Espinoza, A.T., Zhang, B., Cheng, L., Israel, A., Alexandridis, P., Abbott, N.L. (2007). Using nonuniform electric fields to accelerate the transport of viruses to surfaces from media of physiological ionic strength. Langmuir, 23, 3840-3848.

9. Grom, F., Kentsh, J., Muller, T., Schnelle, T., Stelzle, M. (2006). Accumulation and trapping of hepatitis A virus particles by electrohydrodynamic flow and dielectrophoresis. Electrophoresis, 27, 1386-1393.

10. Hughes, M.P., Morgan, H. (1999). Diffuse double layer effects observed by dielectrophoresis of Herpes Simplex Virus, type 1 (HSV-1). Annual International Conference of the IEEE Engineering in Medicine and Biology – Proceedings, 1, 90.

11. Morgan, H., Green, N.G. (1997). Dielectrophoretic manipulation of rod-shaped viral particles. Journal of Electrostatics, 42, 279-293.

12. Tuukkanen, S., Toppari, J.J., Kuzyk, A., Hirviniemi, L., Hytonen, V.P., Ihalainen, T., Torma, (2006). P. Carbon nanotubes as electrodes for dielectrophoresis of DNA. Nano Letters, 6, 1339-1343.

13. Zou, H., Mellon, S., Syms, R.R.A., Tanner, K.E. (2006). 2-dimensional MEMS dielectrophoresis device for osteoblast cell stimulation. Biomedical Microdevices, 8, 1339-1343.

14. Hunt, T.P., Westervelt, R.M. (2006). Dielectrophoresis tweezers for single cell manipulation. Biomedical Microdevices, 8, 227-230.

15. Cen, E.G., Dalton, C., Li, Y., Adamia, S., Pilarski, L.M., Kaler, K.V.I.S. (2004). A combined dielectrophoresis, traveling wave dielectrophoresis and electrorotation microchip for the manipulation and characterization of human malignant cells. Journal of Microbiological Methods, 58(3), 387-401.

16. Green, N.G., Morgan, H. (1999). Dielectrophoresis of submicrometer latex spheres. 1. Experimental results. Journal of Physical Chemistry B, 103(1), 41-50.

17. Fuhr, G., Arnold, W.M., Hagedorn, R., Muller, T., Benecke, W., Wagner, B., Zimmermann, U. (1992). Levitation, holding, and rotation of cells within traps made by high-frequency fields. Biochimica et Biophysica Acta - Biomembranes, 1108 (2), 215-223.

18. Winslow, M.W. (1949). Induced fibration of suspensions. Journal of Applied Physics, 20(12), 1137-1140.

19. Whitesides, G.M. (2006). The origins and the future of microfluidics. Nature, 442 (7101), 368-373.

20. Srinivasan, V., Pamula, V.K., Fair, R.B. (2004). An integrated digital microfluidic lab-on-a-chip for clinical diagnostics on human physiological fluids. Lab on a Chip - Miniaturization for Chemistry and Biology, 4 (4), 310-315.

21. Fan, S.-K., Huang, P.-W., Wang, T.-T., Peng, Y.-H., (2008). Cross-scale electric manipulations of cells and droplets by frequency-modulated dielectrophoresis and electrowetting. Lab on a Chip - Miniaturisation for Chemistry and Biology 8 (8), 1325-1331

22. Chin, C.D., Linder, V., Sia, S.K. (2007). Lab-on-a-chip devices for global health: Past studies and future opportunities. Lab on a Chip, 7(1), 41-57.

23. Manz, A., Eijkel, J.C.T. (2001). Miniaturization and chip technology. What can we expect. Pure and Applied Chemistry, 73(10), 1555-1561.

24. Markx, G.H., Pethig, R., and Rousselet, J. (1997). The dielectrophoretic levitation of latex beads, with reference to field-flow fractionation. Journal of Physics. D: Appl.Phys. 30, 2470-2477.

25. Morgan, H., Green, N.G., Hughes, M.P., Monaghan, W., and Tan, T.C. (1997). Large-area travelling-wave dielectrophoresis particle. Journal of Micromechanics and Microengineering. 7(2), 65–70.

26. Cui, L., Morgan, H. (2000). Design and fabrication of traveling wave di-electrophoretic structures. Journal of Micromechanics and Microengineering, 10, 72–79.

27. Goater, A.O., Burt, J.P.H., Pethig, R. (1997). A combined travelling wave dielectrophoresis and electrorotation device: Applied to the concentration and viability determination of cryptosporidium. Journal of Physics D: Applied Physics, 30 (18), L65-L69.

28. Pethig, R. (1996). Dielectrophoresis: Using inhomogeneous AC electrical fields to separate and manipulate cells, Critical Reviews in Biotechnology, 16, 331–348.

29. Wang, X.-B., Huang, Y., Becker, F.F., Gascoyne, P.R.C. (1994). Unified theory of dielectrophoresis and travelling wave dielectrophoresis. Journal of Physics D: Applied Physics, 27 (7), 1571-1574.

30. Morgan, H., Izquierdo, A.G., Bakewell, D., Green, N.G., Ramos, A. (2001). The dielectrophoretic and travelling wave forces generated by interdigitated electrode arrays: Analytical solution using Fourier series. Journal of Physics D: Applied Physics, 34 (10), 1553-1561.

31. Green, N.G., Ramos, A., Morgan, H. (2002). Numerical solution of the dielectrophoretic and travelling wave forces for interdigitated electrode arrays using the finite element method. Journal of Electrostatics, 56 (2), 235-254.

32. Wang, X., Wang, X.-B., Becker, F.F., Gascoyne, P.R.C. (1996). A theoretical method of electrical field analysis for dielectrophoretic electrode arrays using Green's theorem. Journal of Physics D: Applied Physics, 29 (6), 1649-1660.

33. Huang, Y., Wang, X.-B., Tame, J.A., Pethig, R. (1993). Electrokinetic behaviour of colloidal particles in travelling electric fields: studies using yeast cells. Journal of Physics D: Applied Physics, 26 (9), 1528-1535.

34. Singh, P. and Aubry, N. (2007). Transport and deformation of droplets in a microdevice using dielectrophoresis, Electrophoresis, 29 (4), 644-657.

35. Klass, D. L., Martinek, T. W. (1967), Electroviscous fluids. II. Electrical properties. Journal of Applied Physics, 38, 75-80.

36. Uejima, H. (1972). Dielectric mechanism and rheological properties of electrofluids. Japanese Journal of Applied Physics, 11, 319-326.

37. Stangroom, J. E. (1991). Basic considerations in flowing electrorheological fluids. Journal of Statistical Physics, 64, 1059-1072.

38. Stangroom, J. E. (1996). Basic observations on electrorheological fluids. Journal of Intelligent Material System and Structures, 7, 479-483.

39. Marshall, L., Goodwin, J.W., Zukoski, C. F. (1989). Effects of electric fields on the rheology of nonaqueous concentrated suspensions. Journal of Chemical Society Faraday Transactions I, 85, 2785-2795.

40. Song, H., Tice, J.D. and Ismagilov, R.F. Angew. (2003). A microfluidic system for controlling reaction networks in time. Angewandte Chemie - International Edition 42 (7), 768-772.

41. Tawfik, D.S., Griffiths, A.D. (1998). Man-made cell-like compartments for molecular evolution. Nature Biotechnology, 16, 652-656.

42. Millman, J. R., Bhatt, K. H., Prevo, B. G., and Velev, O. D. (2005). Anisotropic particle synthesis in dielectrophoretically controlled microdroplet reactors. Nature Materials 4, 98-102.

43. Ozen, O., Aubry, N., Papageorgiou, D. and Petropoulos, P. (2006). Electrohydrodynamic linear stability of two immiscible fluids in channel flow, Electrochimica Acta, 51, 11425.

44. Ozen, O., Aubry, N., Papageorgiou, D., and Petropoulos, P. (2006). Monodisperse drop formation in square microchannels, Physical Review Letters, 96, 144501.

45. Binks, B.P. (2002). Particles as surfactants - similarities and differences. Current opinion in Colloid Interface Science. 7, 21-41.

46. Ramsden, W. (1903). Separation of solids in the surface-layers of solutions and 'suspensions' - Preliminary account. Proceedings of Royal Society, (London), 72, 156.

47. Pickering, S.U. (1907). Emulsions. Journal Chemical Society, London, 91(2), 2001-2021.

48. Menon, V.B., and Wasan, D.T. (1986). Particle-fluid interactions with application to solid-stabilized emulsions. Part 1, The effect of asphaltene adsorption. Colloids Surfaces, 19, 89-105.

49. Auroux, P.-A., Iossifidis, D., Reyes, D.R., Manz, A. (2002). Micro total analysis systems. 2. Analytical standard operations and applications. Analytical Chemistry, 74 (12), 2637-2652.

50. Li, F., Ozen, O., Papageorgiou, D., and Petropoulos, P. (2007). Linear instability of a two-fluid interface for electro-hydrodynamic mixing in a channel. Journal of Fluid Mechanics. 583, 347-377.

51. Bresme, F., Quirke, N. (1999). Nanoparticulates at liquid/liquid interfaces. Physical Chemistry Chemical Physics, 1 (9), 2149-2155.

52. Finkle, P., Draper, H.D., Hildebrand, J.H. (1923). The theory of emulsification. The Journal of the American Chemical Society, 45 (12), 2780-2788.

53. Binks, B.P., Lumsdon, S.O. (1999). Stability of oil-in-water emulsions stabilised by silica particles. Physical Chemistry Chemical Physics, 1 (12), 3007-3016.

54. Midmore, B.R. (1998). Preparation of a novel silica-stabilized oil/water emulsion. Colloids and Surfaces A: Physicochemical and Engineering Aspects, 132 (2-3), 257-265.

55. Yan, N., Masliyah, J. H. (1994). Adsorption and desorption of Clay Particles at the Oil-Water Interface. Journal of Colloid Interface Science 168, 386–392.

56. O'Konski, C. T., Thacker, H. C. (1953). The distortion of aerosol droplets by an electric field. Journal of Physical Chemistry, 57, 955–958.

57. Garton, C. G., Krasuchi, Z. (1964). Bubbles in insulating liquids: Stability in an electric field. Proceedings of the Royal Society, London A, 280, 211–226.

58. Taylor, G. (1966). Studies in electrohydrodynamics. I. The circulation produced in a drop by electrical field. Proceedings of the Royal Society, London A, 291(1425), 159–166.

59. Allen, R. S., Mason, S. G. (1962). Particle behaviour in shear and electric fields. I. Deformation and burst of fluid drops. Proceedings of the Royal Society, London A, Math. Phys.Sci, 267, 45–61.

60. Torza, S., Cox, R. G., Mason, S. G. (1971). Electrohydrodynamic deformation and burst of liquid drops. Phil. Trans. R. Soc. Lond.A Math. Phys. Sci., 269, 295–310.

61. Melcher, J. R., Taylor, G. I. (1969). Electrohydrodynamics: A review of the interfacial shear stresses. Annual. Review of Fluid Mechanics, 1, 111–146.

62. Sherwood, J. D. (1988). Breakup of fluid droplets in electric and magnetic fields. Journal of Fluid Mechanics, 188, 133–146.

63. Saville, D. A. (1997). Electrohydrodynamics: The taylor-melcher leaky dielectric model. Annual Review of Fluid Mechanics, 29, 27–64.

64. Darhuber, A. A., Troian, S. M. (2005). Principles of microfluidic actuation by modulation of surface stresses. Annual Review of Fluid Mechanics, 37, 425–455.

65. Bei, Z.M., Jones, T.B., Tucker-Schwartz, A. (2008). Electric field mediated droplet centering. Applied Physics Letters, 93(18), 184101.

66. Jomni, F., Denat, A., Aitken, F. (2009). The dynamics of microscopic bubbles in viscous insulating liquids. Journal of Applied Physics 105 (5), 053301.

67. Arp, P.A., Foister, R.T., Mason, S.G. (1980). Some electrohydrodynamic effects in fluid dispersions. Advances in Colloid and Interface Science, 12 (4), 295-356.

68. Atten, P., Castellanos, A. (1995). Injection induced electrohydrodynamic flows. Handbook of Electrostatic Processes, 121-146.

69. Baygents, J.C., Saville, D.A. (1989). The circulation produced in a drop by an electric field: A high field strength electrokinetic model. Drops & Bubbles, Third International Colloquium, Monterey. AIP Conference Proceedings, 7-17.

70. Brazier-Smith, P.R. (1971). Stability and shape of isolated and pairs of water drops in an electric field. Physics of Fluids, 14 (1), 1-6.

71. De La Mora, J.Fernandez, Loscertales, I.G. (1994). Current emitted by highly conducting taylor cones. Journal of Fluid Mechanics, 260, 155-184.

72. Hayati, I. (1992). Eddies inside a liquid cone stressed by interfacial electrical shear. Colloids and Surfaces, 65 (1), 77-84.

73. Hayati, I., Bailey, A.I., Tadros, Th.F. (1986). Mechanism of stable jet formation in electrohydrodynamic atomization. Nature, 319 (6048), 41-43.

74. Singh, P and Aubry, N. (2007). Dielectrophoresis and deformation of droplets in micro devices, Electrophoresis, 28, 644–657.

75. Singh, P. and Aubry, N. (2005). Trapping force on a finite sized particle in a dielectrophoretic cage. Physical Review E, 72, 016602.

76. Aubry, N. and Singh, P. (2006). Control of electrostatic particle-particle interactions in dielectrophoresis. European Physics Letters 74(4), 623-629.

77. Glowinski, R. T., Pan, W., Hesla, T. I and Joseph, D.D. (1998). Direct numerical simulation of viscoelastic particulate flows. International Journal of Multiphase Flows, 25, 755-794.

78. Singh, P., Joseph, D. D., Hesla, T. I., Glowinski, R. T. and Pan, W. (2000). A distributed lagrange multiplier/fictitious domain method for particulate flows. Journal of Non-Newtonian Fluid Mechanics, 91, 165-188.

79. Singh, P. and Joseph, D.D. (2005). Fluid dynamics of floating particles. Journal of fluid Mechanics. 530, 31-80.

80. Basaran, O.A. and Scriven, L.E. (1990). Axisymmetric shapes and stability of pendant and sessile drops in an electric field. Journal of Colloid Interface Science. 140, 10-30.

81. Fernandez, de la Mora J. (2007). The fluid dynamics of Taylor cones, Annual Review of Fluid Mechanics. 39, 217-243.

82. Reznik, S.N., Yarin, A.L., Theron, A. and Zussman, E. (2004). Transient and steady shapes of droplets attached to a surface in a strong electric field. Journal of Fluid Mechanics, 516, 349-377.

83. Wohlhuter, F.K. and Basaran, O.A. (1992). Shapes and stability of pendant and sessile dielectric drops in an electric field. Journal of Fluid Mechanics, 235, 481-510.

84. Baygents, J.C. Rivette N.J., and Stone, H.A. (1998). Electrohydrodynamic deformation and interaction of drop pairs. Journal of Fluid Mechanics. 368, 359-375.

85. Aubry, N. and Singh, P. (2006). Influence of particle-particle interactions and particle rotational motions in traveling wave dielectrophoresis, Electrophoresis, 27, 703-715.

86. Huang, J.P., Karttunen, M., Yu, K.W., Dong, L., and Gu, G.Q. (2004). Electrokinetic behavior of two touching inhomogeneous biological cells and colloidal particles: Effects of multipolar interactions. Physical Review. E, 69(5), 051402.

87. Kadaksham, J., Singh, P., Aubry, N. (2006). Manipulation of particles using dielectrophoresis. Mechanics Research Communications, 33, 108-122.

88. Kadaksham, J., Singh, P., Aubry, N. (2005). Dielectrophoresis induced clustering regimes of viable yeast cells. Electrophoresis, 26, 3738-3744.

89. Kadaksham, J., Singh, P., Aubry, N. (2004). Dielectrophoresis of nanoparticles. Electrophoresis 25, 3625-3632.

90. Kadaksham, J., Singh, P., Aubry, N. (2004). Dynamics of electrorheological suspensions subjected to spatially nonuniform electric fields. Journal of Fluids Engineering, 120, 170-179.

91. Perch-Nielsen, I.R., Green, N.G., Wolff, A. (2005). Numerical simulation of travelling wave induced electrothermal fluid flow. Journal of Physics. D: Appl. Phys, 37, 2323-2330.